

THE  
TETRAKIS(TRI-PARA-TOLYL PHOSPHITE)NICKEL(0)  
HYDRIDE SYSTEM

DEDICATION

To my husband Mark for his continual  
support and encouragement

SYNTHESIS AND NUCLEAR MAGNETIC RESONANCE  
STUDIES OF THE  
TETRAKIS(TRI-PARA-TOLYL PHOSPHITE)NICKEL(0)  
HYDRIDE SYSTEM.

BY

Karen Ann Moffat B.Sc.

A THESIS

Submitted to the School of Graduate Studies  
in Partial Fulfilment of the Requirements  
For The Degree  
MASTER OF SCIENCE

McMaster University

(March, 1984)

MASTER OF SCIENCE (1984)  
(Chemistry)

McMaster University  
Hamilton, Ontario

TITLE: Synthesis and Nuclear Magnetic Resonance Studies of  
the Tetrakis(Tri-para-tolyl phosphite)Nickel(0)  
Hydride System.

AUTHOR: Karen Ann Moffat, B.Sc. (McMaster University)

SUPERVISOR: Professors D.R. Eaton, M.J. McGlinchey.

NUMBER OF PAGES: 114

## ABSTRACT

This thesis is primarily concerned with an investigation of the reaction of tetrakis(tri-p-tolyl phosphite)nickel(0) with strong acids, using  $^1\text{H}$ ,  $^{31}\text{P}$  and  $^2\text{H}$  NMR. The results differ from those previously obtained for similar reactions with other Ni(0) phosphites, in that both five and four-coordinate nickel hydrides are formed in concentrations sufficient for spectroscopic studies. The four-coordinated hydride is believed to be the catalytically active species in a number of reactions catalyzed by Ni(0) phosphites. Variable-temperature studies show that the four-coordinate hydride complex is a fluxional molecule. The exchange process is exclusively intramolecular in nature.

A very simple method was used to analyze the NMR data and obtain activation parameters for the exchange process. These parameters were compared with those reported in the literature for related intramolecular and intermolecular reactions. The large negative entropy of activation is interpreted in terms of ion pairing in the transition state. NMR evidence for the structure of the products resulting from the reactions of acids with both the metal complexes and the free phosphite ligands is presented. The conditions necessary for the observation of four-coordinated nickel hydrides are also discussed.

## ACKNOWLEDGEMENTS

A special thank you is extended to Drs. D.R. Eaton and M.J. McGlinchey for their guidance and enthusiastic support throughout the course of my research. Appreciation is also extended to Dr. D.P. Santry and Mr. R.J. Buist for their invaluable contributions to this work. The excellent typing skills of Ms. L. Palmer are greatly appreciated. A special thanks is directed to Joanne Weegar for proof reading this thesis. Finally, I am grateful for the support of my family, and all the people at McMaster who have made my stay a very enjoyable one.

## TABLE OF CONTENTS

	<u>PAGE</u>
Descriptive Note	ii
Abstract	iii
Acknowledgements	iv
CHAPTER 1: Literature Survey of Transition Metal Hydrides	
1.1 Introduction	1
1.1.1 The Metal-Hydrogen Bond	2
1.1.2 The Trans Effect of Hydride Ligands	3
1.1.3 NMR Studies of the M-H Bond	4
1.1.4 Electronic and Steric Effects	7
1.1.5 General Preparative Methods for Metal Hydrides	8
1.1.6 Protonation of Metal Complexes	9
1.2 The Role of Transition Metal Hydrides in Homogeneous Catalysis	10
1.3 The Stereochemical Nature of the Hydride Ligand	15
1.3.1 Nonrigidity of Transition Metal Hydrides	16
i) Z=4 Complexes	17
ii) Z=5 Complexes	17
1.4 Nickel Hydrides	20
1.4.1 $\text{HML}_3$ and $\text{HML}_3\text{CN}$ Complexes	20
1.4.2 $\text{HNiXL}_2$ Complexes	22
1.4.3 $\text{HNiL}_4^+$ Complexes	23
1.4.4 $\text{HNiXL}_3$ , $\text{H}_2\text{NiL}_3$ and Other Nickel Complexes	24
1.5 Objectives of This Research	25

	<u>PAGE</u>
CHAPTER 2: Experimental Details	27
2.1 Synthesis of Metal Complexes	27
2.2 NMR Instruments	29
CHAPTER 3: Reactions of $\text{Ni}[\text{P}(\text{O}-\text{p}-\text{C}_6\text{H}_4\text{CH}_3)_3]_4$ with Strong Acids	31
3.1 Other Complexes Similar to $\text{Ni}[\text{P}(\text{O}-\text{p}-\text{C}_6\text{H}_4\text{CH}_3)_3]_4$	31
3.2 Reaction of Strong Acids with $\text{NiL}_4$ System	47
3.3 Identification of the $^1\text{H}$ and $^{31}\text{P}$ NMR Spectra of the $\text{HNiL}_4^+$ and $\text{HNiL}_3^+$ Compounds of Tri-p-tolyl Phosphite	49
CHAPTER 4: Discussion of Variable-Temperature and Spin- Saturation Experiments	79
4.1 Spin-Saturation Transfer	79
4.2 The Intramolecular Exchange Process in $\text{HNiL}_3^+$	84
4.3 The Temperature Dependence of $\text{HNiL}_3^+$	89
4.4 Enthalpy and Entropy of Activation for the $\text{HNiL}_3^+$ System	94
4.5 Proposals for Future Research	108
REFERENCES	109



LIST OF TABLES

	<u>PAGE</u>	
Table 1.1	Spectroscopic data for $[\text{PtHL}_3]^+\text{X}^-$ complexes	21
Table 3.1	$^1\text{H}$ NMR hydride data of $\text{HNi}[\text{P}(\text{OR})_3]_4^+\text{X}^-$ , $\text{HCo}[\text{P}(\text{OR})_3]_4$ , $\text{H}_2\text{Fe}[\text{P}(\text{OR})_3]_4$ referenced to TMS	43
Table 3.2	$^{31}\text{P}$ NMR low field data for $\text{HNi}[\text{P}(\text{OR})_3]_4^+\text{X}^-$ , $\text{Ni}[\text{P}(\text{OR})_3]_4$ , $\text{HCo}[\text{P}(\text{OR})_3]_4$ referenced to 85% $\text{H}_3\text{PO}_4$	45
Table 4.1	Temperature and rate data for activation energy parameters	100
Table 4.2	Activation parameters for metal complex reactions	104

## LIST OF FIGURES

	<u>PAGE</u>
Figure 1.1	13
Synthesis of hexadienes using the $\text{HNiL}_4^+$ system as the catalyst	
Figure 1.2	15
Trigonal bipyramid with equatorial ligands displaced toward the H atom	
Figure 1.3	18
Schematic representation of the Berry mechanism with a square pyramidal transition state	
Figure 3.1	33
$^{31}\text{P}$ NMR spectrum of $\text{HNi}[\text{P}(\text{OCH}_2\text{CH}_3)_3]_4^+\text{HSO}_4^-$ in $\text{CD}_2\text{Cl}_2$ at 253°K	
Figure 3.2	35
Observed and calculated 220 MHz $^1\text{H}$ hydride NMR spectra of $\text{H}_2\text{Fe}[\text{P}(\text{OCH}_2\text{CH}_3)_3]_4$ as a function of temperature	
Figure 3.3	36
$^1\text{H}$ NMR spectrum of $\text{HNi}[\text{P}(\text{OC}_6\text{H}_5)_3]_4^+\text{HSO}_4^-$ of both low and high field regions	
Figure 3.4	39
$^{31}\text{P}$ NMR spectrum (101.26 MHz) low field of $\text{HNi}[\text{P}(\text{OC}_6\text{H}_5)_3]_4^+\text{HSO}_4^-$ in $\text{CD}_2\text{Cl}_2$ at 253°K	
Figure 3.5	41
$^1\text{H}$ NMR spectrum of the hydride resonance of $\text{HCo}[\text{P}(\text{O}-p\text{-C}_6\text{H}_4\text{CH}_3)_3]_4$ at 294°K	
Figure 3.6	50
The $^1\text{H}$ NMR spectrum of $\text{P}(\text{O}-p\text{-C}_6\text{H}_4\text{CH}_3)_3$	
Figure 3.7	52
$^1\text{H}$ NMR spectra of $\text{P}(\text{O}-p\text{-tolyl})_3 + \text{H}_2\text{SO}_4$ at 273°K and 233°K	
Figure 3.8	54
$^1\text{H}$ NMR spectra of $\text{HNiL}_4^+$ , $\text{HNiL}_3^+$ downfield from TMS at 268°K and 193°K	

LIST OF FIGURES (CONT..)

	<u>PAGE</u>	
Figure 3.9	$^1\text{H}$ NMR spectrum of $\text{HNi}[\text{P}(\text{O-p-tolyl})_3]_4^+$ and $\text{HNi}[\text{P}(\text{O-p-tolyl})_3]_3^+$ upfield from TMS at 253°K	56
Figure 3.10	$^{31}\text{P}$ NMR spectrum of $\text{P}(\text{O-p-C}_6\text{H}_4\text{CH}_3)_3$ at 213°K	57
Figure 3.11	$^{31}\text{P}$ NMR spectra of $\text{P}(\text{O-p-C}_6\text{H}_4\text{CH}_3)_3$ and $\text{H}_2\text{SO}_4$ at 253°K using 1:0.6 and 1:6 mole ratio of L: $\text{H}_2\text{SO}_4$	59
Figure 3.12	$^{31}\text{P}$ NMR spectra of $\text{P}(\text{O-p-C}_6\text{H}_4\text{CH}_3)_3$ reacting with $\text{H}_2\text{O}$ at room temperature	62
Figure 3.13	$^{31}\text{P}$ NMR spectrum of $\text{Ni}[\text{P}(\text{O-p-C}_6\text{H}_4\text{CH}_3)_3]_4$ at 253°K	63
Figure 3.14	$^{31}\text{P}$ NMR spectra of $\text{HNiL}_4^+$ , $\text{HNiL}_3^+$ coupled and decoupled at 253°K and 233°K downfield from 85% $\text{H}_3\text{PO}_4$	65
Figure 3.15	$^{31}\text{P}$ NMR spectrum downfield from 85% $\text{H}_3\text{PO}_4$ of $\text{HNiL}_4^+$ and $\text{HNiL}_3^+$ at 253°K where $\text{HNiL}_4^+$ is the dominant species	67
Figure 3.16	$^{31}\text{P}$ NMR spectra at 253°K of $\text{HNi}[\text{P}(\text{O-p-C}_6\text{H}_4\text{CH}_3)_3]_4^+$ and $\text{HNi}[\text{P}(\text{O-p-C}_6\text{H}_4\text{CH}_3)_3]_3^+$ with excess free phosphite downfield from 85% $\text{H}_3\text{PO}_4$	68
Figure 3.17	$^{31}\text{P}$ NMR spectra at 253°K of the high field region of $\text{HNiL}_4^+$ , $\text{HNiL}_3^+$ system	69
Figure 3.18	$^{31}\text{P}$ NMR spectra of $\text{Ni}[\text{P}(\text{O-p-tolyl})_3]_4$ , free ligand and various concentrations of $\text{H}_2\text{SO}_4$ upfield from 85% $\text{H}_3\text{PO}_4$	71

## LIST OF FIGURES (CONT..)

	<u>PAGE</u>	
Figure 3.19	$^{31}\text{P}$ NMR spectrum of $\text{HP}(\text{O})(\text{O-p-tolyl})_2$ and $^2\text{HP}(\text{O})(\text{O-p-tolyl})_2$ in $\text{CD}_2\text{Cl}_2$ at $253^\circ\text{K}$	74
Figure 3.20	The $^2\text{H}$ NMR spectra downfield from TMS of the $\text{DNiL}_4^+$ , $\text{DNiL}_3^+$ system at $263^\circ\text{K}$ and $283^\circ\text{K}$	75
Figure 3.21	The $^2\text{H}$ NMR spectra of the hydride region of $\text{DNiL}_4^+$ and $\text{DNiL}_3^+$ at $263^\circ\text{K}$ and $273^\circ\text{K}$	76
Figure 3.22	The $^2\text{H}$ NMR spectrum of the hydride complex $\text{DNiL}_4^+$ at $253^\circ\text{K}$	78
Figure 4.1	Spin-saturation experiments of the hydride resonance of $\text{HNi}[\text{P}(\text{O-p-C}_6\text{H}_4\text{CH}_3)_3]_3^+$ at $253^\circ\text{K}$ in $\text{CD}_2\text{Cl}_2$	82
Figure 4.2	The $^1\text{H}$ NMR variable-temperature spectra of the hydride resonance of $\text{HNi}[\text{P}(\text{O-p-C}_6\text{H}_4\text{CH}_3)_3]_3^+$	91
Figure 4.3	$^2\text{H}$ NMR spectrum of $^2\text{HNiL}_3^+$ at $288^\circ\text{K}$	92
Figure 4.4	The $^1\text{H}$ simulated and experimental spectra of the hydride resonance of $\text{HNi}[\text{P}(\text{O-p-C}_6\text{H}_4\text{CH}_3)_3]_3^+$	95
Figure 4.5	The $^{31}\text{P}$ simulated and observed spectra of $\text{HNi}[\text{P}(\text{O-p-C}_6\text{H}_4\text{CH}_3)_3]_3^+$	97
Figure 4.6	The plot of $\log k_r$ versus $1/T$	99
Figure 4.7	The plot of $\log(k_r/T)$ versus $1/T$	102

## CHAPTER ONE

### Literature Survey of Transition Metal Hydrides

#### 1.1 Introduction

Transition metal hydrides (1) contain one or more hydrogen atoms bonded directly to a transition metal ion by an essentially covalent two-electron bond (2). The interest in metal hydrides is due largely to the wide variety of chemical reactions they undergo. Thus, they participate in catalytic reactions such as hydroformylation, olefin isomerization, and hydrogen exchange.

The first paper written on transition metal hydrides appeared in 1939 but the subject was not extensively pursued until 1955. In 1960, the first X-ray diffraction study was published and in 1964 a neutron diffraction study appeared. Ewens and Lister reported molecular structures for gaseous  $\text{CoH}(\text{CO})_4$  and  $\text{FeH}_2(\text{CO})_4$  determined by electron diffraction (3). From this they concluded that the transition metal was surrounded by carbonyl ligands in a tetrahedral array, with the hydrogen atom showing no stereochemical influence. It was suggested that the hydrogen was attached to an oxygen of a carbonyl group. Hieber (4a) proposed that the hydrogen atom was buried in the metal orbitals. This would account for the chemical evidence for hydrogen atoms attached to the metal. NMR studies showed a hydride chemical shift of  $-12.8$  ppm (4b,4c) for  $\text{ReH}(\pi\text{-C}_5\text{-H}_5)_2$  which was evidence for a metal hydrogen bond (4d). This "buried" hydrogen concept

was used to explain the large shifts to high field observed in the  $^1\text{H}$  NMR of  $\text{CoH}(\text{CO})_4$  (5).

The first X-ray diffraction study on transition metal hydrides was performed on  $\text{PtHBr}[\text{P}(\text{C}_2\text{H}_5)_3]_2$ . The Br and phosphorus atoms occupy three corners of a quadrilateral around Pt and the hydrogen atom, which was not located, but was assured to occupy the fourth position(6). The complex  $\text{OsHBr}(\text{CO})[\text{P}(\text{C}_6\text{H}_5)_3]_3$  similarly shows that the hydrogen atom occupies this sixth position (vertex) in a distorted octahedron around Os (7). The X-ray diffraction study of  $\text{RhH}(\text{CO})[\text{P}(\text{C}_6\text{H}_5)_3]_3$  located the H atom and gave a bond length of  $1.72(15) \text{ \AA}$ (8). From the information obtained from X-ray diffraction, it was concluded that the hydrogen atom does exert some stereochemical influence and is not buried in the metal orbitals. This was supported by a neutron diffraction investigation of  $\text{K}_2\text{ReH}_9$  (9).

### 1.1.1 The Metal-Hydrogen Bond

A characteristic of metal hydrides is the appearance of chemical shifts to high field of TMS. These high field proton resonances were considered to be consistent with a hydride proton "buried" in the metal electron cloud. However, as noted above, later X-ray structural analysis showed that the hydride ligand occupies a specific site in the coordination sphere of the metal ion. The model, therefore, changed to one with geometrically well behaved ligands with short M-H bond lengths (M-H distance was less than the sum of the covalent radii). The short-

bond observed was believed to explain the high field  $^1\text{H}$  chemical shift by through-space electrostatic interactions and also to explain the strong trans-directing ability of the hydride ligand. It was later discovered that the bond lengths were longer and that the hydride ligand was well behaved in bond length as well as geometry. Neutron diffraction was used to determine the Mn-H distance in  $\text{HMn}(\text{CO})_5$  by LaPlace et al. (10). This procedure produced a reliable and meaningful value for a M-H bond length of  $1.601 \text{ \AA}$ . This established that a terminally bonded hydride distance from the metal is a normal covalent distance.

#### 1.1.2 The Trans-Effect of Hydride Ligands

The trans-effect and trans-influence are structural characteristics of transition metal hydrides. The hydrogen bonded to a metal is a good trans directing ligand in substitution reactions of metal complexes. This effect arises from destabilization of the ground state in a complex or stabilization of the transition state or both. Subsequently, Pidcock, Richards, and Venanzi (11) introduced a term called trans-influence which is defined as the weakening of the bond by a trans ligand in the ground state of a complex. The inductive effect of hydrogen gives rise to a large component of the s-character in  $\sigma$  bonds and thus weakens the  $\sigma$  bonds of all other ligands but especially the ligand in the trans position because of the use of common orbitals. The electron density on the metal is increased due to the ligand in the trans position to the hydride donating the s electron density along the  $\sigma$  bond. Ligands

that are better  $\pi$  acceptors are preferred to be trans to hydrogen than those which are better  $\sigma$  donors due to competition of these for metal  $\sigma$ -bonding orbitals with hydrogen. Ligands trans to hydrogen are more labile than ligands cis to hydrogen. Also, M-L bonds trans to hydrogen can be slightly longer than bonds cis to hydrogen.

### 1.1.3 NMR Studies of M-H Bonds

All transition metal hydrides show a high field proton resonance which generally occurs in the range of -10 to -20 ppm but can be as high as -35 ppm. The only other resonance found in this region are resonances from paramagnetic complexes which are broader than resonances due to protons of diamagnetic complexes. Metal hydrides show the largest high field shift for first-row transition metals. The second and third row metals produce shifts that are approximately 25% less than first row transition metals. An exception is the larger  $^1\text{H}$  chemical shift value for the diamagnetic complex  $\text{IrHCl}_2(\text{PBu}_2^t\text{Me})_2$  of -50.5 ppm reported by Masters et al. (12).

The spin-spin coupling of metal hydrides to other nuclei such as  $^{31}\text{P}$  provides strong evidence for direct metal-hydrogen bonds. Phosphorus ligands trans to hydrogen show coupling constants in the range of 80 to 160 Hz and phosphorus ligands cis to hydrogen are in the range of 10 to 40 Hz.



Direct evidence for metal hydrogen bonds is provided by the coupling of the hydride to metals such as  $^{103}\text{Rh}$ ,  $^{195}\text{Pt}$ ,  $^{183}\text{W}$  and  $^{187}\text{Os}$  with non-zero nuclear spins. The factors affecting the metal-hydrogen coupling constants ( $J_{\text{M-H}}$ ) are electronic effects and the magnetogyric ratios of the nuclei concerned. Since the magnetogyric ratios are known for different nuclei, this factor can be eliminated. Pople and Santry suggested a reduced coupling constant  $K_{\text{AB}}$  (13) where;

$$K_{\text{AB}} = \frac{2\pi}{\pi\gamma_{\text{A}}\gamma_{\text{B}}} J_{\text{AB}} \quad [1.1]$$

The reduced coupling constant  $K_{\text{AB}}$  is a measure of the electronic environment on the nuclear spin-spin coupling. The dominant factor in determining the magnitude of  $J_{\text{H-M}}$  as shown by Pople and Santry, is the Fermi contact interaction (13). Electronic factors depend on s-electron densities at the two nuclei, the degree of s-character in the metal hydrogen bond and on the mean excitation energy as determined by perturbation theory.

The s electron density at a nucleus depends on the effective nuclear charge; thus the large coupling of platinum to hydrogen has been ascribed (84) to a high effective nuclear charge and generally, reduced coupling constants for 5d hydrides are larger than for 4d complexes. The coupling constant also increases with increasing s electron character in the metal hydrogen bond.

The effect of changing the electronegativity of other ligands is twofold for complexes such as  $\text{Pt}[\text{P}(\text{C}_2\text{H}_5)_3]_2\text{HX}$ . Increasing the electronegativity of X would increase the effective nuclear charge on platinum and, therefore, increase  $K_{\text{M-H}}$ . For halide complexes  $J_{\text{M-H}}$  would decrease according to the series  $\text{Cl} > \text{Br} > \text{I}$ . Electron density is withdrawn from the metal to the halide due to the polar nature of the Pt-X bond, therefore, s-electron density at the metal (Pt) is reduced with increasing electronegativity of the halide. This observation predicts  $K_{\text{M-H}}$  for the halide of  $\text{I} > \text{Br} > \text{Cl}$ . But the presence of a more electronegative ligand trans to the M-H bond would be expected to increase the s-character of the bond, which predicts  $K_{\text{M-H}}$ ,  $\text{Cl} > \text{Br} > \text{I}$ . Therefore, changes in electronegativity have several opposing effects and thus, the size of the effects are very important (2).

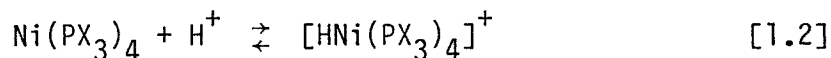
There are two theories which account for the magnitude of chemical shifts to high field for transition metal hydrides. Both theories involve shielding by the nonbonding electrons of the metal. The difference in the theories lies in dealing with electrons in orbitals corresponding to an excited state of the metal atom. Stevens et al. (14) ignored this contribution and evaluated the chemical shift (in terms of diamagnetic shielding ( $\sigma_d$ ) of protons) from calculated electron densities in metal orbitals confined to metals of the first row transition series e.g.,  $\text{HCo}(\text{CO})_4$ . When the M-H distances are taken as normal, i.e., the sum of covalent radii, the results indicate the correct order of the shifts.

The other theory proposed by Buckingham and Stephens (15) shows that contributions from excited states are significant for complexes in which the metal atom has partially filled d orbitals. These contributions are responsible for temperature independent paramagnetism and this leads to the introduction of the paramagnetic shielding term ( $\sigma_p$ ). This paramagnetic shielding term is important in the second and third row transition metals. The average shielding ( $\sigma = \sigma_d + \sigma_p$ ) of protons is very sensitive to anisotropy in metal atoms, so neglecting distortions from regular symmetry can lead to errors in the calculation of shielding constants.

#### 1.1.4 Electronic and Steric Effects

The effectiveness of metal complexes as catalysts depends largely on the interaction of the surrounding ligands with the central metal atom. An example is the trans-effect or trans-influence where the interactions between ligands occur by two mechanisms:

- 1) electronic effects transmitted by metal-ligand bonds and
- 2) steric effects which are due to interligand repulsion in sterically crowded complexes. Electronic effects are shown in the reaction of protonic acids with  $\text{Ni}(\text{PX}_3)_4$  (16).



Trialkylphosphines are primarily  $\sigma$ -donor ligands which transfer considerable electron density to the metal atom, nickel which therefore becomes a strong base. Weak acids have been used to protonate  $\text{Ni}[\text{P}(\text{C}_2\text{H}_5)_3]_4$ . Strong

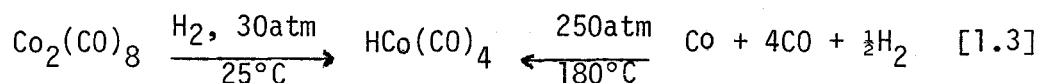
electron acceptors such as  $\text{PF}_3$  and  $\text{CO}$  produce nickel complexes  $\text{Ni}(\text{PF}_3)_4$  which have significant basicity but not very much electron density is transferred to the nickel atom. Trialkyl and triaryl phosphite complexes are protonated by various reasonably strong mineral acids which is consistent with an intermediate electron density on the metal.

Steric effects are measured by the cone angle of the ligand which determines the bulk or size of the ligand (77). The cone angle is a measure of the space that a ligand occupies in the coordination sphere of the metal. For example, the ligand trimethyl phosphite has a cone angle of  $107^\circ$ . When coordinated to nickel to give  $\text{Ni}[\text{P}(\text{OCH}_3)_3]_4$  a tetrahedral geometry is observed and it is not distorted because  $\text{P}(\text{OCH}_3)_3$  fits in nicely. On the other hand tri-*o*-tolyl phosphite has a cone angle of  $141^\circ$ , so when it is coordinated to nickel to give  $\text{NiL}_4$  the geometry is distorted due to the size of the ligand. The complex is distorted so much that  $\text{NiL}_3$  is formed by ligand dissociation at room temperature (77).

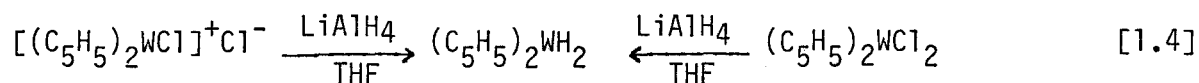
### 1.1.5 General Preparative Methods for Metal Hydrides

Green and Jones (2) organized the methods of synthesis of transition metal hydrides into five categories;

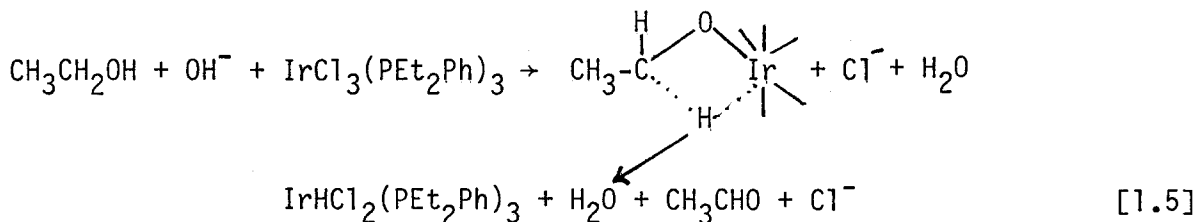
1) direct hydrogenation



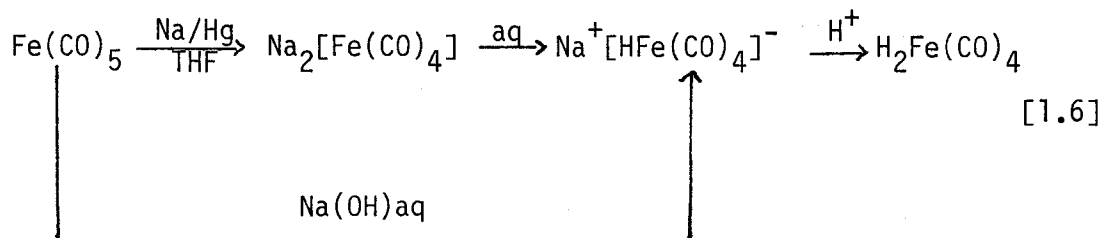
2) reduction of metal halide complexes



## 3) hydride-transfer and reverse carbonylation reactions

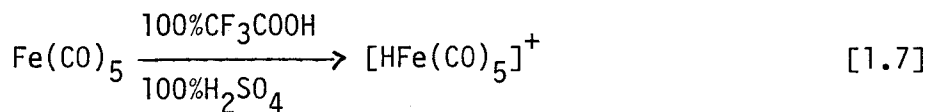


## 4) hydrolysis of alkali metal salts of complex carbonyls



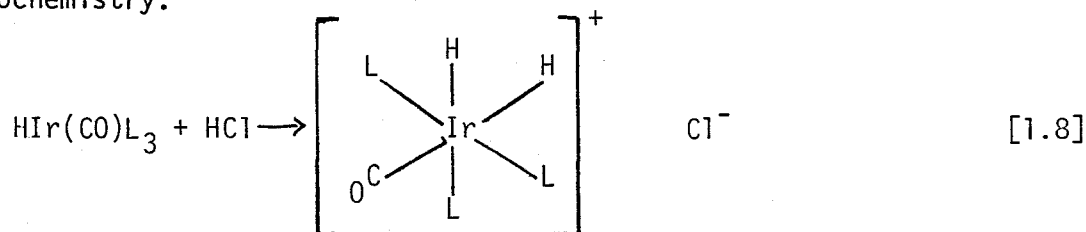
## 5) protonation

Neutral species are protonated to form cationic hydride complexes. Weaker bases require strong acids such as concentrated  $\text{H}_2\text{SO}_4$  or trifluoroacetic acid  $\text{CF}_3\text{COOH}$ .

1.1.6 Protonation of Metal Complexes

Donor properties of transition metals usually appear in complexes in which all the low-lying orbitals are filled through interactions with various donor ligands. If a transition metal complex has fewer than 18 electrons in bonding and/or nonbonding orbitals, then treatment with acid

usually leads to oxidative addition except for derivatives of  $\text{HPtL}_2^+\text{A}^-$  which are ionic. Kotz and Pedrotty (17) reported that triphenylphosphonium (tricarbonylchromium, -molybdenum, or-tungsten) cyclopentadienylides dissolve in  $\text{CF}_3\text{COOH}$  to give highly coloured solutions and NMR spectra showing a high field resonance at -5 to -8 ppm corresponding to metal protonation  $[\text{HM}(\text{cplid})(\text{CO})_3]^+$ . Drinkard et al. (18) reported protonation of  $\text{Ni}[\text{P}(\text{OC}_2\text{H}_5)_3]_4$  and Schunn (19) was able to isolate protonated derivatives from addition of strong nonaqueous acids to solution of  $\text{Ni}(\text{diphos})_2$ . Vaska (20) reported the protonation of 18 electron complexes such as  $\text{HIr}(\text{CO})\text{L}_3$  where  $\text{L}=\text{PPh}_3$  giving dihydride cations with the following stereochemistry.



Knight and Mays (21) dissolved  $\text{Ir}_4(\text{CO})_{12}$  in concentrated  $\text{H}_2\text{SO}_4$  and observed a high field singlet at -18.4 ppm in the  $^1\text{H}$  NMR spectrum which was due to the dicationic species  $\text{H}_2\text{Ir}_4(\text{CO})_{12}^{2+}$ . The protons are equivalent due to a rapid scrambling mechanism which exchanges the protons on the  $\text{C}_2$  axes of the tetrahedral array of the carbonyl ligands.

## 1.2 Role of Transition Metal Hydrides in Homogeneous Catalysis

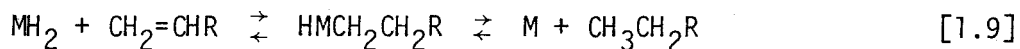
Transition metal hydrides play important roles in many homogenous catalytic reactions, particularly those involving olefins. Examples of such catalytic reactions are hydrogenation, isomerization, hydroformyla-

tion, polymerization, deuteration and hydrosilation. Transition metal hydride complexes that are coordinately saturated and unable to interact with unsaturated substrates until one of the ligands of the complex dissociates to give a free coordination site. A coordinately saturated complex has 18 electrons and a coordinately unsaturated complex usually has 16 metal valence electrons for many compounds of catalytic interests.

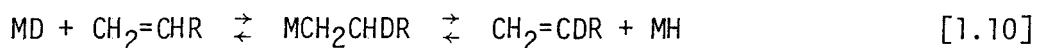
Formation of transition metal hydrides by protonation can have a dramatic effect on the properties of the original ligands. An increase in the CO stretching frequencies of approximately  $150\text{cm}^{-1}$  is a result of protonation of transition metal carbonyl complexes. Protonation weakens the M-CO bond and also makes the other ligands more labile. The rate constant for dissociation of  $\text{L}=\text{P}(\text{OC}_2\text{H}_5)_3$  from  $\text{NiL}_4$  is increased on protonation of the complex from  $4.9 \times 10^{-6} \text{sec}^{-1}$  (benzene,  $35.9^\circ\text{C}$ ) (22) to  $1.5 \times 10^{-2} \text{sec}^{-1}$  ( $\text{CH}_3\text{OH}$ ,  $25^\circ\text{C}$ ) (23). The reaction of  $\text{HNiL}_4^+$  with 1,3-butadiene was shown to involve ligand dissociation from a coordinatively saturated complex as the first step of the reaction (23). The rate of reaction was independent of butadiene concentration in the absence of added ligand.

Transition metal hydrides in homogeneous catalysis are able to add to unsaturated substrates to form catalytic intermediates containing metal-carbon bonds. One reaction is the addition to olefins to form alkyls.

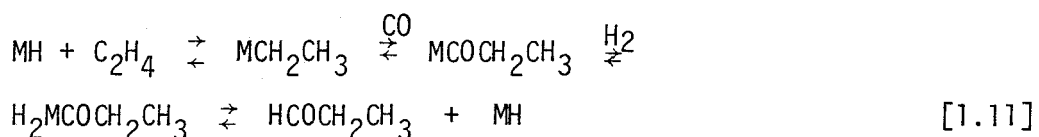
Alkyl formation can occur by hydrogenation as shown by the following sequence;



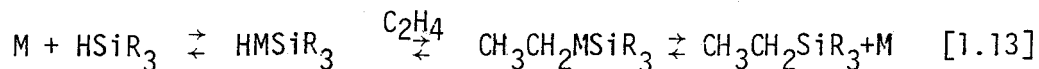
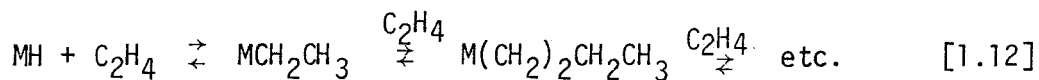
or by polymerization, isomerization, hydroformylation, deuterium exchange, and hydrosilation of olefins. An example of hydrogen-deuterium exchange is given by an Anti-Markovnikov addition.



Hydroformylation of ethylene can occur by the sequence shown in the following reaction



The next two reactions are examples of polymerization and hydrosilation of ethylene respectively.



Another area of addition is to conjugated dienes to form  $\sigma$  and  $\pi$ -allyls. The following example is of the reaction of dienes with olefins to form 1,4-hexadienes. The best illustration of the synthesis of hexadienes was studied using  $Ni[P(OC_2H_5)_3]_4$  (abbreviated to  $NiL_4$ ) and  $H_2SO_4$



in  $\text{CH}_3\text{OH}$  which lead to a 20-step mechanism reaction. Figure 1.1 (23)

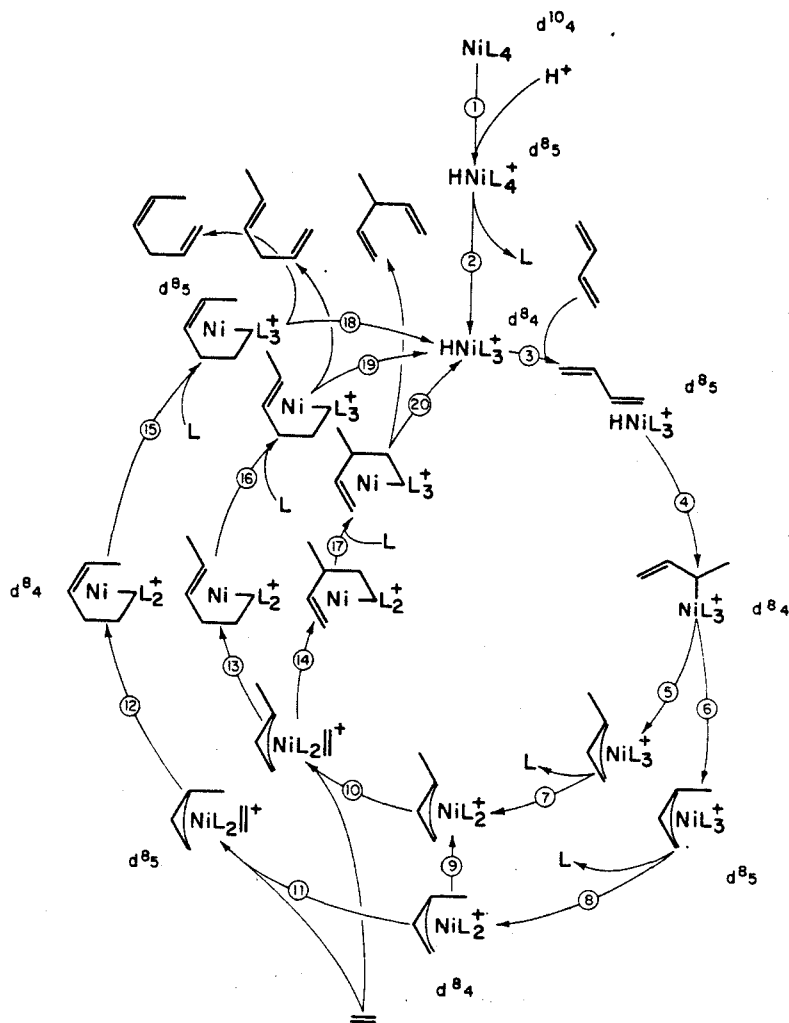


Figure 1.1 Synthesis of Hexadienes using the  $\text{HNiL}_4^+$  system as the catalyst.

The essential features of the mechanism include

- a) "reversible and rapid protonation of  $\text{NiL}_4$  to give a five-coordinate (18 electron) hydride  $\text{HNiL}_4^+$  (step 1),

- b) reversible dissociation of ligand  $L=P(OC_2H_5)_3$  to give a reactive coordinately unsaturated (16 electron) hydride  $HNiL_3^+$  (step 2),
- c) rapid reaction of  $HNiL_3^+$  with butadiene to give  $\pi-C_4H_7NiL_3^+$  with anti-isomer kinetically preferred (step 3 to 6),
- d) rapid and reversible dissociation of L to give  $\pi-C_4H_7NiL_2^+$  species (steps 7 and 8) and isomerization of anti to a more stable syn isomer (step 9),
- e) reaction with ethylene to give  $[\pi-C_4H_7NiL_2(C_2H_4)]^+$  complexes (steps 10 and 11), and
- f) subsequent ethylene insertion followed by  $\beta$ -hydrogen abstraction to give the observed products and regenerate  $HNiL_3^+$  (1).

The hydride  $HNi[P(OC_2H_5)_3]_4^+$  (18) was characterized by  $^1H$  and  $^{31}P$  NMR spectra. The complex is an unstable yellow oil when isolated as the bisulfate salt (24). The hydride formation is very rapid and occurs with a rate constant of  $k_1=1550m^{-1}sec^{-1}$  for  $HClO_4$  in  $CH_3OH$  at  $25^\circ C$ . The polymerization of butadiene by protonic acids and Ni(0) complexes such as  $Ni[P(OC_6H_5)_3]_4$  or  $Ni[1,5-cyclooctadiene]$  (25) probably also proceeds by  $\pi$ -alkyl complexes formed by the reaction of nickel hydrides with the dienes. Nickel hydrides have also been involved in the addition to alkynes to form metal vinyl complexes.

### 1.3 The Stereochemical Nature of the Hydride Ligand

The stereochemically active hydride ligand occupies a coordination site but exerts little or no influence on the geometry of the complex. In  $\text{RhH}[\text{P}(\text{C}_6\text{H}_5)_3]_4$  the phosphorus atoms form a regular tetrahedron around Rh (26). In just about all crystal structures of transition metal hydride complexes, the ligands adjacent to the hydride ligand are displaced towards hydrogen. This degree of distortion varies according to the coordination number. The distortion is evident in four- and six-coordinate complexes but it is more difficult to assess in five-coordinate complexes. The structure of most five-coordinate species are trigonal bipyramidal with the hydrogen in the axial or equatorial position. Figure 1.2

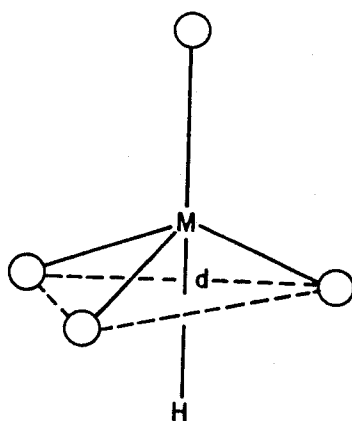


Figure 1.2 Trigonal bipyramid with equatorial ligands displaced toward the H atom. The distance of the metal from the plane of the equatorial ligands is defined by  $d$  (1).

The three equatorial ligands define a plane, and the distance that the central metal atom lies from the plane is a measure of distortion. To account

for the distortion, you must look at steric effects of the bulky ligands such as  $P(C_6H_5)_3$ . The bulkier the ligand, the greater the distortion. Shorter metal-ligand bond distances trans to the hydride ligand create a greater molecular distortion. Short M-L distances are indicative of multiple bonding, which is due to electron pair repulsion between M-L bonds and M-P bonds. Therefore, the molecular geometry of transition metal hydride complexes is a function of the number and size of ligands, the degree of distortion increasing with bulkiness of ligands, and the amount of multiple bonding present in the bond trans to the hydride ligand.

### 1.3.1 Nonrigidity of Transition Metal Hydrides

Stereochemically non-rigid molecules are those molecules in which permutation of nuclear positions (stereoisomerism) takes place at an "appreciable" rate by an intramolecular process (27). A hydride is defined or regarded as stereochemically non-rigid if isomerization occurs at a rate sufficiently rapid to produce effects on line shapes in the NMR spectrum of hydrides, while at the same time spin correlation is maintained between coupled nuclei in the fast exchange limit. It is necessary to have other nuclei in the molecule possessing spins to which the hydride protons are coupled in order to establish spin correlation. Intermolecular exchange processes are manifested by the loss of spin-spin coupling.

Many transition metal hydrides contain phosphorus ligands which show  $J_{H-P}$  couplings that are easily resolved. Depending on the coordination number and on steric and electronic factors, the barriers to rearrangement can vary. Five-coordinate systems and complexes with a coordination number

greater than six generally have low barriers. The majority of four- and six-coordinate hydrides are more rigid. Many hydrides of the form  $\text{HML}_4$  show a quintet when the ligands contain phosphorus and this could indicate that the molecule has square pyramidal structure. Structure determination by X-ray crystallography shows that all five-coordinate solid hydrides studied so far have  $C_{3v}$  symmetry, and low temperature NMR experiments show this in solution (28). Therefore, the apparent equivalence of the four phosphorus ligands in solution is attributable to a low barrier to intramolecular rearrangement instead of magnetic equivalence in the equilibrium configuration.

i) Z=4 Complexes

In many four-coordinate transition metal complexes fast polytopal rearrangements are observed (29). Before 1971 there were no four-coordinate hydrides known to be non-rigid. The best characterized four-coordinate compounds are of Pt which appear to be planar and rigid as demonstrated by separate couplings for phosphorus in the cis and trans positions with respect to hydrogen. This thesis will later illustrate the presence of a non-rigid four-coordinate nickel phosphite.

ii) Z=5 Complexes

In five-coordinate chemistry non-rigidity is a common feature (30,31). A mechanism for isomerization in these systems was proposed by Berry (32). The mechanism is depicted as follows

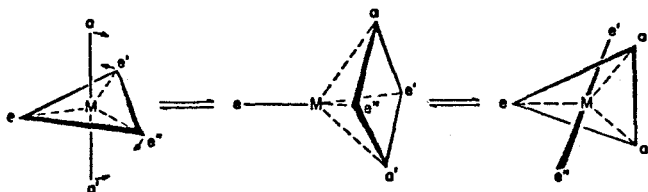


Figure 1.3 Schematic representation of the Berry mechanism with a square-pyramidal transition state. In one rearrangement the two axial nuclei exchange positions with two of the equatorial nuclei (33).

in Figure 1.3 (33). The process exchanges pairs of axial ligands for a pair of equatorial ligands in a trigonal bipyramid while passing through a square pyramidal form. In a five-coordinate system, the two idealized limiting geometries are trigonal bipyramidal and square pyramidal but in monohydrides, distortion of bipyramidal forms may be so large that the ligands are in a near tetrahedral array. This is largely a steric effect which is observed in solids by X-ray diffraction.

There are many examples of hydride complexes that are either fluxional or rapidly exchanging hydrides intramolecularly. Meakin et al. (34) have observed similar NMR properties for  $\text{H}_2\text{Fe}[\text{P}(\text{OC}_2\text{H}_5)_3]_4$  and established that room temperature equivalence of hydrido or phosphite ligands is due to stereochemical non-rigidity. The temperature-dependent hydride spectra are invariant to concentration changes or addition of free phosphite. The chemical shift for the hydride resonance occurs at  $-13.86$  ppm at  $30^\circ\text{C}$

for  $\text{H}_2\text{Fe}[\text{P}(\text{OC}_2\text{H}_5)_3]_4$ . Tebbe et al. (35) showed that for this Fe hydride, bimolecular or solvent-assisted hydride exchange is not observed. The stereochemical non-rigidity shown by NMR line-shape analysis of  $\text{H}_2\text{Fe}[\text{P}(\text{OC}_2\text{H}_5)_3]_4$  is probably due to the movement of the hydrogen nucleus from one  $\text{C}_3$  axis in the tetrahedron skeleton of four  $\text{P}(\text{OC}_2\text{H}_5)_3$  ligands across the edge of the tetrahedron to another  $\text{C}_3$  axis. A distorted tetrahedron is another possibility where one mechanism is the consequence of mixing of nonbonding Fe orbital electron density with the Fe-H bond. The second mechanism involved the mixing of Fe-H molecular orbitals with the orbital bonding scheme for tetrahedral coordinated phosphite ligands.

The process of hydrogen exchange across the edge of a tetrahedron for  $\text{H}_4\text{M}_4(\text{CO})_{12}$  was suggested by Knox and Kaesz (36). Titus et al. (37) stated that phosphite ligands in  $\text{HCo}[\text{P}(\text{OC}_2\text{H}_5)_3]_4$  are arranged in an approximate trigonal bipyramidal configuration with H<sup>+</sup> along the  $\text{C}_3$  axis. Dewhirst et al. (38) suggested that, if stereochemical non-rigidity in monohydrides is due to the exchange of hydrogen ligands (inter-or-intramolecular) then all hydride line-widths in NMR spectra should broaden with increase in temperature. If the ligand is exchanging then only some of the hydride lines will broaden with an increase in temperature (assuming only one ligand exchanges at a time). Other experimental techniques used to establish the stereochemistry of transition metal hydrides are IR spectra, Raman spectra, Mössbauer spectra, mass spectrometry, electron paramagnetic resonance spectra, dipole moments, and incoherent inelastic neutron spectra which are discussed in reference (1).

## 1.4 Nickel Hydrides

Nickel hydrides and the other members of this triad (Ni, Pd, Pt) are more stable than the Co triad complexes but the nickel forms the least stable hydrides in that group. Bond (39) observed that the heat of adsorption of  $H_2$  is approximately 10 kcal/mol greater for the Ni triad than for the Co triad. An increase in M-H bond energy is responsible for the ability of  $Ni^0$ ,  $Pd^0$  and  $Pt^0$  to undergo a two electron oxidative-addition as well as a one electron oxidative-addition which is found for  $Co^0$ ,  $Rh^0$  and  $Ir^0$ . Reversible addition of  $H_2$  to  $Ni^0$  was reported by Gasser et al. (40). The thermal stability order of the Ni triad hydrides ( $Pt > Pd > Ni$ ) pointed out by Green et al. (41, 42) follows the energy separation between the lowest unoccupied molecular orbital (LUMO) and the highest occupied molecular orbital (HOMO). The stability of nickel hydrides are a result of bulky ligands which prevent geometric deformation.

### 1.4.1 HML<sub>3</sub> and HML<sub>3</sub>CN Complexes

There are a variety of cationic platinum 16-electron complexes known (43-49). Some are listed in Table 1.1 along with infrared and NMR data (1) but no nickel compounds of similar structure had been reported up to 1971. The structure of the  $HPtL_3^+$  compounds were determined by  $^1H$  and  $^{31}P$  NMR data. A new class of five-coordinate nickel hydrides  $HNiL_3CN$  were formed by the addition of HCN to phosphorus complexes of  $NiL_4$  nickel (0) which were characterized by  $^1H$  and  $^{31}P$  NMR in solution. Also, some  $HNiL_2CN$  complexes were observed when the ligand was bulky enough to create a large steric effect (50).



Table I.1: Spectroscopic Data for [PtHL<sub>3</sub>]<sup>+</sup>X<sup>-</sup> Complexes

Compound	$\nu_{\text{MH}}$	$\delta$	$J_{\text{Pt-H}}$	$J_{\text{PHcis}}$	$J_{\text{PH trans}}$	Ref.
trans- PtH[P(C <sub>2</sub> H <sub>5</sub> ) <sub>3</sub> ] <sub>2</sub> (C <sub>5</sub> H <sub>5</sub> N) <sup>+</sup> C <sub>10</sub> <sub>4</sub> <sup>-</sup>	2216	-19.32	1106	14.4		44
trans- PtH[P(C <sub>2</sub> H <sub>5</sub> ) <sub>3</sub> ] <sub>2</sub> (CO) <sup>+</sup> C <sub>10</sub> <sub>4</sub> <sup>-</sup>	2167	- 4.76	967	13.5		44
trans- PtH[P(C <sub>2</sub> H <sub>5</sub> ) <sub>3</sub> ] <sub>2</sub> [(CH <sub>3</sub> ) <sub>3</sub> CNC] <sup>+</sup> C <sub>10</sub> <sub>4</sub> <sup>-</sup>	2104	- 7.13	895	14.4		44
trans- PtH[P(C <sub>2</sub> H <sub>5</sub> ) <sub>3</sub> ] <sub>2</sub> (p-CH <sub>3</sub> OC <sub>6</sub> H <sub>4</sub> NC) <sup>+</sup> C <sub>10</sub> <sub>4</sub> <sup>-</sup>	2096	- 6.56	890	14.0		44
trans- PtH[P(C <sub>2</sub> H <sub>5</sub> ) <sub>3</sub> ] <sub>2</sub> [P(OC <sub>6</sub> H <sub>5</sub> ) <sub>3</sub> ] <sup>+</sup> C <sub>10</sub> <sub>4</sub> <sup>-</sup>	2090	- 5.21	872	14.4	289	44
trans- PtH[P(C <sub>2</sub> H <sub>5</sub> ) <sub>3</sub> ] <sub>2</sub> [P(OCH <sub>3</sub> ) <sub>3</sub> ] <sup>+</sup> C <sub>10</sub> <sub>4</sub> <sup>-</sup>	2067	- 4.54	846	15.2	268	44
trans- PtH[P(C <sub>2</sub> H <sub>5</sub> ) <sub>3</sub> ] <sub>2</sub> [P(C <sub>6</sub> H <sub>5</sub> ) <sub>3</sub> ] <sup>+</sup> C <sub>10</sub> <sub>4</sub> <sup>-</sup>	2100	- 6.51	890	14.4	165	44
trans- PtH[P(C <sub>2</sub> H <sub>5</sub> ) <sub>3</sub> ] <sub>3</sub> <sup>+</sup> C <sub>10</sub> <sub>4</sub> <sup>-</sup>	2090	- 6.24	790	15.0	156	44
trans- PtH[P(C <sub>2</sub> H <sub>5</sub> ) <sub>3</sub> ] <sub>2</sub> (C <sub>2</sub> H <sub>4</sub> ) <sup>+</sup> [B(C <sub>6</sub> H <sub>5</sub> ) <sub>4</sub> ] <sup>-</sup>		- 7.2	908	12.0		49
trans- PtH[P(C <sub>6</sub> H <sub>5</sub> ) <sub>3</sub> ] <sub>3</sub> <sup>+</sup> [B(C <sub>6</sub> H <sub>5</sub> ) <sub>4</sub> ] <sup>-</sup>	2110	- 5.9	788	15.0	157	47

### 1.4.2 HNiXL<sub>2</sub> Complexes

Ni, Pd and Pt produce 16-electron M(II) compounds of the form HMXL<sub>2</sub> where nickel and palladium complexes are less stable than the platinum complexes. The first well-characterized nickel complex was NiHCl[P(C<sub>6</sub>H<sub>11</sub>)<sub>3</sub>]<sub>2</sub> (51) which showed a triplet hydride resonance in the NMR spectrum and this indicated that the complex had a trans structure. Later the trans-[(C<sub>6</sub>H<sub>11</sub>)<sub>3</sub>P]<sub>2</sub>NiHX complex was investigated using other anions such as SCN<sup>-</sup> and CN<sup>-</sup> (41). Since Green's initial report, a series of nickel hydrides have been discovered, (52) such as HNiCH<sub>3</sub>[P(C<sub>6</sub>H<sub>11</sub>)<sub>3</sub>]<sub>2</sub>, HNiCpP(C<sub>6</sub>H<sub>11</sub>)<sub>3</sub> and HNi[P(C<sub>6</sub>H<sub>11</sub>)<sub>3</sub>]<sub>2</sub> (OAc).

The crystal structure of NiHCl[P(i-C<sub>3</sub>H<sub>7</sub>)<sub>3</sub>]<sub>2</sub> was studied by X-ray diffraction (53). Later π-allyl hydridonickel complexes were discovered (54). These NiH(π-C<sub>3</sub>H<sub>5</sub>)L complexes gave NMR spectra for the allylic protons in which the syn protons have a separate chemical shift. This supports a planar type structure. In NiH(BH<sub>4</sub>)[P(i-C<sub>3</sub>H<sub>7</sub>)<sub>3</sub>]<sub>2</sub> the hydride proton is coupled to two equivalent phosphorus nuclei and four equivalent protons from the BH<sub>4</sub><sup>-</sup> ligand (J<sub>HH</sub>=6Hz) (55).

Other nickel complexes of this type are formed from dichlorobis-(tricyclohexylphosphine) nickel and NaBH<sub>4</sub> which is reduced upon exposure to air to HNiCl[P(C<sub>6</sub>H<sub>11</sub>)<sub>3</sub>]<sub>2</sub>. This complex rapidly decomposes in solution and somewhat more slowly in the solid state. The stability is due to the bulkiness of the cycloalkylphosphine ligands. The trans configuration is assigned based on the high field triplet at -24.6 ppm and J<sub>P-H</sub> = 73.5 Hz. Also a series of cationic hydride complexes of nickel

$[\text{NiH}(\text{L})(\text{Pcy}_3)_2]^+\text{BPh}_4^-$  ( $\text{Pcy}_3$  = tricyclohexylphosphine, L = pyridines, pyrazole, imidazole) were synthesized and characterized by  $^1\text{H}$  NMR (56).

#### 1.4.3. $\text{HNiL}_4^+$ Complexes

A series of five-coordinate nickel phosphine and phosphite hydrides (18 electron systems) have been generated by protonation of zerovalent nickel complexes  $\text{NiL}_4$  in strong acids. The five-coordinate cationic complex  $\text{HNi}[(\text{C}_6\text{H}_5)_2\text{PCH}_2\text{CH}_2\text{P}(\text{C}_6\text{H}_5)_2]^+$  was isolated as an orange salt with various anions to give a  $J_{\text{PH}} = 6\text{Hz}$  and the chemical shift of the hydride resonance was at  $-13.0$  ppm (19). The salts decompose slowly in air.  $\text{HNi}[\text{P}(\text{OC}_2\text{H}_5)_3]_4^+$  with a coupling constant of  $26\text{Hz}$  was prepared by Drinkard et al. (18). The phosphite cation was isolated as an air sensitive yellow oil from a chilled ( $-50^\circ\text{C}$ ) diethyl ether solution to which  $\text{H}_2\text{SO}_4$  was added.  $^1\text{H}$  and  $^{31}\text{P}$  spectra led to a square-pyramidal geometry with the hydrogen at the apex. Protonation preceded ligand dissociation although there was also evidence for a species  $\text{HNi}[\text{P}(\text{OC}_2\text{H}_5)_3]_3^+$  which could not be characterized (24).

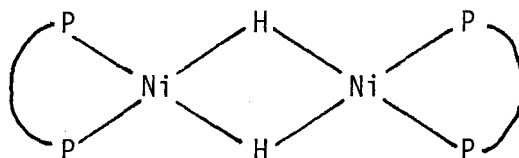
Protonation of a tetrakis(bicyclic phosphite)nickel(0) derivative with  $\text{HCl}$ ,  $\text{HBF}_4$  or  $\text{HPF}_6$  led to the isolation of solid hydrido-nickel phosphite complexes of the type  $\text{HNi}(\text{bicyclic phosphite})_4^+ \text{X}^-$  ( $\text{X} = \text{HCl}_2^-, \text{BF}_4^-, \text{PF}_6^-$ ). These complexes are cream powders which are stable at room temperature under vacuum and were identified by analysis and IR spectrometry. The complexes were not soluble in common solvents therefore no NMR work was done (57). Meakin et al. (58) investigated, by NMR, the rate of ligand association in a series of four-coordinate group

VIIIA complexes ( $\text{HML}_3^+$ ) relative to the rate of intramolecular rearrangement with the five-coordinate intermediate or transition state ( $\text{HML}_4^+$ ) where the metals are ( $\text{M}=\text{Ni}(\text{II}), \text{Pd}(\text{II}), \text{Pt}(\text{II}), \text{L} = \text{P}(\text{C}_2\text{H}_5)_3$ ). Also, preparation and reaction of nickel hydride salts such as  $\text{HNiL}_4^+\text{B}(\text{C}_6\text{H}_5)_4^-$  ( $\text{L} = \text{P}(\text{CH}_3)_3$  and  $\text{P}(\text{CH}_3)_2(\text{C}_6\text{H}_5)$ ) were prepared from bis(1,5-cyclooctadiene) nickel (0), free ligand and  $\text{NaB}(\text{C}_6\text{H}_5)_4$  in ethanol (59). Further work was done on the  $\text{HNi}[\text{P}(\text{OC}_2\text{H}_5)_3]_4^+\text{X}^-$  system by Tolman (23, 24, 60, 61). A wide range of similar cationic nickel hydride complexes of the type  $\text{HNiL}_4^+$  were formed by protonation with  $\text{H}_2\text{SO}_4$  in  $\text{CH}_3\text{OH}$ . The ligands used are  $\text{P}(\text{O}-p\text{-C}_6\text{H}_4\text{OCH}_3)_3$ ,  $\text{P}(\text{O}-p\text{-tolyl})_3$ ,  $\text{P}(\text{OCH}_3)_3$ ,  $\text{P}(\text{OCH}_2\text{CH}_2\text{Cl})_3$ ,  $\text{PPh}(\text{OC}_2\text{H}_5)_2$  and  $\text{P}(\text{CH}_3)_3$  and the complexes were characterized by  $^1\text{H}$  NMR (62).

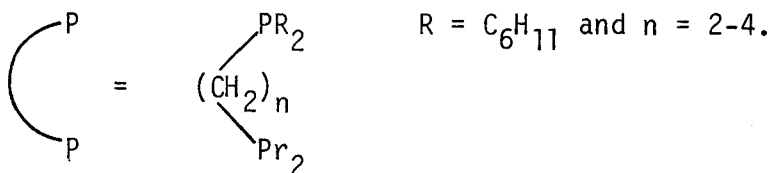
#### 1.4.4 $\text{HNiXL}_3$ , $\text{H}_2\text{NiL}_3$ and Other Nickel Complexes

The only example of a nickel hydride in the  $\text{HNiXL}_3$  or  $\text{H}_2\text{NiL}_3$  category is  $\text{NiH}(\pi\text{-C}_5\text{H}_5)[\text{P}(\text{C}_6\text{H}_{11})_3]_3$  (52). The complex  $\text{PtH}_2[\text{P}(\text{C}_6\text{H}_5)_3]_3$  has been reported but not characterized in detail (63).

A well defined series of diamagnetic bridged nickel hydrides have been prepared with the following configuration (64)



where



The NMR data for two of the species are as follows:

	$\delta$ (ppm)	$J_{\text{PH}}$ (Hz)
$n = 2$	-11.4	23.5 (quintet)
$n = 4$	-10.4	15.0 (quintet)

There are two equivalent protons and four equivalent phosphorus ligands. Complexes with triangular metal cluster hydrides have been reported such as  $\text{Ni}_3\text{H}_2(\text{CO})_8$  but have not been characterized in detail (65). Another such nickel cluster is  $[\text{Ni}_4(\text{CO})_9\text{H}]^-$  which is a dark red salt (66).

### 1.5 Objectives of Present Research

Stereochemical non-rigidity of nickel phosphine hydrides have been studied in some detail by Meakin et al. (33, 67, 68). There has been no corresponding study of phosphite hydrides. Tolman has reported detailed studies on the chemistry of  $\text{HNi}[\text{P}(\text{OC}_2\text{H}_5)_3]_4^+$  (23,24,60 61) particularly as it pertains to catalytic reactions. In this case, dissociation to a four-coordinated hydride occurs only to a very small extent ( $K$  estimated to be  $< 4 \times 10^{-5}\text{M}$ ) and this compound could not be detected spectroscopically but was postulated to be the key intermediate in the catalytic reactions. NMR studies on the series of Ni(0) phosphite hydrides have been cursory and reported only in two brief notes in Inorganic Chemistry (18,62). The objectives of the present project were, therefore:

- 1) to extend NMR studies of nickel phosphite hydrides by examining their formation with a variety of acids and phosphite ligands,
- 2) to obtain, if possible, spectroscopic evidence for the four-coordinated hydrides postulated as catalytic intermediates, and
- 3) to investigate the fluxional behaviour of both the four and five-coordinated hydride compounds and to compare the rates of isomerization with those of previously studied phosphine complexes.

## CHAPTER TWO

### Experimental Details

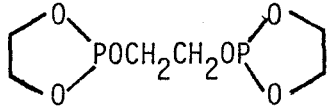
#### 2.1 Synthesis

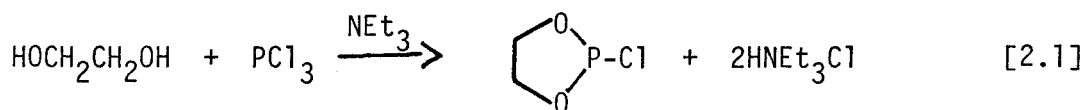
$\text{Ni}[\text{P}(\text{O}-\text{p}-\text{C}_6\text{H}_4\text{CH}_3)_3]_4$  was prepared according to the procedure for tetrakis(triphenyl phosphite)nickel(0) reported by Levison and Robinson (69). Under a nitrogen atmosphere in a dry box, the four and five-coordinate nickel hydride compounds  $\text{HNi}[\text{P}(\text{O}-\text{p}-\text{C}_6\text{H}_4\text{CH}_3)_3]_3^+\text{HSO}_4^-$  and  $\text{HNi}[\text{P}(\text{O}-\text{p}-\text{C}_6\text{H}_4\text{CH}_3)_3]_4^+\text{HSO}_4^-$  were formed. Into a 30ml beaker, which was placed in dry ice ( $-40^\circ\text{C}$ ), was added 0.1-0.2g of solid white  $\text{Ni}[\text{P}(\text{O}-\text{p}-\text{C}_6\text{H}_4\text{CH}_3)_3]_4$ . To this was added concentrated  $\text{H}_2\text{SO}_4$  using a syringe, followed by 3-4g of  $\text{CD}_2\text{Cl}_2$  and free phosphite when required. Then the beaker was removed from the dry ice and warmed slowly to combine all the reagents. When the solid  $\text{NiL}_4$  had dissolved and the solution was an orange-red colour, the beaker was placed back in the dry ice to make sure the solvent did not evaporate. Immediately following, the top organic layer was transferred into NMR tubes which were finally stored in dry ice in a dewar in the freezer. The lower layer which was oily dark red remained in the beaker and was not analyzed. It was probably excess acid and a small amount of decomposed nickel hydride which forms upon the initial reaction of the strong acid with the nickel complex. The samples could not be stored for longer than 24 hours without total decomposition occurring even at  $-40^\circ\text{C}$ . To favour the four-coordinate hydride, an excess of concentrated  $\text{H}_2\text{SO}_4$

(~1 ml) was required and no free phosphite was added. For the five-coordinate hydride to be the dominant species, an excess of free phosphite (0.25-0.5 ml) was required along with 1 ml of concentrated  $\text{H}_2\text{SO}_4$ . Therefore, depending on whether the four or five-coordinate species is the desired product, the quantities of reagents required for synthesis will vary. For the deuterated nickel phosphite complexes,  $\text{D}_2\text{SO}_4$  replaced  $\text{H}_2\text{SO}_4$  and the sample preparation previously stated above was followed.

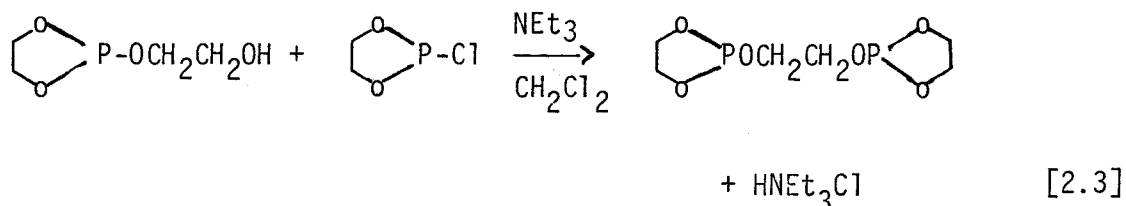
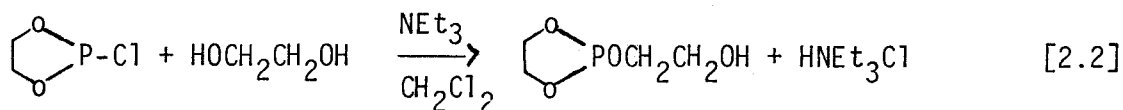
The preparation of the four-coordinate nickel hydride was attempted by another route in which the tetraphenyl boron salt was formed  $\text{HNi}[\text{P}(\text{O}-p\text{-C}_6\text{H}_4\text{CH}_3)_3]_3^+\text{B}(\text{C}_6\text{H}_5)_4^-$ . This method was reported by Schunn (59) and was originally used to prepare  $\text{HNi}[\text{P}(\text{C}_2\text{H}_5)_3]_3^+\text{B}(\text{C}_6\text{H}_5)_4^-$  from  $\text{Ni}[\text{P}(\text{C}_2\text{H}_5)_3]_4$ . It was adapted by changing the phosphine to a phosphite ligand. The final product was a red oil that was fairly stable in ethanol but could not be isolated for analysis, therefore, the preparation of  $\text{HNi}[\text{P}(\text{O}-p\text{-C}_6\text{H}_4\text{CH}_3)_3]_3^+$  was carried out by the protonation route.

The following complexes were prepared by the method reported by Levison and Robinson (70),  $\text{HCo}[\text{P}(\text{OC}_6\text{H}_5)_3]_4$ ,  $\text{HCo}[\text{P}(\text{OCH}_2\text{CH}_3)_3]_4$ ,  $\text{HCo}[\text{P}(\text{O}-p\text{-C}_6\text{H}_4\text{CH}_3)_3]_4$ ,  $\text{Ni}[\text{P}(\text{OC}_6\text{H}_5)_3]_4$ ,  $\text{Ni}[\text{P}(\text{OC}_2\text{H}_5)_3]_4$  and  $\text{Ni}[\text{P}(\text{OCH}(\text{CH}_3)_2)_3]_4$ .

The formation of  was prepared according to the following reactions (71-73):







$\text{H}_2\text{Fe}[\text{P}(\text{OCH}_2\text{CH}_3)_3]_4$  was prepared according to the method given by Gerlach et al.(74). The synthesis of the hydride nickel compounds was the same as that used to form  $\text{HNi}[\text{P}(\text{O-p-C}_6\text{H}_4\text{CH}_3)_3]_4^+$ . The only difference is that  $\text{CF}_3\text{COOH}$  was substituted for  $\text{H}_2\text{SO}_4$  in some cases. The phosphite ligands used were obtained from BDH and Kodak chemicals and were used without further purification.

## 2.2 NMR Instruments

The  $^1\text{H}$  and  $^{31}\text{P}$  NMR spectra were recorded on Bruker WM-250 and WP-400 spectrometers. The proton resonances at 250MHz and 400MHz were measured relative to an internal standard of tetramethylsilane ( $\delta=0$  ppm) in  $\text{CD}_2\text{Cl}_2$  or toluene- $d_8$  solvent. The solvent was used to provide a lock signal. The phosphorus signals resonating at 101.26MHz and 161.98 MHz, respectively, were referenced to an external sample of 85%  $\text{H}_3\text{PO}_4$  ( $\delta=0$ ppm). A mixture of  $\text{CD}_2\text{Cl}_2$  and  $\text{CH}_2\text{Cl}_2$  ( $\delta=5.32$ ppm) was used as an internal standard for the deuterium NMR spectra, this resonates at 38.39MHz on the Bruker WM250 spectrometer.

Variable temperature control was provided by a Bruker variable-temperature unit B-VT 1000 with an error of  $\pm 3^\circ\text{K}$ . In a few cases  $^1\text{H}$  spectra were obtained on a Varian CW EM-390MHz spectrometer or a Bruker WP 80MHz spectrometer.

## CHAPTER THREE

### REACTIONS OF Ni[P(O-p-C<sub>6</sub>H<sub>4</sub>CH<sub>3</sub>)<sub>3</sub>]<sub>4</sub> WITH STRONG ACIDS

#### 3.1 Other Complexes Similar to Ni[P(O-p-C<sub>6</sub>H<sub>4</sub>CH<sub>3</sub>)<sub>3</sub>]<sub>4</sub>

Initially the objective of this research project was to investigate the preparation and characterization of various zero-valent metal phosphite hydrides. They are prepared by reaction of Ni(0) phosphites with strong acids and characterized by NMR techniques. Many of the nickel hydrides examined by <sup>1</sup>H and <sup>31</sup>P NMR experiments produced only limited information due to chemical instability. These limitations include temperature instability, decomposition in air and a rapid intramolecular exchange process. Analogous cobalt (I) (69, 75, 76) and iron (II) (34, 74) hydrides which are more stable than the nickel hydrides, were also prepared. Again the data obtained from these compounds are limited and are presented in the following section.

The <sup>31</sup>P NMR spectrum of P(OCH<sub>2</sub>CH<sub>3</sub>)<sub>3</sub> was obtained in a deuterated chloroform solvent. It shows a septet at 138.38 ppm at 293°K which shifts to 137.97 ppm upon lowering the temperature to 253°K. The three-bond coupling constant between proton and phosphorus was 8 Hz. The literature chemical shift for the <sup>31</sup>P resonance of P(OCH<sub>2</sub>CH<sub>3</sub>)<sub>3</sub> is 137.8 ppm reported by Tolman (77). The phosphorus resonance of the Ni[P(OCH<sub>2</sub>CH<sub>3</sub>)<sub>3</sub>]<sub>4</sub> complex in toluene at 273°K appeared as a singlet at 159.50 ppm shifting to 160.19 ppm when the temperature was lowered to 213°K. The reported chemical shift value for the nickel compound of triethyl phosphite is given as 158.4 ppm by Tolman (77). Drinkard et al. (18) also reported a value of 159 ppm for

the chemical shift of  $\text{Ni}[\text{P}(\text{OCH}_2\text{CH}_3)_3]_4$ . Thus, the NMR spectra we obtain for these compounds agree well with literature reports.

The  $\text{Ni}[\text{P}(\text{OCH}_2\text{CH}_3)_3]_4$  complex was acidified with  $\text{CF}_3\text{COOH}$  in toluene- $d_8$  to form the nickel hydride  $\text{HNi}[\text{P}(\text{OCH}_2\text{CH}_3)_3]_4^+\text{CF}_3\text{COO}^-$ . The  $^1\text{H}$  spectrum consisted of a high field quintet centered at -15 ppm with a coupling constant of  $^2J_{\text{H-P}} = 27$  Hz. Drinkard et al. (18) reported a quintet at -14.4 ppm with  $^2J_{\text{H-P}} = 27$  Hz for  $\text{HNi}[\text{P}(\text{OCH}_2\text{CH}_3)_3]_4^+\text{CF}_3\text{COO}^-$  in benzene- $d_6$ . The low field region from TMS showed a triplet at 1.2 ppm with a three-bond proton-proton coupling constant of 6 Hz, assigned to the methyl resonance. The  $-\text{CH}_2-$  resonance which appeared at 4 ppm was a broad singlet, not a quartet as was expected. As the temperature was lowered the hydride resonance broadened and began to collapse. The lowest temperature at which a proton spectrum was obtained was 218°K. At temperatures lower than this the solvent (toluene- $d_8$ ) begins to freeze and therefore, the low temperature limiting spectrum was not resolved. If the geometry of  $\text{HNi}[\text{P}(\text{OCH}_2\text{CH}_3)_3]_4^+$  is trigonal bipyramidal with the proton in an equatorial position, then the theoretical low temperature limiting spectrum would consist of a triplet of triplets.

The  $^{31}\text{P}$  NMR spectrum of  $\text{HNi}[\text{P}(\text{OCH}_2\text{CH}_3)_3]_4^+\text{HSO}_4^-$  was obtained using deuterated methylene chloride as the solvent. The low field region showed a doublet centered at 131.1 ppm with a  $^2J_{\text{H-P}} = 25$  Hz. The doublet is a result of four equivalent phosphorus atoms coupled to one proton which is illustrated in Figure 3.1. This is consistent with the hydride resonance in the  $^1\text{H}$  NMR spectrum and confirms that the nickel hydride is a five-coordinate complex undergoing a fast intramolecular exchange of  $^{31}\text{P}$  atoms.

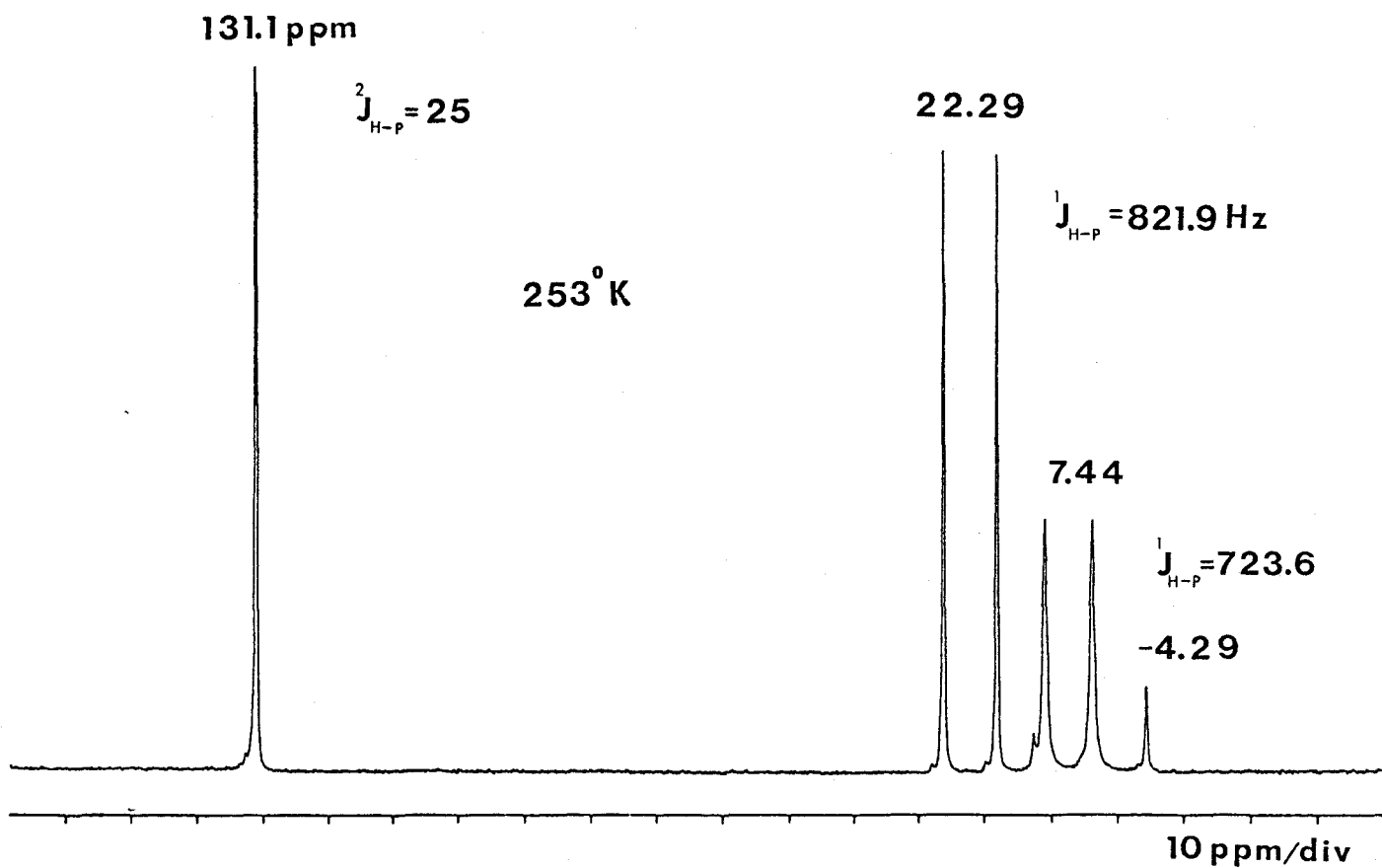


Figure 3.1:  $^{31}\text{P}$  NMR Spectrum of  $\text{HNi}[\text{P}(\text{OCH}_2\text{CH}_3)_3]_4^+\text{HSO}_4^-$  in  $\text{CD}_2\text{Cl}_2$  at  $253^\circ\text{K}$  (101.26 MHz)

The high field region consists of two sets of doublets and a singlet also shown in Figure 3.1. The singlet occurring at -4.29 ppm is characteristic of  $\text{O}=\text{P}(\text{OCH}_2\text{CH}_3)_3$  which is compared to a similar phosphite ligand that was reported by Dillon et al. (80). The doublet centered at 7.44 ppm with  $^1J_{\text{H-P}} = 723.6$  Hz, according to Tolman (24) corresponds to  $\text{H}(\text{O})\text{P}(\text{OCH}_2\text{CH}_3)_2$ . Tolman reported the same doublet at -10 ppm with  $^1J_{\text{H-P}} = 710$  Hz which he assigned to  $\text{H}(\text{O})\text{P}(\text{OCH}_2\text{CH}_3)_2$ . The largest doublet centered at 22.29 ppm with a coupling constant of 821.9 Hz belongs to  $\text{H}-\overset{\oplus}{\text{P}}(\text{OCH}_2\text{CH}_3)_3$  which agrees with the results of the work done by Hudson et al. (81). Large coupling constants are characteristic of a proton directly bonded to a  $^{31}\text{P}$  atom.

Previous research done by Kruse and Atalla (76) on the analogous Co(I) complex  $\text{HCo}[\text{P}(\text{OCH}_2\text{CH}_3)_3]_4$  reported a  $^{31}\text{P}$  NMR spectrum consisting of a singlet at 168.3 ppm relative to 85%  $\text{H}_3\text{PO}_4$  which broadened due to the quadrupole moment of cobalt. The  $^1\text{H}$  NMR spectrum showed a high field proton hydride resonance which was a quintet centered at -15.8 ppm. Levison and Robinson (69) and Muetterties and Hirsekorn (78) have also investigated this system and report a singlet in the  $^{31}\text{P}$  NMR spectrum.

The iron six-coordinate dihydride  $\text{H}_2\text{Fe}[\text{P}(\text{OCH}_2\text{CH}_3)_3]_4$  was prepared and the NMR spectrum of the high field region was obtained. It consisted of an unresolved quintet at -14.3 ppm. The three central peaks were broader than the outer two lines. Meakin et al. (34, 35, 79) observed a high temperature spectrum consisting of a quintet centered at -13.86 ppm in the  $^1\text{H}$  NMR spectrum which undergoes an intramolecular exchange to give a low temperature limiting spectrum of a triplet of doublets which is illustrated

in Figure 3.2 (34). The  $^1\text{H}$  and  $^{31}\text{P}$  NMR spectrum establishes the stereo-

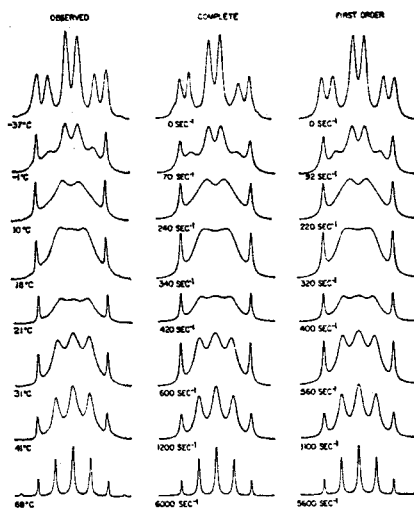


Figure 3.2: Observed and calculated 220 MHz  $^1\text{H}$  hydride NMR spectra of  $\text{H}_2\text{Fe}[\text{P}(\text{OCH}_2\text{CH}_3)_3]_4$  as a function of temperature.

chemical nonrigidity of the iron dihydride  $\text{H}_2\text{Fe}[\text{P}(\text{OCH}_2\text{CH}_3)_3]_4$  (34).

Similar compounds such as  $\text{Ni}[\text{P}(\text{OR})_3]_4$ ,  $\text{HNi}[\text{P}(\text{OR})_3]_4^+$  and  $\text{HCo}[\text{P}(\text{OR})_3]_4$  were prepared using a triphenyl phosphite ligand. The free ligand in the  $^{31}\text{P}$  NMR spectrum produced a singlet at 127.46 ppm at 293°K and 126.54 ppm at 253°K (literature 127.3 ppm (77)). The phosphorus spectrum of tetrakis-(triphenyl phosphite)nickel(0) consisted of a singlet at 130.15 ppm at 273°K which shifted downfield to 130.46 ppm at 213°K (literature 128.8 ppm (77)). The tetrakis nickel phosphite compound was protonated with  $\text{H}_2\text{SO}_4$  to form  $\text{HNi}[\text{P}(\text{OC}_6\text{H}_5)_3]_4^+\text{HSO}_4^-$  in  $\text{CD}_2\text{Cl}_2$ . The  $^1\text{H}$  NMR spectrum for this com-

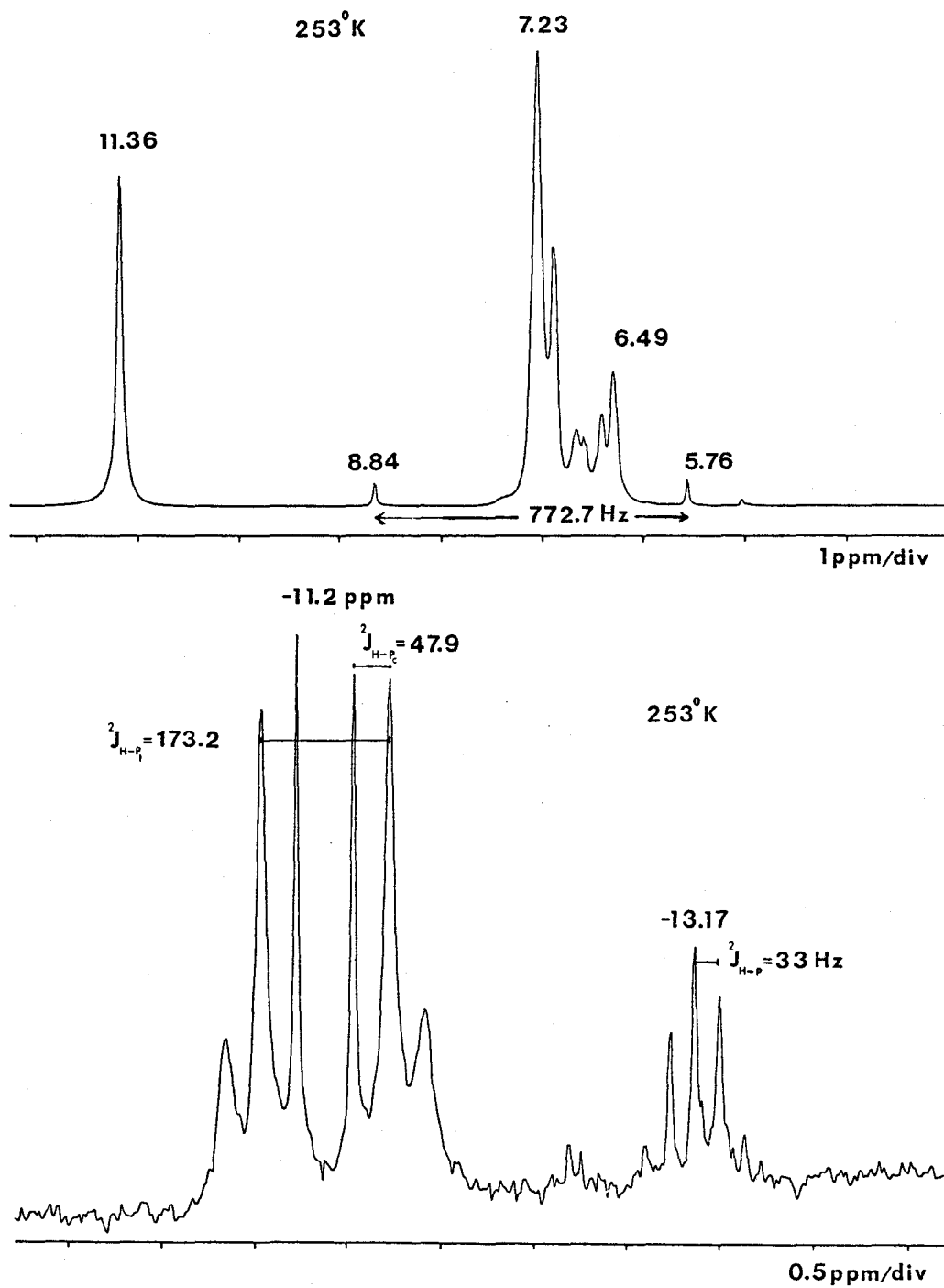


Figure 3.3:  $^1\text{H}$  NMR Spectrum of  $\text{HNi}[\text{P}(\text{OC}_6\text{H}_5)_3]_4^+\text{HSO}_4^-$  of both low and high field regions (250.13 MHz).



plex contained a complex multiplet at 7.2 ppm characteristic of the non-equivalent phenyl groups, a large doublet centered at 7.3 ppm with a  $^1J_{\text{H-P}} = 772.7$  Hz, a small singlet at 11.4 ppm due to the excess free acid  $\text{H}_2\text{SO}_4$ , and in the high field region a poorly resolved quintet centered at -13.2 ppm with a coupling constant of  $^2J_{\text{P-H}} = 33$  Hz and a doublet of triplets centered at -11.2 ppm. These resonances are illustrated in Figure 3.3.

The quintet is characteristic of the five-coordinate nickel hydride  $\text{HNi}[\text{P}(\text{OC}_6\text{H}_5)_3]_4^+$  and the doublet of triplets is due to a four-coordinate species such as  $\text{HNi}[\text{P}(\text{OC}_6\text{H}_5)_3]_3^+$  where the phosphorus atoms are no longer equivalent. The proton is coupled to one trans  $^{31}\text{P}$  atom which produces the doublet and then is further coupled to two cis  $^{31}\text{P}$  atoms which results in the formation of the triplets. The four-coordinate hydride involving the tri-p-tolyl phosphite ligand is discussed in greater detail later on in this chapter. The addition of the methyl in the para position to the phenyl ring increases the stability of the system, especially the four-coordinate hydride. This results in better resolved spectra which is the reason for this research focusing on the tri-p-tolyl phosphite ligand and not the nickel complex of triphenyl phosphite.

The phosphorus spectrum of  $\text{HNi}[\text{P}(\text{OC}_6\text{H}_5)_3]_4^+\text{CF}_3\text{COO}^-$  in toluene- $d_8$  consisted of three single resonances downfield from 85%  $\text{H}_3\text{PO}_4$  ( $\delta=0$  ppm). At 273°K, the singlet at 125.39 ppm was free phosphite, the resonance at 129.22 ppm was characteristic of  $\text{Ni}[\text{P}(\text{OC}_6\text{H}_5)_3]_4$  and the singlet at 141.97 ppm was attributed to impurities or a product of hydrolysis, but not the

hydride complex. In comparison with  $\text{HNi}[\text{P}(\text{O}-\text{p}-\text{C}_6\text{H}_4\text{CH}_3)_3]_4^+$ , the acidified nickel phosphite compound  $\text{HNi}[\text{P}(\text{OC}_6\text{H}_5)_3]_4^+$  should appear upfield from the free ligand resonance which places it in the 110-120 ppm range. This is not observed when the solvent used is toluene- $d_8$  and the protonating agent is  $\text{CF}_3\text{COOH}$ .

When the solvent was changed to  $\text{CD}_2\text{Cl}_2$  and the protonating agent was  $\text{H}_2\text{SO}_4$ ; forming the compound  $\text{HNi}[\text{P}(\text{OC}_6\text{H}_5)_3]_4^+\text{HSO}_4^-$ , resonances were found in the 110-120 ppm range in the phosphorus spectrum. A doublet centered at 113 ppm with a  $^2J_{\text{H-P}} = 34.2$  Hz was characteristic of the five-coordinate species  $\text{HNi}[\text{P}(\text{OC}_6\text{H}_5)_3]_4^+$ . The four phosphorus atoms are equivalent which couple to the hydride proton. A broad unresolved singlet centered at 114.93 ppm was assigned to the four-coordinate complex  $\text{HNi}[\text{P}(\text{OC}_6\text{H}_5)_3]_3^+$  where the  $\text{P}_{\text{trans}}$  and  $\text{P}_{\text{cis}}$  resonances have not been resolved as shown in Figure 3.4. When the ligand is changed to  $\text{P}(\text{O}-\text{p}-\text{C}_6\text{H}_4\text{CH}_3)_3$  the four-coordinate hydride shows well resolved resonances for  $\text{P}_{\text{trans}}$  and  $\text{P}_{\text{cis}}$  in the spectrum. This will be discussed in greater detail in Section 3.3.

The high field region of the  $^{31}\text{P}$  spectrum of  $\text{HNi}[\text{P}(\text{OC}_6\text{H}_5)_3]_4^+\text{CF}_3\text{COO}^-$  in toluene- $d_8$  consisted of a large doublet centered at 3.03 ppm with  $^1J_{\text{H-P}} = 758$  Hz and a singlet at -17.75 ppm. The singlet is characteristic of  $\text{O} = \text{P}(\text{OC}_6\text{H}_5)_3$  which is reported in the literature by Dillon et al. as a singlet resonating at -18.2 ppm (80). The large doublet is characteristic of a proton directly bonded to a phosphorus. Similar doublets have been observed in the  $^{31}\text{P}$  NMR spectrum of  $\text{HNi}[\text{P}(\text{O}-\text{p}-\text{C}_6\text{H}_4\text{CH}_3)_3]_4^+$  and  $\text{HNi}[\text{P}(\text{OCH}_2\text{CH}_3)_3]_4^+$

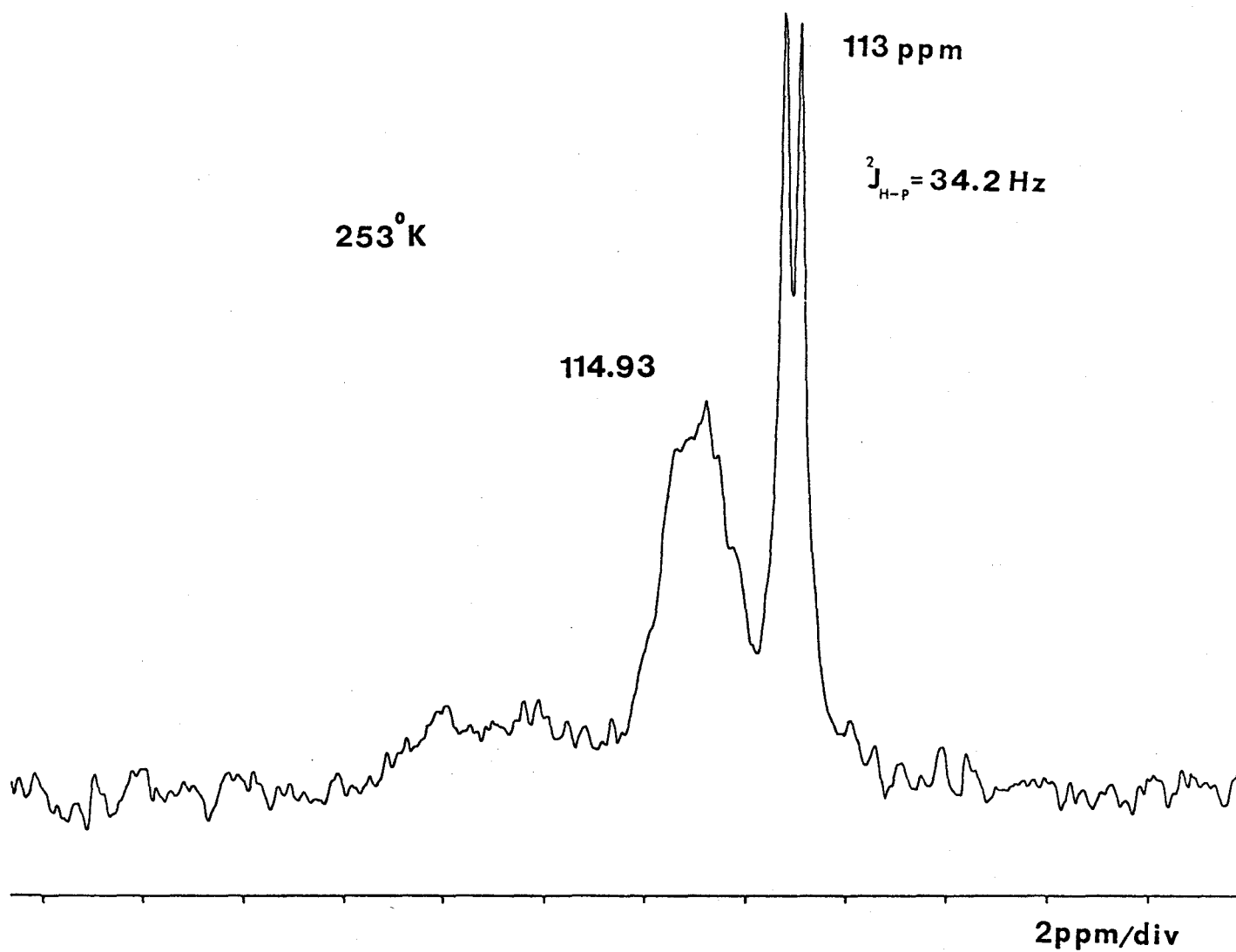
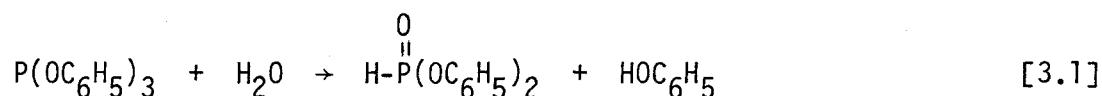


Figure 3.4:  $^{31}\text{P}$  NMR Spectrum (101.26 MHz) Low Field of  $\text{HNi}[\text{P}(\text{OC}_6\text{H}_5)_3]_4^+\text{HSO}_4^-$  in  $\text{CD}_2\text{Cl}_2$  at 253°K.

as noted previously. The doublet is assigned to  $\text{HP}(0)(\text{OC}_6\text{H}_5)_2$  which is a hydrolysis product of the reaction of the triphenyl phosphite with water present in the acid.



Other such doublets have been reported by Tolman (24) and Hudson (81).

The analogous cobalt hydride was also synthesized  $\text{HCo}[\text{P}(\text{OC}_6\text{H}_5)_3]_4$  and the  $^1\text{H}$  and  $^{31}\text{P}$  NMR spectra were observed. The proton spectrum consisted of a phenyl resonance at approximately 7.0 ppm and a high field triplet at -13.87 ppm which was actually an unresolved quintet at 273°K. The coupling constant was  $^2J_{\text{H-P}} = 15\text{-}17$  Hz. This is in agreement with the reported values of Levison and Robinson (69). The high field quintet was observed at -13.58 ppm with  $^2J_{\text{H-P}} = 17$  Hz for  $\text{HCo}[\text{P}(\text{OC}_6\text{H}_5)_3]_4$ . The  $^{31}\text{P}$  NMR spectrum consisted of a singlet at 142.52 ppm (literature is 141.2 ppm (69)). This singlet has broadened due to the interaction with the  $^{59}\text{Co}$  quadrupole moment and the doublet structure expected for coupling with the hydride proton is not resolved.

The similar cobalt hydride of tri-para-tolyl phosphite,  $\text{HCo}[\text{P}(\text{O-p-C}_6\text{H}_4\text{CH}_3)_3]_4$  was synthesized and the  $^1\text{H}$  NMR spectrum of the high field region was obtained. At -14.21 ppm a poorly resolved quintet was observed with a  $^1\text{H}-^{31}\text{P}$  coupling constant of 17 Hz at 294°K (literature quintet at -13.44 ppm,  $^2J_{\text{H-P}} = 17$  Hz (69)). This quintet is illustrated in Figure 3.5. The  $^{31}\text{P}$  NMR spectrum was also obtained for  $\text{HCo}[\text{P}(\text{O-p-tolyl})_3]_4$  which showed a singlet

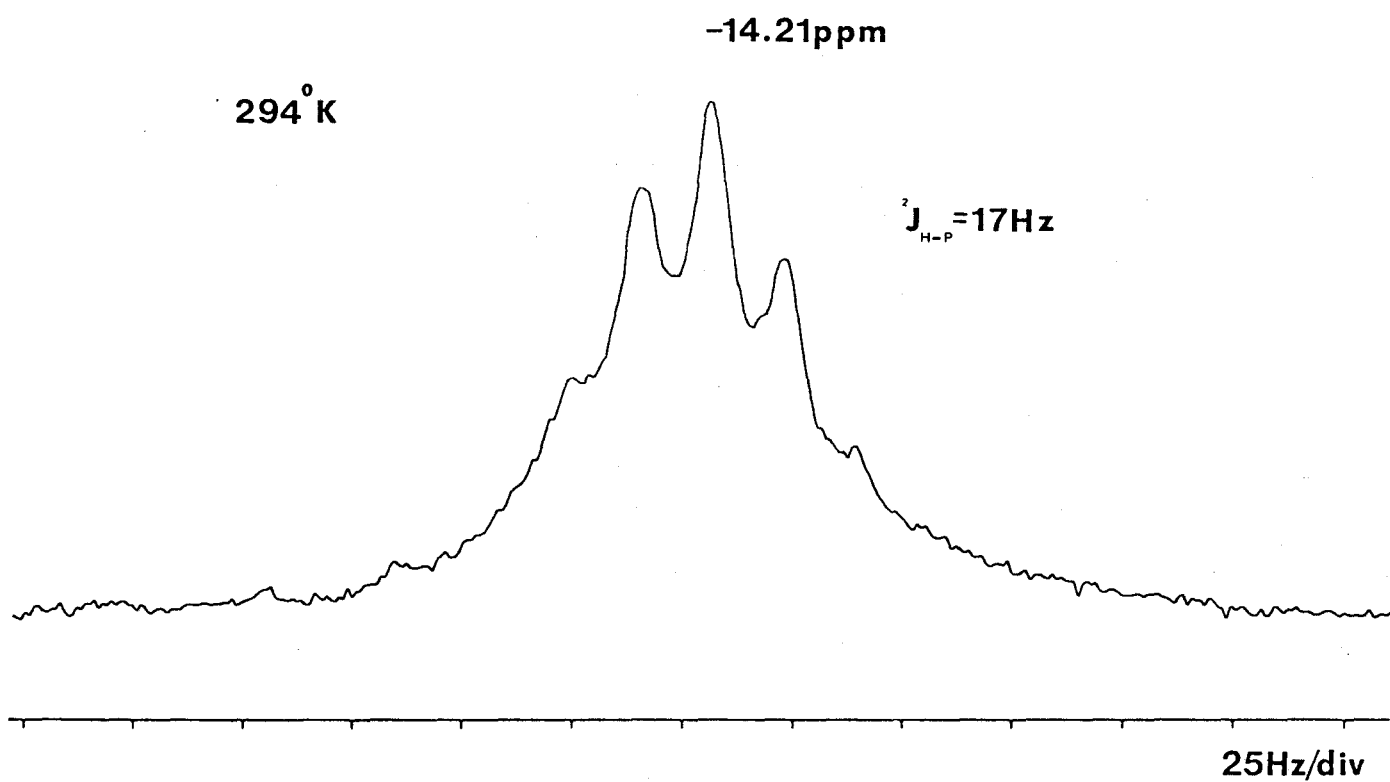


Figure 3.5:  $^1\text{H}$  NMR Spectrum (250 MHz) of the Hydride Resonance of  $\text{HCo}[\text{P}(\text{O}-p\text{-C}_6\text{H}_4\text{CH}_3)_3]_4$  at  $294^\circ\text{K}$ .

at 144.16 ppm (literature 142.7 ppm (69)).

In comparison with the other phosphite cobalt hydrides, this tri-p-tolyl phosphite cobalt complex was the most thermally stable hydride prepared. The other cobalt and nickel hydrides decomposed at 273°K or below.

A tetrakis (tri-isopropyl phosphite) nickel (0) hydride  $\text{HNi}[\text{P}(\text{OCH}(\text{CH}_3)_2)_3]_4^+ \text{CF}_3\text{COO}^-$  was synthesized and attempts were made to obtain the  $^1\text{H}$  spectrum. This compound is thermally stable only below a temperature of 233°K. The  $^1\text{H}$  spectrum of the hydride resonance at -40°C was a broad, poorly resolved triplet at -13.8 ppm with a coupling of approximately 37 Hz. Upon warming the sample to give the high temperature limiting quintet, the sample decomposed so the quintet was never observed.  $\text{HCo}[\text{P}(\text{O-p-C}_6\text{H}_4\text{CH}_3)_3]_4$  was shown to be an extremely stable complex producing a partially resolved quintet for the high field hydride resonance. As a result of this stability the analogous nickel complex was synthesized. The investigation of this nickel tri-p-tolyl phosphite complex lead to the discovery of the first four-coordinate nickel hydride formed in sufficient concentration to be observed spectroscopically by NMR. This nickel hydride system is discussed in the remaining portion of this thesis. Tabulated summaries of the proton hydride resonances and the phosphorus resonances for the compounds mentioned in this research are given in the following two tables (Table 3.1 and 3.2).

Table 3.1  
 $^1\text{H}$  NMR Hydride Data of  $\text{HNi}[\text{P}(\text{OR})_3]_4^+\text{X}^-$ ,  $\text{HCo}[\text{P}(\text{OR})_3]_4$ ,  $\text{H}_2\text{Fe}[\text{P}(\text{OR})_3]_4$   
 Referenced to TMS

Ligand	$\text{X}^-$	T(°K), Solvent	Multiplicity	$\delta$ (ppm)	$^2J_{\text{H-P}}$ (Hz)	Reference
$\text{P}(\text{OEt})_3^{\text{a}}$	$\text{CF}_3\text{COO}^-$	258, tol- $d_8$	quintet	-15.0	27	This work
$\text{P}(\text{OEt})_3^{\text{a}}$	$\text{CF}_3\text{COO}^-$	233, ben- $d_6$	quintet	-14.4	27	18
$\text{P}(\text{OEt})_3^{\text{b}}$			quintet	-15.8		76
$\text{P}(\text{OEt})_3^{\text{c}}$		253, tol- $d_8$	quintet	-14.3		This work
$\text{P}(\text{OEt})_3^{\text{c}}$			quintet	-13.86		34
$\text{P}(\text{OCH}(\text{CH}_3)_2)_3^{\text{a}}$	$\text{CF}_3\text{COO}^-$	233, acetone- $d_6$	triplet	-13.8	37	This work
$\text{P}(\text{OPh})_3^{\text{a}}$	$\text{CF}_3\text{COO}^-$	253, tol- $d_8$	quintet	-13.0	33	This work
$\text{P}(\text{OPh})_3^{\text{a}}$	$\text{HSO}_4^-$	253, $\text{CD}_2\text{Cl}_2$	quintet d of triplet	-13.2 -11.2	33 H- $P_t$ = 173 H- $P_c$ = 48	This work
$\text{P}(\text{OPh})_3^{\text{b}}$		273, $\text{CDCl}_3$	quintet	-13.87	15-17	This work

Cont...

Table 3.1 Cont..

$P(OPh)_3$			quintet	-13.58	17	69
$P(O-p-tolyl)_3$		294, $CDCl_3$	quintet	-14.21	17	This work
$P(O-p-tolyl)_3$			quintet	-13.44	17	69
$P(O-p-tolyl)_3$	$HSO_4^-$	253, $CD_2Cl_2$	quintet	-13.20	32	This work
$P(O-p-tolyl)_3$	$HSO_4^-$	253, $CD_2Cl_2$	d of triplet	-11.00	$H-P_{trans} = 173$ $H-P_{cis} = 47$	This work
$P(O-p-tolyl)_3$	$CF_3COO^-$	$CD_2Cl_2$	quintet	-13.20	33	62

- a)  $HNi[P(OR)_3]_4^+$   
 b)  $HCo[(OR)_3]_4$   
 c)  $H_2Fe[P(OR)_3]_4$



Table 3.2

$^{31}\text{P}$  NMR Low Field Data for  $\text{HNi}[\text{P}(\text{OR})_3]_4^+\text{X}^-$ ,  $\text{Ni}[\text{P}(\text{OR})_3]_4$ ,  $\text{HCo}[\text{P}(\text{OR})_3]_4$   
Referenced to 85%  $\text{H}_3\text{PO}_4$

Complex	T(°K), Solvent	Multiplicity	$\delta$ (ppm)	Reference
$\text{P}(\text{OEt})_3$	253, $\text{CDCl}_3$	Septet	137.97	This work
$\text{P}(\text{OEt})_3$		Septet	137.8	77
$\text{Ni}[\text{P}(\text{OEt})_3]_4$	273, to1-d <sub>8</sub>	Singlet	159.5	This work
$\text{Ni}[\text{P}(\text{OEt})_3]_4$		Singlet	158.4, 159	77, 18
$\text{HNi}[\text{P}(\text{OEt})_3]_4^+\text{HSO}_4^-$	253, $\text{CD}_2\text{Cl}_2$	doublet	131.1	This work
$\text{HCo}[\text{P}(\text{OEt})_3]_4$		singlet	168.3	76
$\text{P}(\text{OPh})_3$	253, $\text{CDCl}_3$	singlet	126.54	This work
$\text{P}(\text{OPh})_3$		singlet	127.3	77
$\text{Ni}[\text{P}(\text{OPh})_3]_4$	273, $\text{CDCl}_3$	singlet	130.15	This work

Cont..

Table 3.2 Cont..

$\text{Ni}[\text{P}(\text{OPh})_3]_4$		singlet	128.8	77
$\text{HNi}[\text{P}(\text{OPh})_3]_4^+\text{HSO}_4^-$	253, $\text{CD}_2\text{Cl}_2$	doublet	113.00	This work
$\text{HCo}[\text{P}(\text{OPh})_3]_4$	253, $\text{tol-d}_8$	singlet	142.52	This work
$\text{P}(\text{O-p-tolyl})_3$	213, $\text{CD}_2\text{Cl}_2$	singlet	128.6	This work
$\text{P}(\text{O-p-tolyl})_3$		singlet	127.7	77
$\text{Ni}[\text{P}(\text{O-p-tolyl})_3]_4$	253, $\text{CD}_2\text{Cl}_2$	singlet	134.1	This work
$\text{Ni}[\text{P}(\text{O(p-tolyl)})_3]_4$		singlet	130.4	77
$\text{HNi}[\text{P}(\text{O-p-tolyl})_3]_3^+\text{HSO}_4^-$	233, $\text{CD}_2\text{Cl}_2$	d of t, t	120, 115	This work
$\text{HNi}[\text{P}(\text{O-p-tolyl})_3]_4^+\text{HSO}_4^-$	233, $\text{CD}_2\text{Cl}_2$	doublet	113	This work
$\text{HCo}[\text{P}(\text{O-p-tolyl})_3]_4$	253, $\text{tol-d}_8$	singlet	144.16	This work

### 3.2 Reaction of Strong Acids with NiL<sub>4</sub> System

Addition of strong aqueous acids such as H<sub>2</sub>SO<sub>4</sub> and CF<sub>3</sub>COOH to tetrakis nickel (0) complexes NiL<sub>4</sub> where L is a triphosphite ligand, yields solutions of nickel hydride cations. These cations have been prepared in various solvents such as methanol, (24) deuterated methylene chloride (62) and deuterated toluene which have been used for the tri-p-tolyl phosphite system. These nickel hydrides are initially five-coordinate species which show a high field proton resonance as a quintet. This resonance is characteristic of a proton directly bonded to a transition metal (18).

A sequence of four reactions describes the behaviour of the tetrakis nickel phosphite NiL<sub>4</sub> with H<sub>2</sub>SO<sub>4</sub> in a deuterated methylene chloride solution.



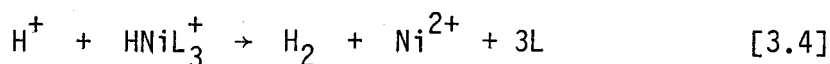
This equilibrium reaction is established very rapidly and is reversible. The ionic organometallic compound HNiL<sub>4</sub><sup>+</sup> is formulated as HNiL<sub>4</sub><sup>+</sup>HSO<sub>4</sub><sup>-</sup>. Similar compounds have been characterized by Tolman such as the hydridotetrakis (triethyl phosphite) nickel bisulfate complex HNi[P(OCH<sub>2</sub>CH<sub>3</sub>)<sub>3</sub>]<sub>4</sub>HSO<sub>4</sub> (24). The hydride chemical shift and coupling to <sup>31</sup>P indicates that the acid anion does not affect the structure of the hydride cation which is a five-coordinate complex. The protonation of NiL<sub>4</sub> precedes ligand dissociation which enables the detection of the quintet by <sup>1</sup>H NMR.

The addition of excess ligand has no effect on the rate of formation of the five-coordinate hydride HNiL<sub>4</sub><sup>+</sup>, which is quite stable in its presence.

The excess ligand only affects the decay of the hydride  $\text{HNiL}_4^+$ .



An excess of acid does not attack the  $\text{HNiL}_4^+$  species but its protonated four-coordinate ligand deficient daughter species  $\text{HNiL}_3^+$ , which is attacked via an oxidation reaction.



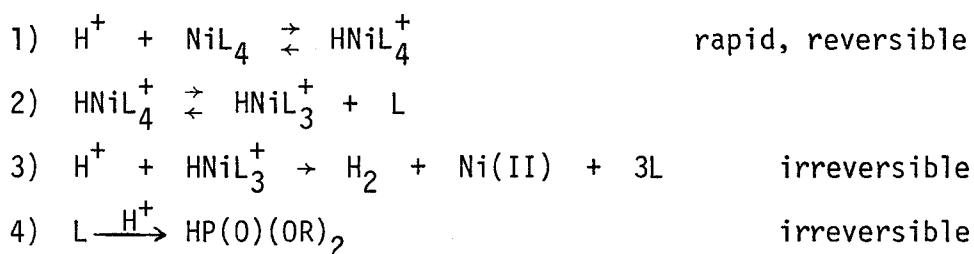
Under these acidic conditions any excess acid will immediately decompose any free ligand  $\text{P(OR)}_3$  present to give  $\text{HP(O)(OR)}_2$ .



Depending on the ligand size further decomposition or hydrolysis can occur resulting in compounds such as  $\text{O=P(OR)}_3$ ,  $\text{HPO(OH)OR}$ ,  $\text{HPO(OH)}_2$  or  $\begin{array}{c} \text{O} \quad \text{O} \\ \parallel \quad \parallel \\ \text{H}^{\text{P}}-\text{O}-\text{P}^{\text{H}} \\ \text{OH} \quad \text{OH} \end{array}$ .

The very concentrated hydride solutions prepared were stable for many hours after some initial decomposition, which was indicated by the bubbles of gas given off as  $\text{H}_2$ . These hydride solutions stabilize themselves by releasing free ligand into the system via the oxidation process as shown in equation 3.4. This suppresses the amount of  $\text{HNiL}_3^+$  formed by equation 3.3 and establishes an equilibrium with  $\text{HNiL}_4^+$ . Therefore, solutions with high concentrations of hydrides of both the four and five-coordinate species should be detected by  $^1\text{H}$  NMR in the same system. When the phosphite ligand used is tri-p-tolyl phosphite, a quintet belonging to  $\text{HNiL}_4^+$  and a

doublet of triplets due to  $\text{HNiL}_3^+$  are indeed observed. There is no spectroscopic evidence for the presence of  $\text{HNiL}_3^+$  when the ligand is triethyl phosphite (24). In a solution of high acid concentration, the dominant species present in the system is shown by  $^1\text{H}$  NMR to be  $\text{HNiL}_3^+$  which means that equation 3.3 becomes rate limiting and favours the right hand side. Thus, the complete reaction sequence is as follows:



where L = triphosphite ligand (61).

### 3.3 Identification of the $^1\text{H}$ and $^{31}\text{P}$ NMR Spectra of the $\text{HNiL}_4^+$ and $\text{HNiL}_3^+$ Compounds of Tri-p-tolyl Phosphite

There are two different nickel compounds observed both in the  $^1\text{H}$  and  $^{31}\text{P}$  NMR spectra where the ligand used is tri-p-tolyl phosphite. The  $^1\text{H}$  NMR spectrum of the free ligand  $\text{P(O-p-C}_6\text{H}_4\text{CH}_3)_3$  consisted of a singlet at 2.20 ppm which is due to methyl protons attached to the aromatic ring in the para position. Also, a singlet was observed at 7.00 ppm which is from the aromatic protons in the ortho and meta positions. This spectrum was referenced to TMS ( $\delta = 0$  ppm) and is illustrated in Figure 3.6. The Sadtler Index gives literature resonances for the ligand  $\text{P(O-p-C}_6\text{H}_4\text{CH}_3)_3$ . The methyl resonance which is a singlet is positioned at 2.21 ppm and the aromatic singlet occurs at 6.98 ppm.

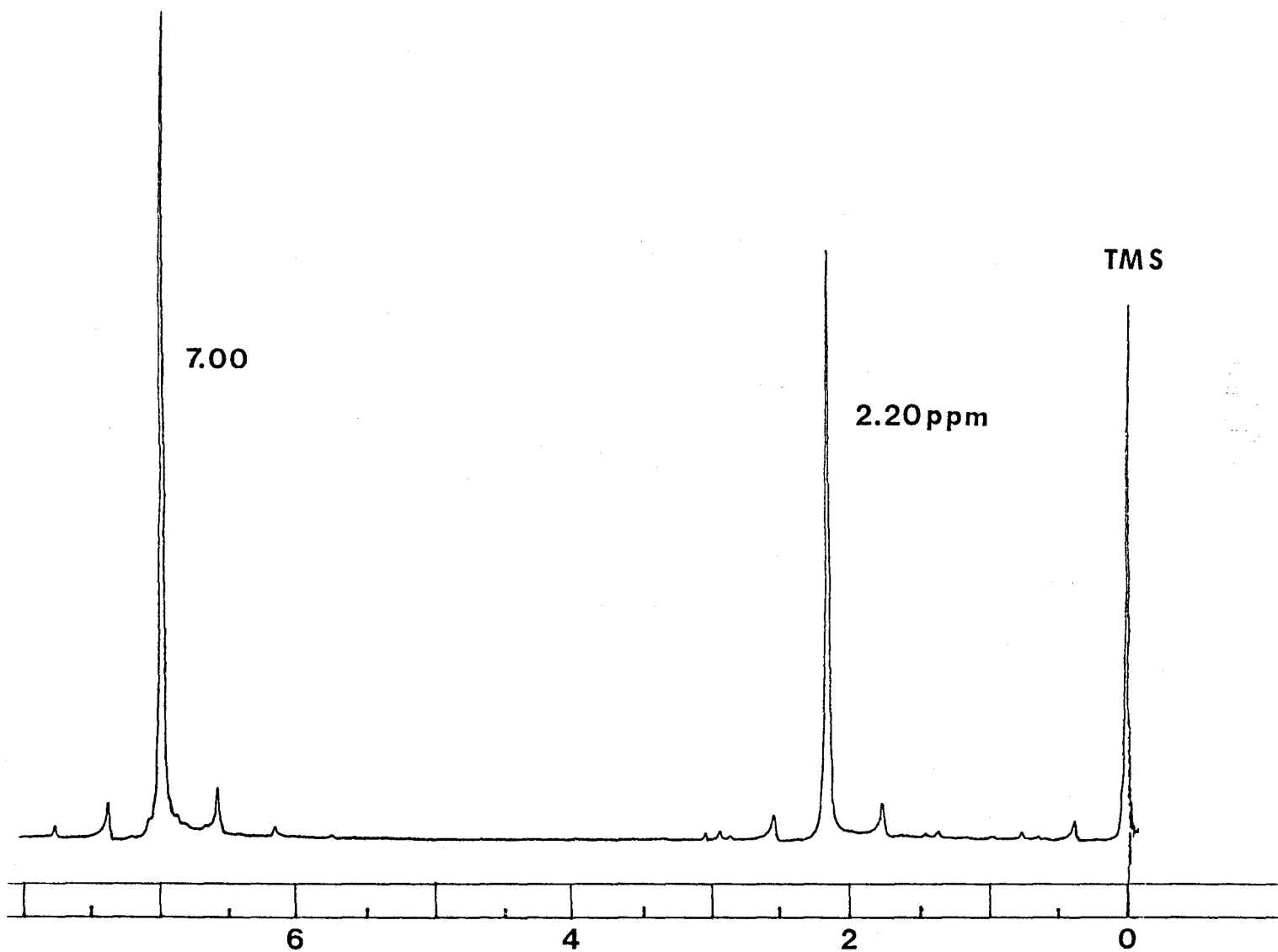
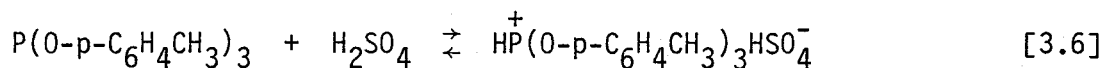


Figure 3.6: The  $^1\text{H}$  NMR Spectrum ( 90 MHz) of  $\text{P}(\text{O}-p\text{-C}_6\text{H}_4\text{CH}_3)_3$ .

Upon acidification of the free ligand with 100% H<sub>2</sub>SO<sub>4</sub>, the phosphorus atom was directly protonated.



The solvent used for this system was CD<sub>2</sub>Cl<sub>2</sub> and the <sup>1</sup>H spectrum was obtained on a WM250 MHz NMR spectrometer. Downfield from TMS (δ=0 ppm) was a singlet at 2.20 ppm which is due to a free ligand methyl resonance and a singlet at 2.30 ppm of greater intensity attributed to the acidified phosphite methyl resonance H-P<sup>+</sup>(O-p-C<sub>6</sub>H<sub>4</sub>CH<sub>3</sub>)<sub>3</sub>. Further downfield was a complex multiplet centered around 7.10 ppm, which is attributable to the aromatic protons of both the free ligand and the acidified phosphite combined. Also, centered at 7.46 ppm was a doublet of equal intensity which had a proton directly bonded to phosphorus to give <sup>1</sup>J<sub>H-P</sub> = 780 Hz. This is from the acidified phosphite HP<sup>+</sup>(O-p-C<sub>6</sub>H<sub>4</sub>CH<sub>3</sub>)<sub>3</sub> taken at 273°K. The same doublet at 233°K had a coupling constant of 787.6 Hz. Further downfield at 11.62 ppm was the acid resonance from excess H<sub>2</sub>SO<sub>4</sub> and HSO<sub>4</sub><sup>-</sup>. (Figure 3.7).

The addition of a strong acid such as 100% H<sub>2</sub>SO<sub>4</sub> to tetrakis(tri-p-tolyl phosphite) nickel (0) produced two nickel hydride compounds, HNiL<sub>4</sub><sup>+</sup> and HNiL<sub>3</sub><sup>+</sup> where L = P(O-p-C<sub>6</sub>H<sub>4</sub>CH<sub>3</sub>)<sub>3</sub> which are formed according to equation 3.2 and 3.3 of section 3.2. The low field region, referenced to CD<sub>2</sub>Cl<sub>2</sub> (δ = 5.32 ppm), consisted of three methyl peaks centered around 2.30 ppm, a complex aromatic multiplet at 7.00 ppm, a doublet centered at 7.30 ppm, and a free acid peak present at 11 ppm. The methyl region showed the free ligand resonance which was the least intense, varying from 2.19 to 2.28 ppm

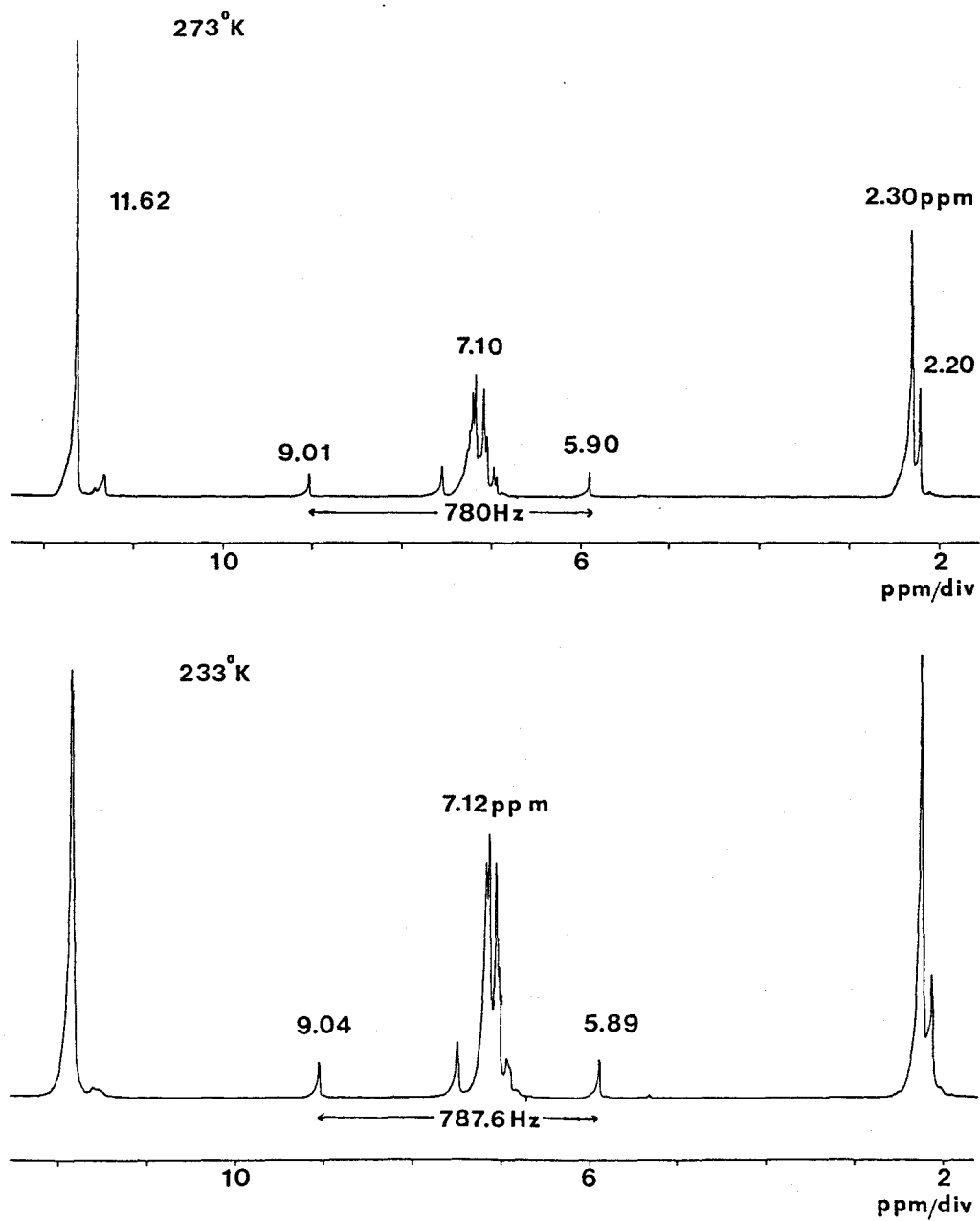


Figure 3.7:  $^1\text{H}$  NMR (250 MHz) Spectra of  $\text{P}(0\text{-}p\text{-tolyl})_3 + \text{H}_2\text{SO}_4$  at 273°K and 233°K.



depending on the temperature and acid concentration of the system. The next two methyl resonances which had moved downfield from the free ligand were assignable to acidified free phosphite,  $\text{HNiL}_4^+$  and  $\text{HNiL}_3^+$ . The resonance for the acidified phosphite is probably combined with  $\text{HNiL}_4^+$  to produce the middle methyl line, leaving the peak with a greater chemical shift belonging to the dominant nickel complex  $\text{HNiL}_3^+$ . This illustrates that the hydride of the four-coordinate compound is the dominant species. The methyl resonance due to  $\text{HNiL}_4^+$  and protonated L ranged from 2.27 ppm to 2.33 ppm, and the  $\text{HNiL}_3^+$  methyl peak could occur between 2.35 ppm and 2.37 ppm depending on the temperature and concentration. The aromatic region was again a complex multiplet with two main peaks at 7.06 ppm and 7.16 ppm. The ortho protons will be shifted slightly downfield from the meta protons since they are deshielded more than the meta protons. A doublet with  $^1J_{\text{H-P}} = 764$  Hz at 268°K increased to 776 Hz when the temperature was lowered to 193°K. This doublet was centered around the aromatic multiplet at approximately 7.30 ppm (Figure 3.8).

In the high field region of the nickel hydride phosphite complexes was a doublet of triplets centered at -11.00 ppm and a quintet centered at -13.20 ppm. The triplets were very symmetrical and have intensity ratios of  $\sim 1:2:1$  at low temperatures. The quintet is due to the hydride proton coupled to four equivalent phosphorus atoms producing a  $^2J_{\text{H-P}} = 32$  Hz. According to Tolman  $\text{HNi}[\text{P}(\text{O-p-C}_6\text{H}_4\text{CH}_3)_3]_4^+\text{CF}_3\text{COO}^-$  shows a quintet at -13.2 ppm with  $^2J_{\text{H-P}} = 33 \pm 2$  Hz in  $\text{CD}_2\text{Cl}_2$  (62). There is no mention of the four-coordinate compound. This hydride resonance is characteristic of  $\text{HNi}[\text{P}(\text{O-p-C}_6\text{H}_4\text{CH}_3)_3]_4^+\text{HSO}_4^-$  where the phosphite ligands have become equivalent

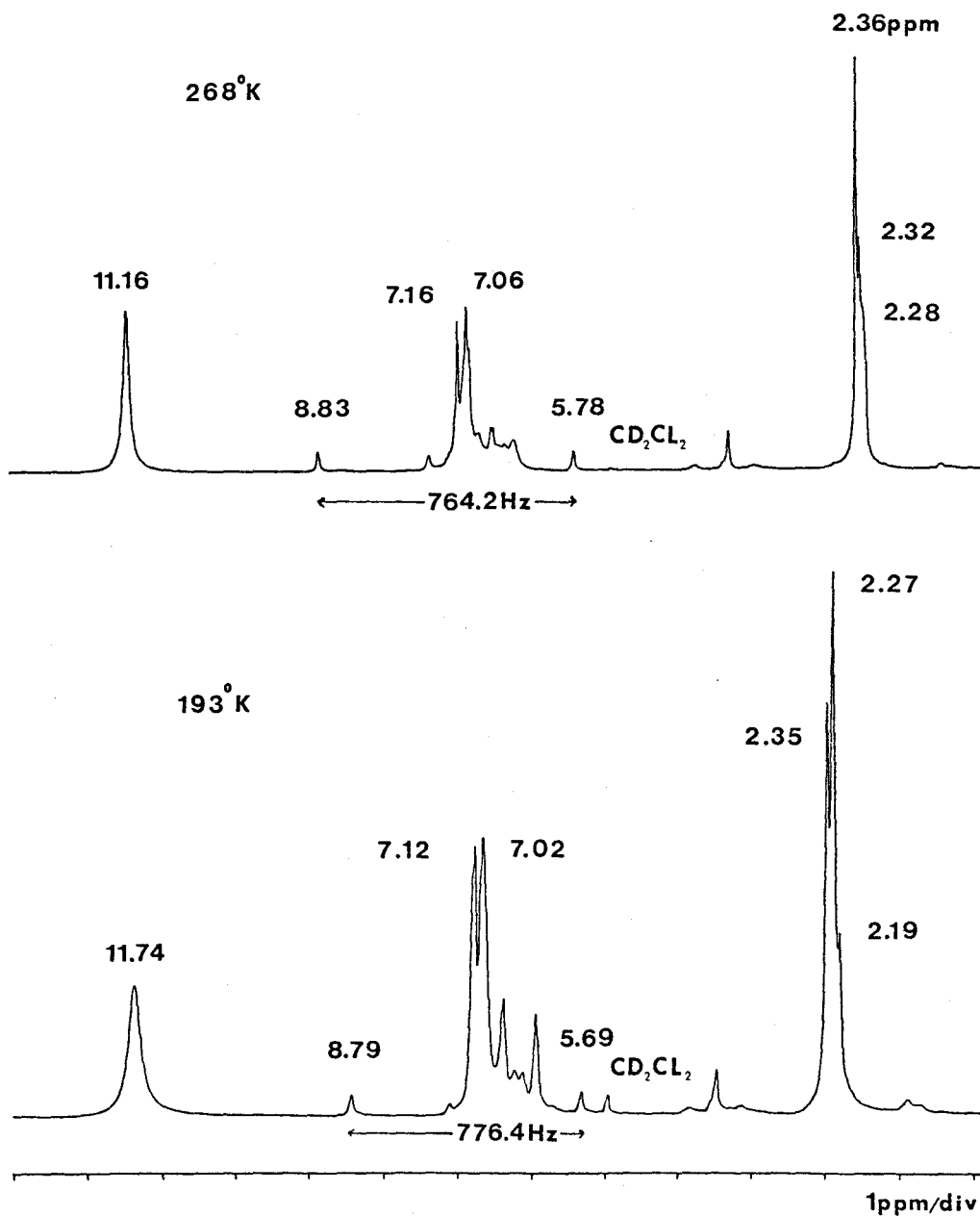
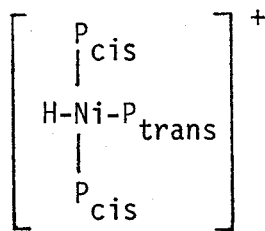


Figure 3.8:  $^1\text{H}$  NMR (250 MHz) Spectra of  $\text{HNiL}_4^+$ ,  $\text{HNiL}_3^+$  Downfield from TMS at  $268^\circ\text{K}$  and  $193^\circ\text{K}$ .

by a rapid intramolecular exchange process. A possible geometry for this complex is a pseudo-square planar or pseudo-tetrahedral with the H-Ni bond on top of the plane of phosphorus atoms or on a face in the tetrahedral geometry.

The doublet of triplets is what is expected for two different phosphorus atoms in a ratio of 1:2 that are coupled to the hydride proton directly bonded to nickel. The nickel complex is a four-coordinate species  $\text{HNi}[\text{P}(\text{O}-p\text{-C}_6\text{H}_4\text{CH}_3)_3]_3^+\text{HSO}_4^-$  where the doublet is due to the single phosphorus trans to the proton giving a coupling constant of  $\pm 172\text{-}174$  Hz and the triplets are due to two equivalent  $^{31}\text{P}$  atoms cis to the hydride proton producing a  $^2J_{\text{H-P}_{\text{cis}}} = \mp 47$  Hz as shown in Figure 3.9. The structure of the complex is approximately of square planar symmetry. This is consistent with a theoretical spectrum expected for a  $\text{XA}_2\text{B}$  ( $\text{X} = ^1\text{H}$ ) system.



Dependence on the concentration of acid will determine which species in the equilibrium will be favoured.



Under highly acidic conditions the four-coordinate compound is favoured resulting in the doublet of triplets being the dominant hydride resonance.

253°K

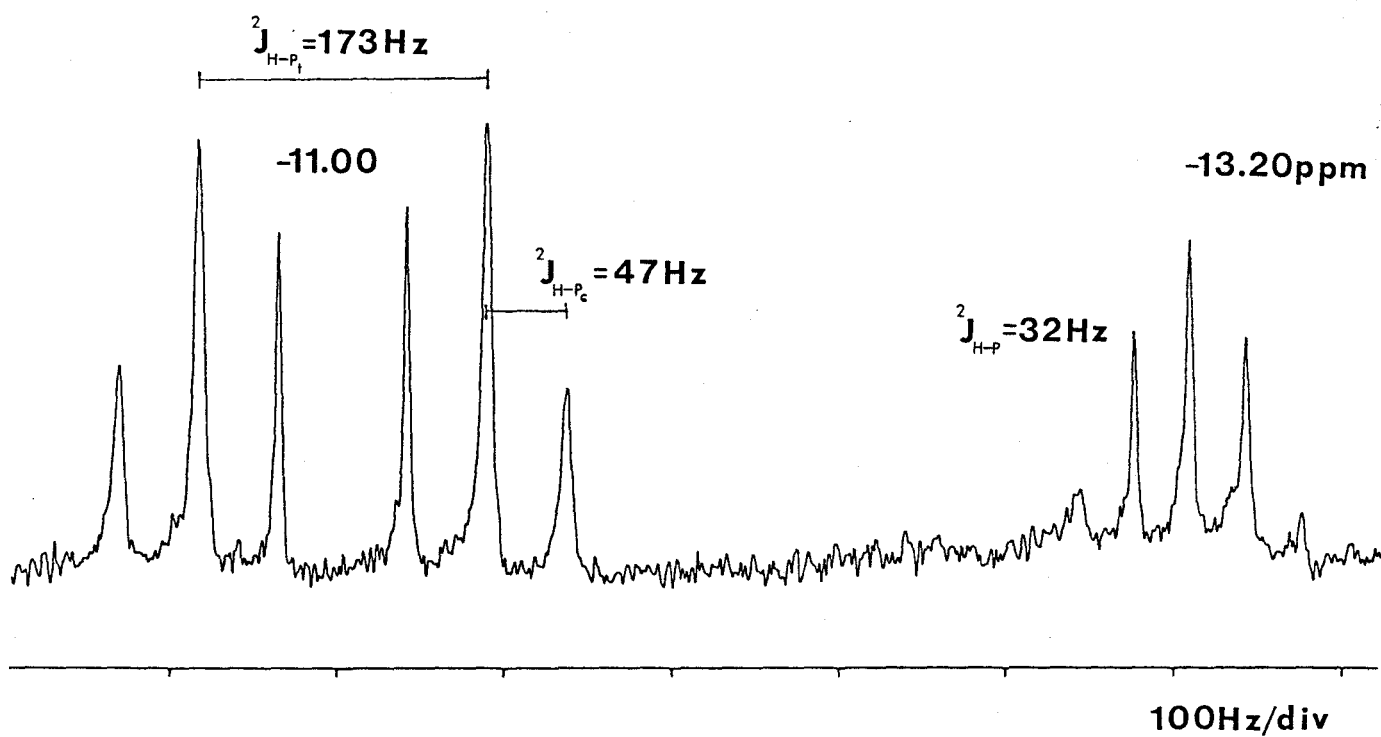


Figure 3.9:  $^1\text{H}$  NMR (250 MHz) Spectrum of  $\text{HNi}[\text{P}(\text{O-p-tolyl})_3]_4^+$  and  $\text{HNi}[\text{P}(\text{O-p-tolyl})_3]_3^+$  Upfield from TMS at  $253^\circ\text{K}$ .

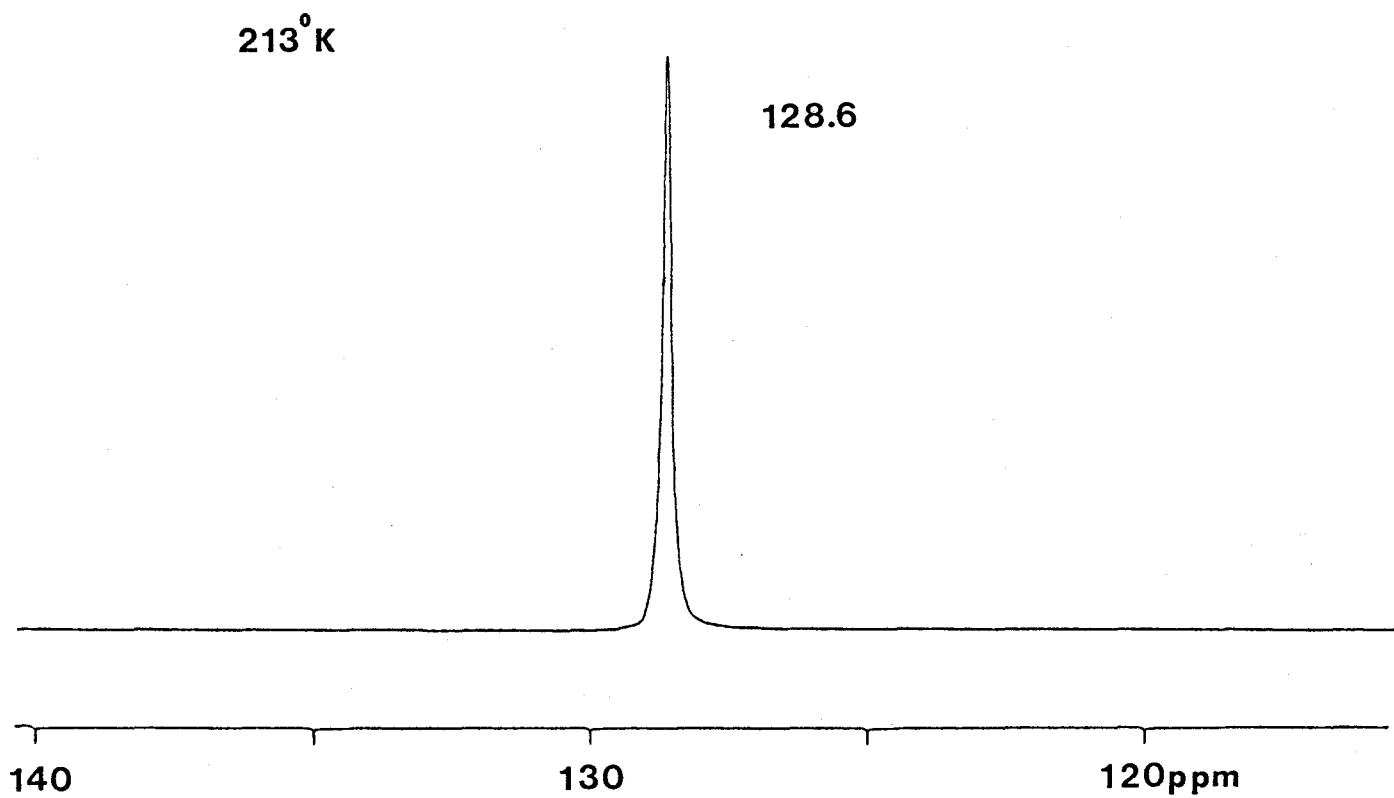
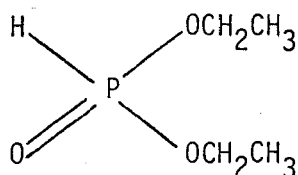


Figure 3.10:  $^{31}\text{P}$  NMR Spectrum (161.98 MHz) of  $\text{P}(\text{O}-p\text{-C}_6\text{H}_4\text{CH}_3)_3$  at 213°K.

When the acid concentration is low or in the presence of excess free ligand, the five-coordinate  $\text{HNiL}_4^+$  species is the major component.

The  $^{31}\text{P}$  NMR spectrum of the free ligand  $\text{P}(\text{O}-p\text{-C}_6\text{H}_4\text{CH}_3)_3$  consisted of a singlet at 128.6 ppm referenced to 85%  $\text{H}_3\text{PO}_4$  ( $\delta=0$  ppm) (Figure 3.10). The literature value is 127.7 ppm (77) also referenced to 85%  $\text{H}_3\text{PO}_4$ .

The reaction of 100%  $\text{H}_2\text{SO}_4$  with the free phosphite produced a  $^{31}\text{P}$  NMR spectrum that contained a doublet centered at 5.10 ppm and a singlet at -16.00 ppm. There was no resonance for unprotonated free ligand. The molar ratio of  $\text{L}:\text{H}_2\text{SO}_4$  was less than 1:1 (1:0.6); therefore, in an acidic environment, any free phosphite is immediately protonated producing peaks at less than 10 ppm. Upon increasing the molar ratio of free L to  $\text{H}_2\text{SO}_4$  to 1:6 (10 fold), other sets of doublets began to appear. The large coupling constant of  $\sim 760$  Hz is characteristic of a proton directly bonded to a phosphorus atom (82) as shown in Figure 3.11. The compound formed is probably  $\text{HP}^+(\text{OH})(\text{O}-p\text{-C}_6\text{H}_4\text{CH}_3)_2$  or  $\text{HP}(\text{O})(\text{O}-p\text{-C}_6\text{H}_4\text{CH}_3)_2$ . Tolman observed a large doublet in the  $^{31}\text{P}$  NMR spectrum with a coupling constant of 710 Hz when he worked with the  $\text{HNi}[\text{P}(\text{OCH}_2\text{CH}_3)_3]_4^+\text{HSO}_4^-$  system. Tolman assigned the doublet to  $\text{HP}(\text{O})(\text{OCH}_2\text{CH}_3)_2$  (24). The singlet at -16.00 ppm is probably due to



$\text{O}=\text{P}(\text{O}-p\text{-C}_6\text{H}_4\text{CH}_3)_3$ . According to Dillon et al., the  $^{31}\text{P}$  chemical shift of  $\text{OP}(\text{OC}_6\text{H}_5)_3$  occurs upfield from 85%  $\text{H}_3\text{PO}_4$  at -18.2 ppm as a singlet in liquid  $\text{HCl}$  (80).

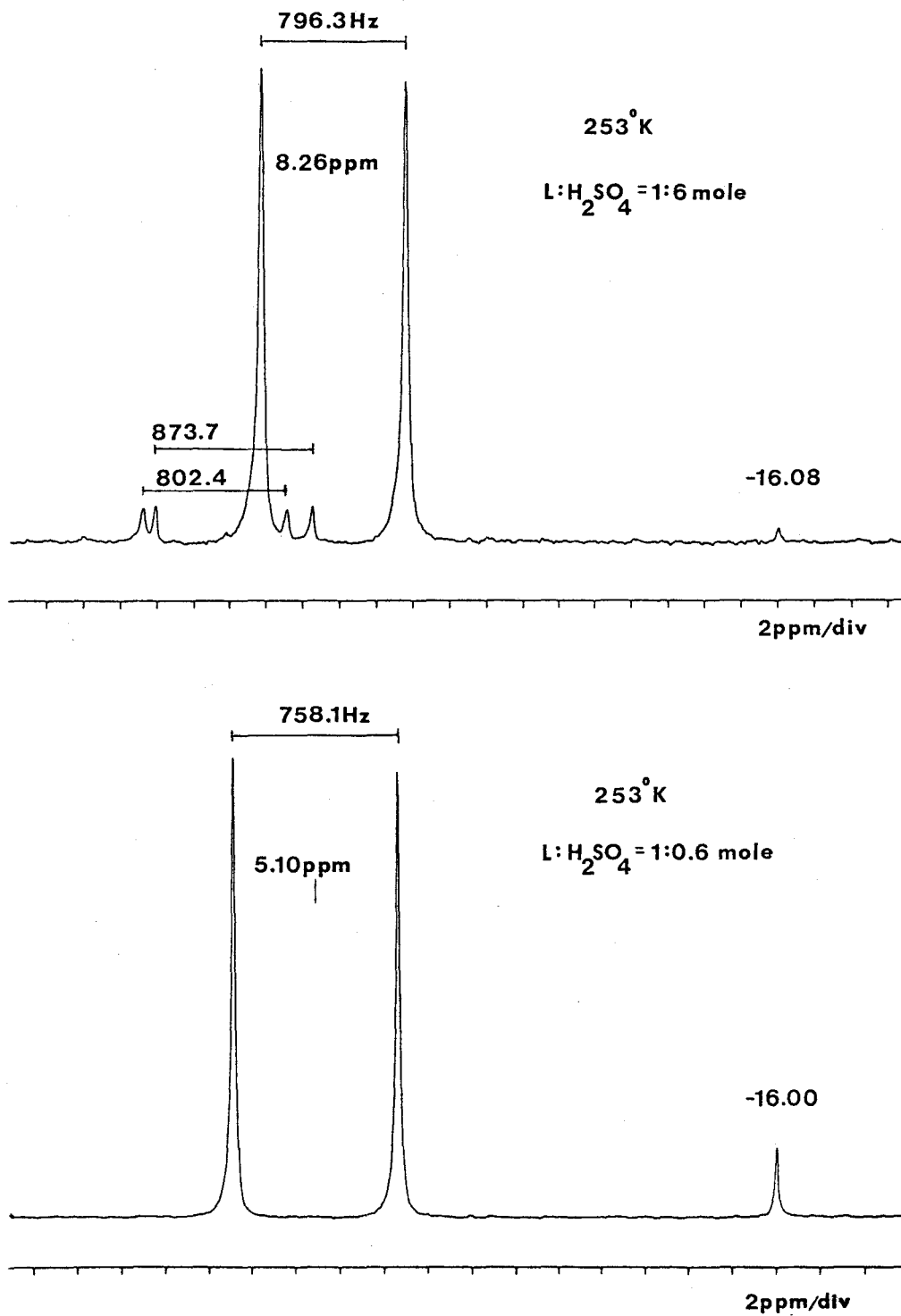
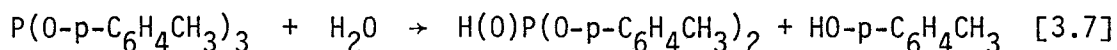


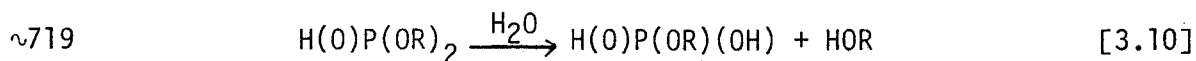
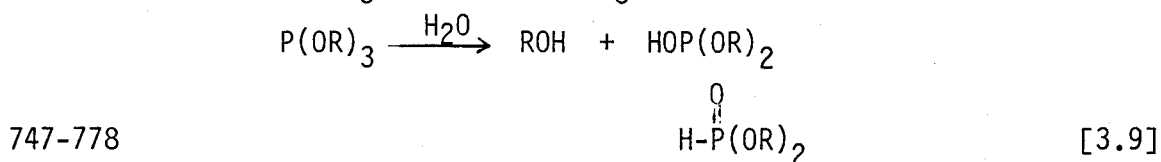
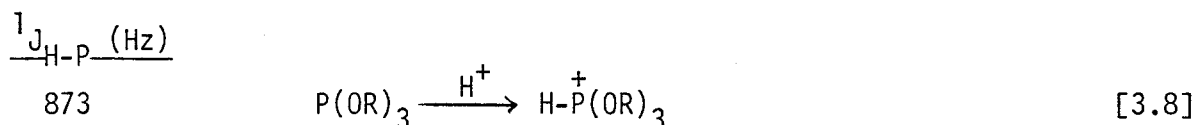
Figure 3.11: <sup>31</sup>P NMR Spectra (101.26 MHz) of P(O-p-C<sub>6</sub>H<sub>4</sub>CH<sub>3</sub>)<sub>3</sub> and H<sub>2</sub>SO<sub>4</sub> at 253°K Using 1:0.6 and 1:6 Mole Ratio of L:H<sub>2</sub>SO<sub>4</sub>.

A competing reaction that occurred along with the protonation of free phosphite ligand was the hydrolysis of the ligand. Since no attempt was made to remove possible water present in the concentrated acid, hydrolysis was very probable. This was shown when one mole of  $H_2O$  reacted with one mole of tri-p-tolyl phosphite.

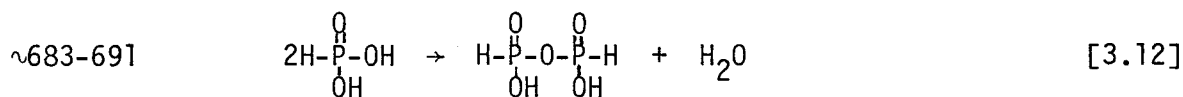
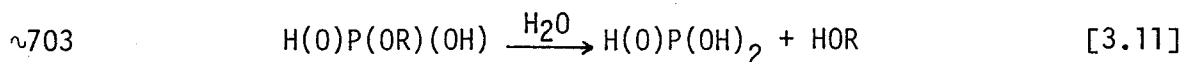


The  $^{31}P$  NMR spectrum consisted of three sets of doublets ranging from 7.22 ppm to 2.20 ppm. The coupling constants also varied from 703 Hz to 746.5 Hz; therefore, more than one hydrolysis product was formed. The doublet centered at 2.20 ppm ( $^1J_{H-P} = 746.5$  Hz) was the major species and the doublet centered at 7.22 ppm ( $^1J_{H-P} = 703$  Hz) was present at approximately half the concentration of the largest doublet (Figure 3.12).

As the ratio of  $H_2O$  to free phosphite increased the doublets furthest downfield increased in intensity. A possible explanation for this is that the doublets further downfield are products of second and third hydrolysis reactions. This further hydrolysis produced smaller  $^1H-^{31}P$  coupling constants.







Therefore, under a very acidic environment the  $\text{H}-\overset{\dagger}{\text{P}}(\text{OR})_3$  complex is the dominant species but when the acid concentration is low, the hydrolysis reactions proceed at a faster rate which forms  $\text{H(O)P(OR)}_2$  as the major complex. Evidence for the phosphate species is given by the weak doublet of doublets resonating at 5.52 ppm. A similar spectrum was obtained by Callis et al.

(83) for the isohypophosphate anion  $\begin{array}{c} \text{O} \quad \text{O}^- \\ \parallel \quad \parallel \\ \text{H}-\text{P}-\text{O}-\text{P}=\text{O}(\text{HP}_2\text{O}_6^{3-}) \\ | \quad | \\ \text{O}^- \quad \text{O}^- \end{array}$ .

The  $^{31}\text{P}$  NMR spectrum of  $\text{NiL}_4 \text{ L} = \text{P}(\text{O}-p\text{-C}_6\text{H}_4\text{CH}_3)_3$  showed a singlet resonating at 134.1 ppm, downfield from the external reference 85%  $\text{H}_3\text{PO}_4$  (Figure 3.13). The literature value is 130.4 ppm (77).

Upon addition of 100%  $\text{H}_2\text{SO}_4$  to  $\text{NiL}_4$ , two nickel hydride species  $\text{HNiL}_4^+$  and  $\text{HNiL}_3^+$  are formed and have been identified in the  $^{31}\text{P}$  NMR spectrum. The low field region consisted of the  $^{31}\text{P}$  resonance for the nickel complexes and then further upfield between 15 ppm and -18 ppm was the region where the protonated phosphites were found.

At approximately 113-114 ppm downfield from 85%  $\text{H}_3\text{PO}_4$  ( $\delta=0$  ppm) was a doublet with a  $^2J_{\text{H-P}} = 27-29$  Hz. This is due to four equivalent phosphorus atoms of the  $\text{HNiL}_4^+$  complex coupled to one proton. Upon addition of free ligand to the system, this doublet increases in intensity relative to the other resonances present in this region. Also, the coupling constant increases to 32 Hz which is comparable to the coupling constant obtained from

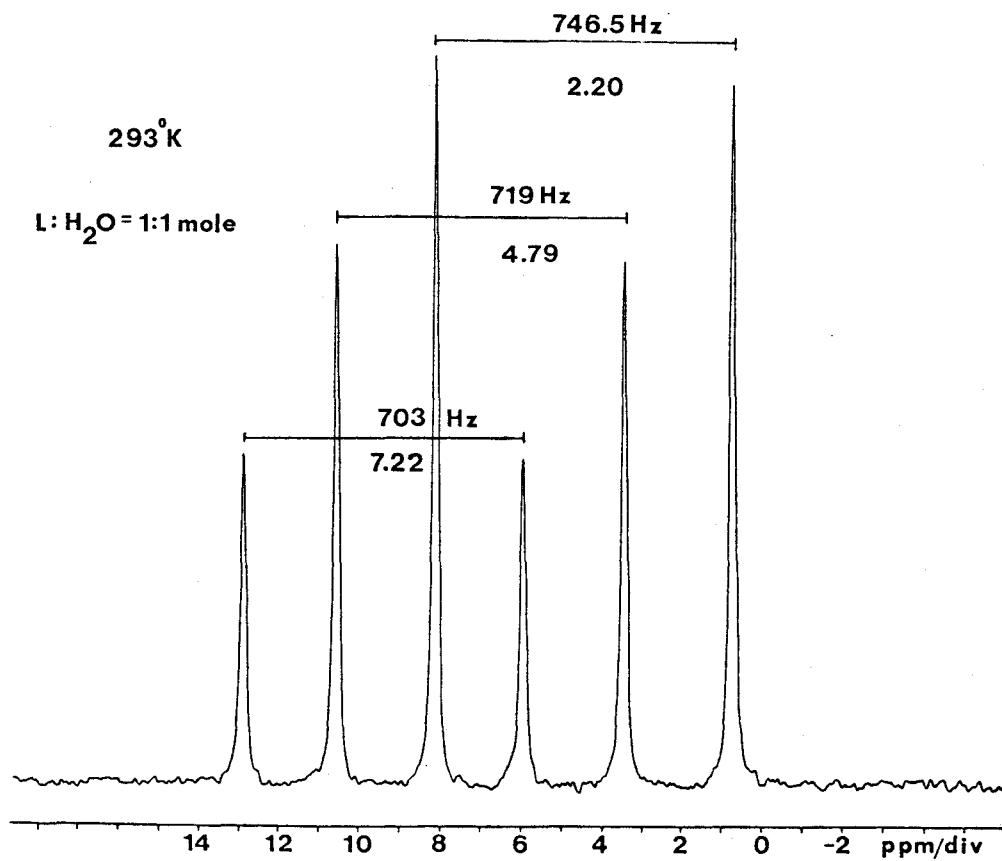
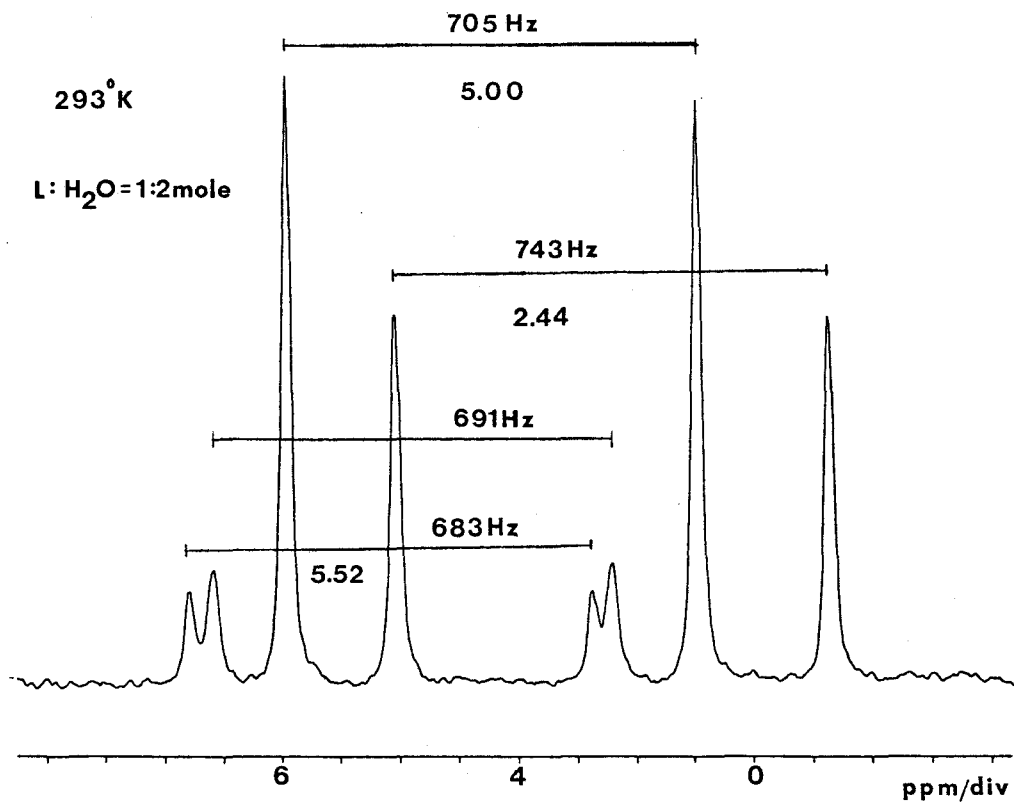


Figure 3.12: <sup>31</sup>P NMR Spectra (101.26 MHz) of P(O-p-C<sub>6</sub>H<sub>4</sub>CH<sub>3</sub>)<sub>3</sub>. Reacting with H<sub>2</sub>O at Room Temperature.

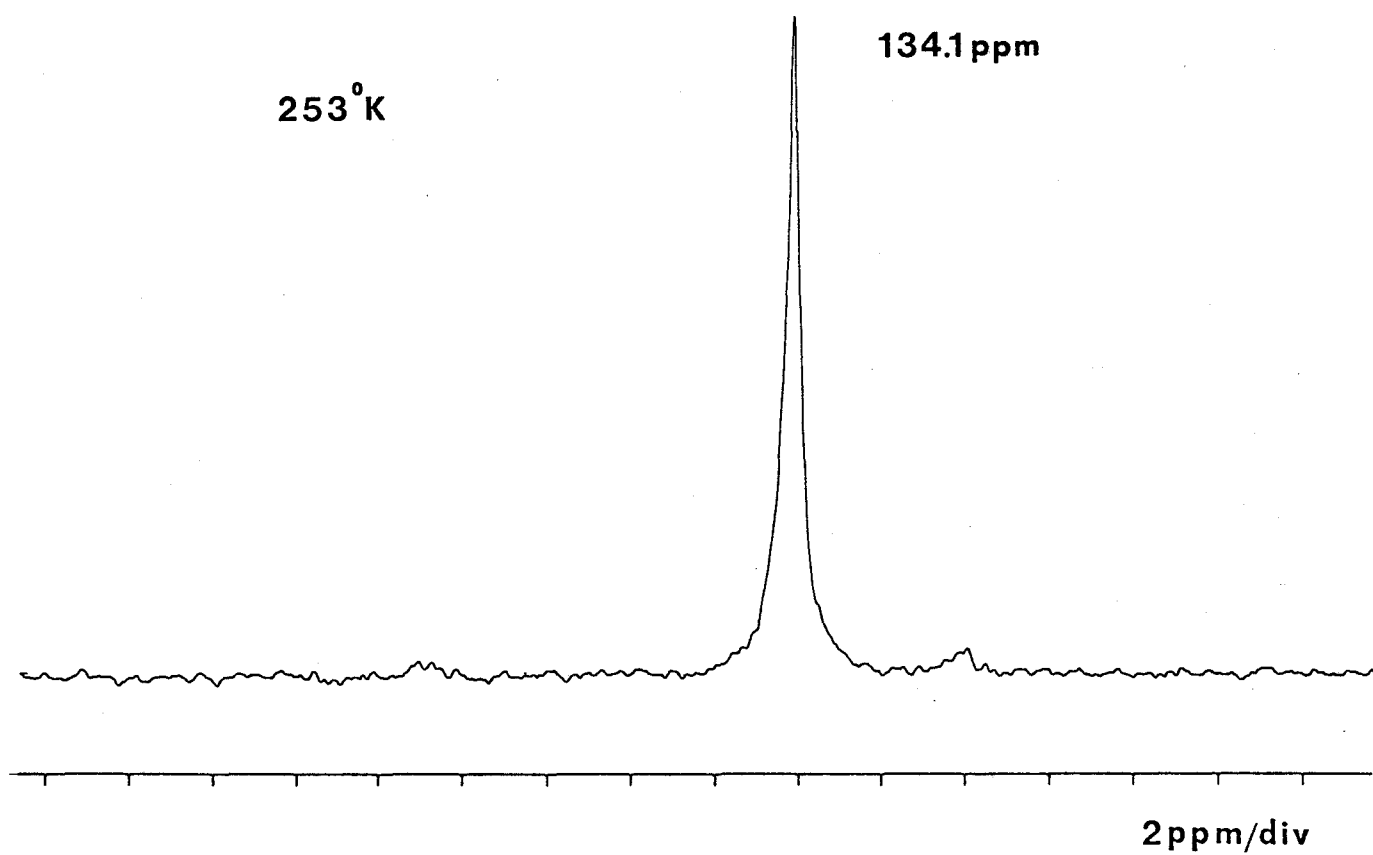


Figure 3.13:  $^{31}\text{P}$  NMR Spectrum of  $\text{Ni}[\text{P}(\text{O}-p\text{-C}_6\text{H}_4\text{CH}_3)_3]_4$  at 253 K (101.26 MHz).

the  $^1\text{H}$  spectrum. When the spectrum was proton decoupled, the doublet collapsed in to a singlet.

Further downfield was a doublet of triplets centered around 120 ppm and a triplet at about 115-117 ppm. The ratio of peak areas of the doublet of triplets to the triplet was approximately 1:2. The doublet of triplets is due to the trans phosphorus in the four-coordinate species  $\text{HNiL}_3^+$  and the triplet is due to the two cis phosphorus atoms also in the  $\text{HNiL}_3^+$  compound. The hydride proton couples to the trans  $^{31}\text{P}$  atom to produce a doublet with a  $^2J_{\text{H-P}_{\text{trans}}} = +174$  Hz and the two cis  $^{31}\text{P}$  atoms couple to the  $\text{P}_{\text{trans}}$  to form the doublet of triplets with a  $^2J_{\text{P}_{\text{trans}}-\text{P}_{\text{cis}}} = 57-58$  Hz. When the proton decoupler was applied this resonance collapsed into a broad singlet. The  $\text{P}_{\text{trans}}-\text{P}_{\text{cis}}$  couplings are not seen because the decoupling power was not strong enough to remove all of the  $^1\text{H}$  coupling. The expected  $^{31}\text{P}[^1\text{H}]$  resonance is a triplet with a splitting of 57-58Hz.

The triplet at 115-117 ppm is actually a doublet of doublets where the center two peaks have overlapped; therefore, the  $\text{P}_{\text{trans}}-\text{P}_{\text{cis}}$  and  $\text{P}_{\text{cis}}-\text{H}$  couplings are mixed to give an average coupling of approximately 50 Hz. When the  $^1\text{H}$  decoupler was applied the triplet changed into a doublet removing the  $^2J_{\text{H-P}_{\text{cis}}}$  and giving a  $^2J_{\text{P}_{\text{trans}}-\text{P}_{\text{cis}}} = 56$  Hz. Also, there was a weak singlet observed at 144-145 ppm which has not been assigned. It may be due to an ortho-metallation product or possibly a combination phosphine, diphosphite complex,  $\text{RP}(\text{OR})_2$  (Figure 3.14).

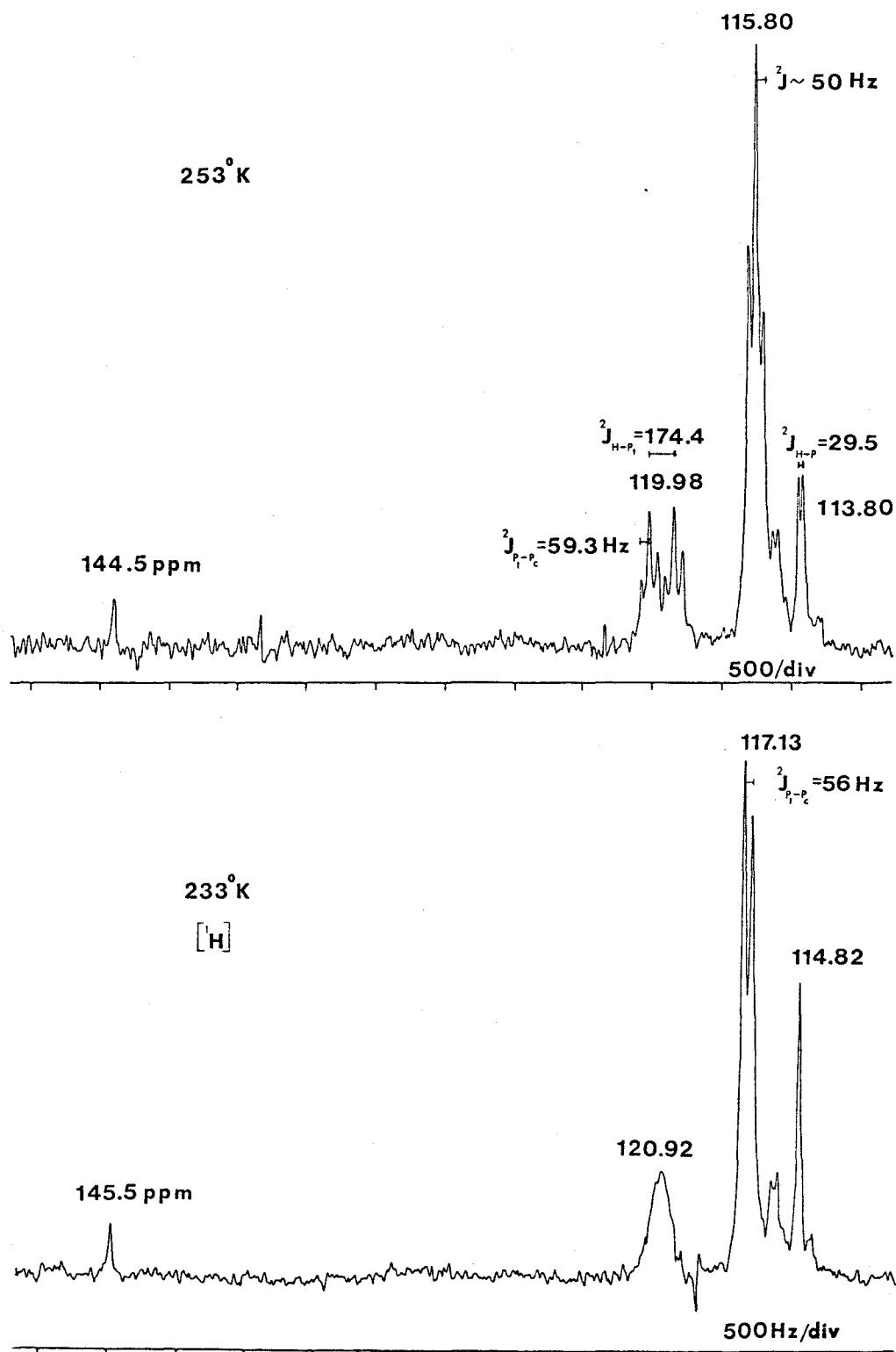
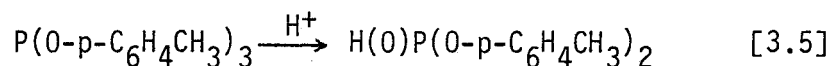
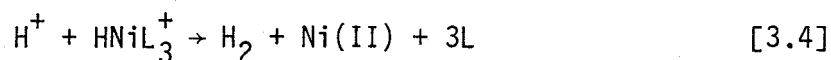


Figure 3.14:  $^{31}\text{P}$  NMR Spectra (161.98 MHz) of  $\text{HNiL}_4^+$ ,  $\text{HNiL}_3^+$  Coupled and Decoupled at 253 K and 233 K Downfield from 85%  $\text{H}_3\text{PO}_4$

The addition of free phosphite to the system does not change the ratio of the doublet of triplets to the triplet, only the intensity of the doublet due to  $\text{HNiL}_4^+$  increases as illustrated in Figure 3.15. The addition of free ligand causes the equilibrium to shift to the left hand side of equation 3.3.



When a large excess of free ligand was added this equilibrium was destroyed and the nickel hydride phosphite compounds decomposed into nickel (II) and protonated phosphites (equation 3.4 and 3.5).



This was observed by the decrease in intensity of the lowfield resonances mentioned above until only a very small singlet was present at  $\sim 115$  ppm (Figure 3.16).

In the  $^{31}\text{P}$  NMR spectra of the  $\text{HNiL}_4^+$  and free ligand system upfield from 85%  $\text{H}_3\text{PO}_4$  are a series of doublets with large coupling constants. One doublet was centered at 12.10 ppm with a  $^1J_{\text{H-P}} = 873$  Hz and a second doublet was centered at 4.90 ppm with a  $^1J_{\text{H-P}} = 778$  Hz. Further upfield was a singlet at -18 ppm (Figure 3.17).

From the literature, Dillon et al. (80) reported a phosphorus chemical shift of -18.2 ppm for  $\text{O=P(OPh)}_3$ ; therefore, the singlet observed at -18 ppm

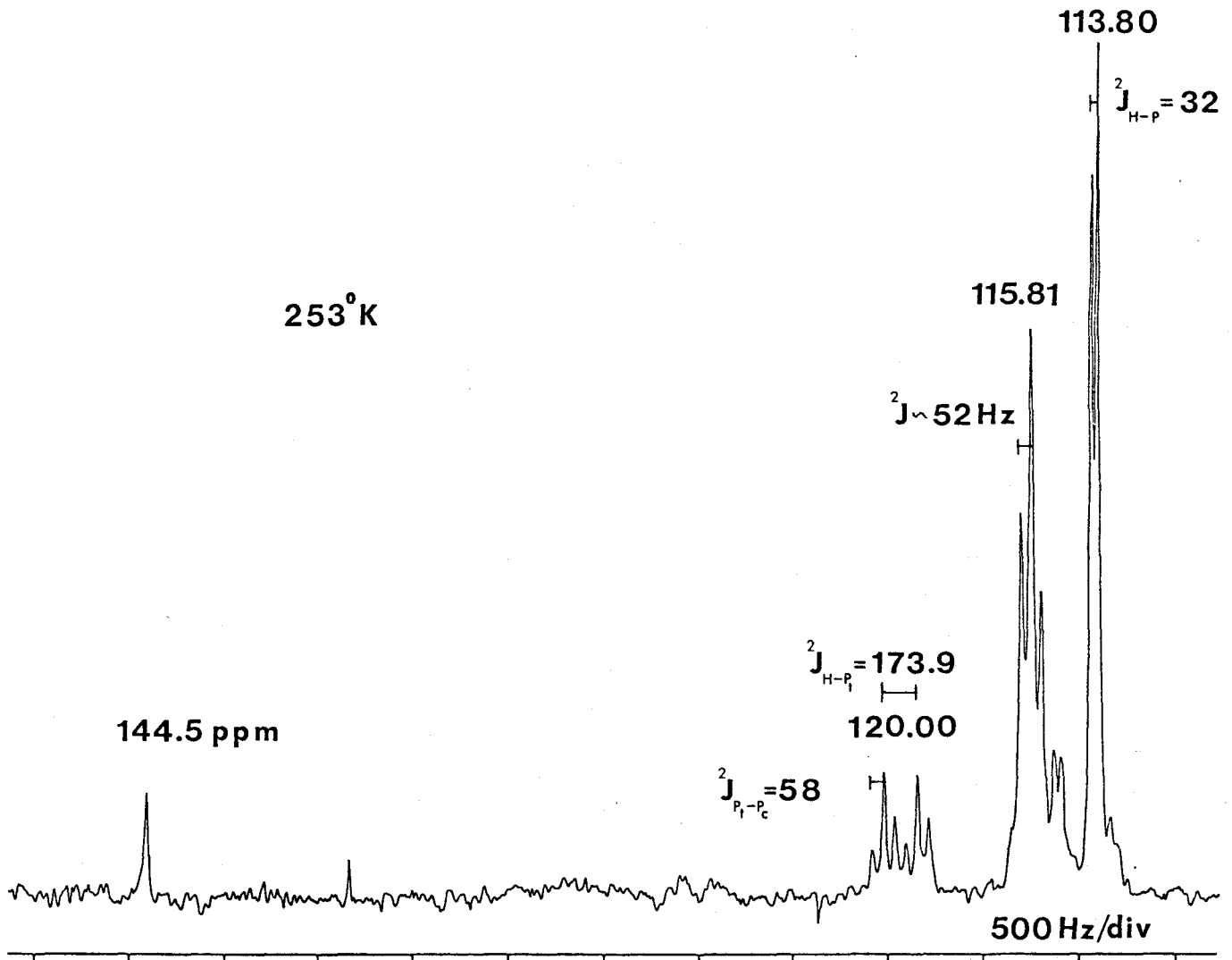


Figure 3.15:  $^{31}\text{P}$  NMR Spectrum (161.98 MHz) Downfield from 85%  $\text{H}_3\text{PO}_4$  of  $\text{HNiL}_4^+$  and  $\text{HNiL}_3^+$  at  $253^\circ\text{K}$  where  $\text{HNiL}_4^+$  is the Dominant Species.

253°K

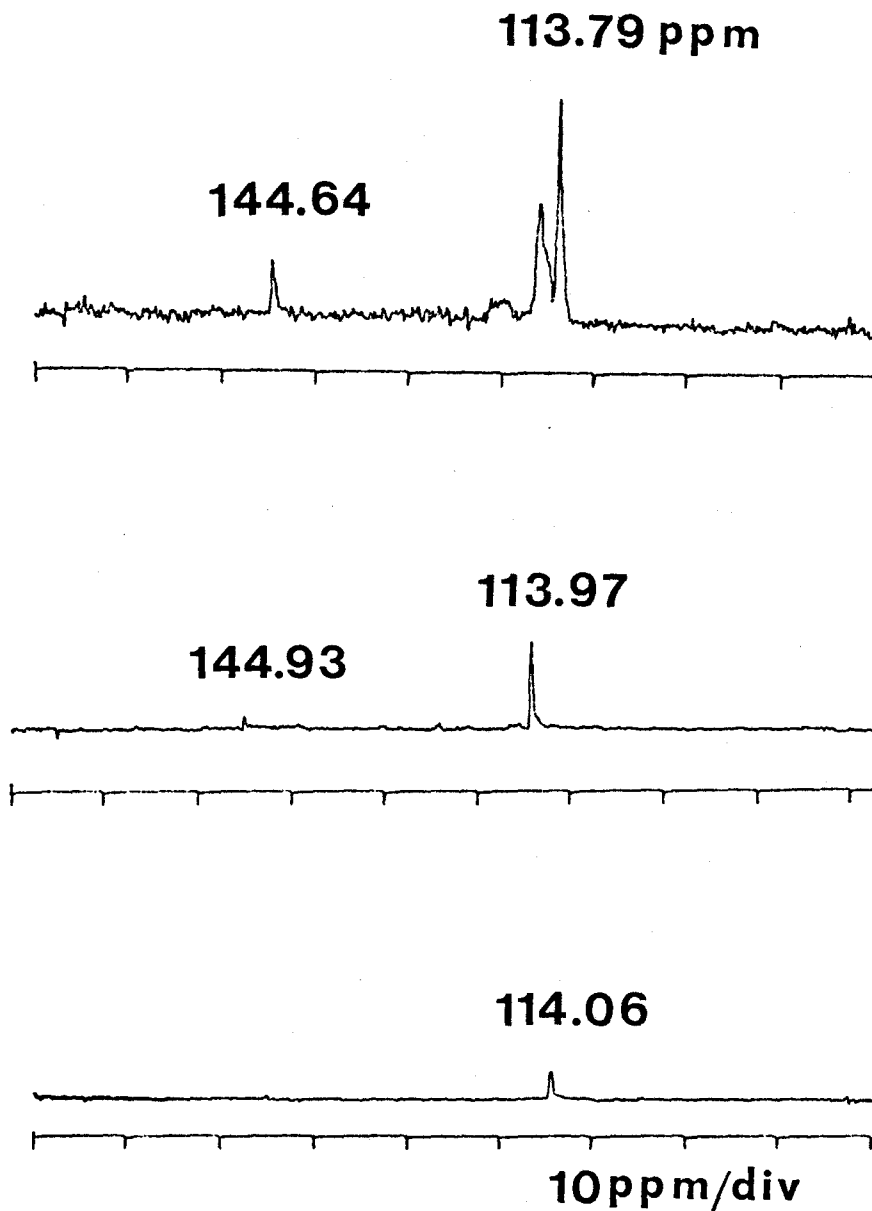


Figure 3.16:  $^{31}\text{P}$  NMR Spectra at 253°K (161.98 MHz) of  $\text{HNi}[\text{P}(\text{O}-p\text{-C}_6\text{H}_4\text{CH}_3)_3]^+$  and  $\text{HNi}[\text{P}(\text{O}-p\text{-C}_6\text{H}_4\text{CH}_3)_3]^+$  with excess free phosphite down-field from 85%  $\text{H}_3\text{PO}_4$ .



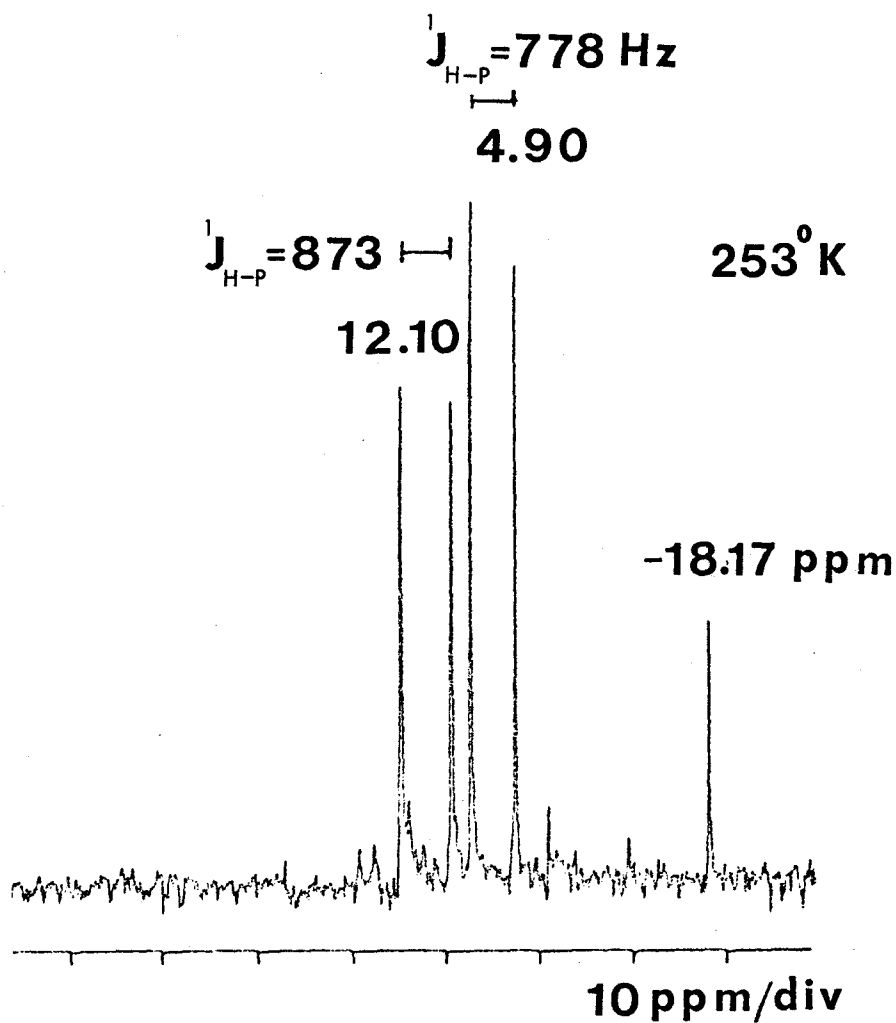
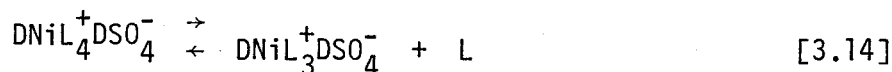
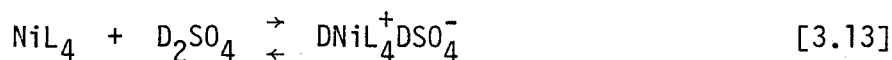


Figure 3.17:  $^{31}\text{P}$  NMR Spectra at  $253^\circ\text{K}$  (161.98 MHz) of the High Field Region of  $\text{HNiL}_4^+$ ,  $\text{HNiL}_3^+$  System.

in the above spectrum corresponds to  $O=P(O-p-C_6H_4CH_3)_3$ . The doublet centered at 12.10 ppm is due to  $HP^+(O-p-C_6H_4CH_3)_3$  which shows an upfield chemical shift and a decrease in P-H coupling constant when the acid concentration is increased. The other doublet centered at 4.90 ppm shows an increase in P-H coupling constant and a downfield chemical shift upon increasing the acid concentration, therefore, this doublet is characteristic of  $HP(O)(O-p-C_6H_4CH_3)_2$  (Figure 3.18). The results obtained are consistent with the work done by Hudson et al. (81).

Upon addition of deuterated  $H_2SO_4$  to the nickel phosphite system, two deuterated nickel phosphite compounds were formed that are analogous to the nickel hydrides.



When a 50/50 percent mixture of  $H_2SO_4/D_2SO_4$  was used to protonate the nickel complexes, the  $^{31}P$  NMR spectrum showed a triplet, each line of equal intensity centered in the middle of a large doublet in the acidified phosphite region of the spectrum. The triplet forms because  $^2H$  has a nuclear spin quantum number  $I = 1$ . The doublet was centered around 3.45 ppm with a  $^1J_{H-P} = 759$  Hz. This doublet is the same as the second doublet in the previous  $^{31}P$  spectrum centered at 4.90 ppm. The triplet was centered at 3.05 ppm with a  $^1J_{D-P} = 114-122$  Hz (Figure 3.19). There was a slight change in chemical shift to high field of about 0.4 ppm (40 Hz) when a proton was

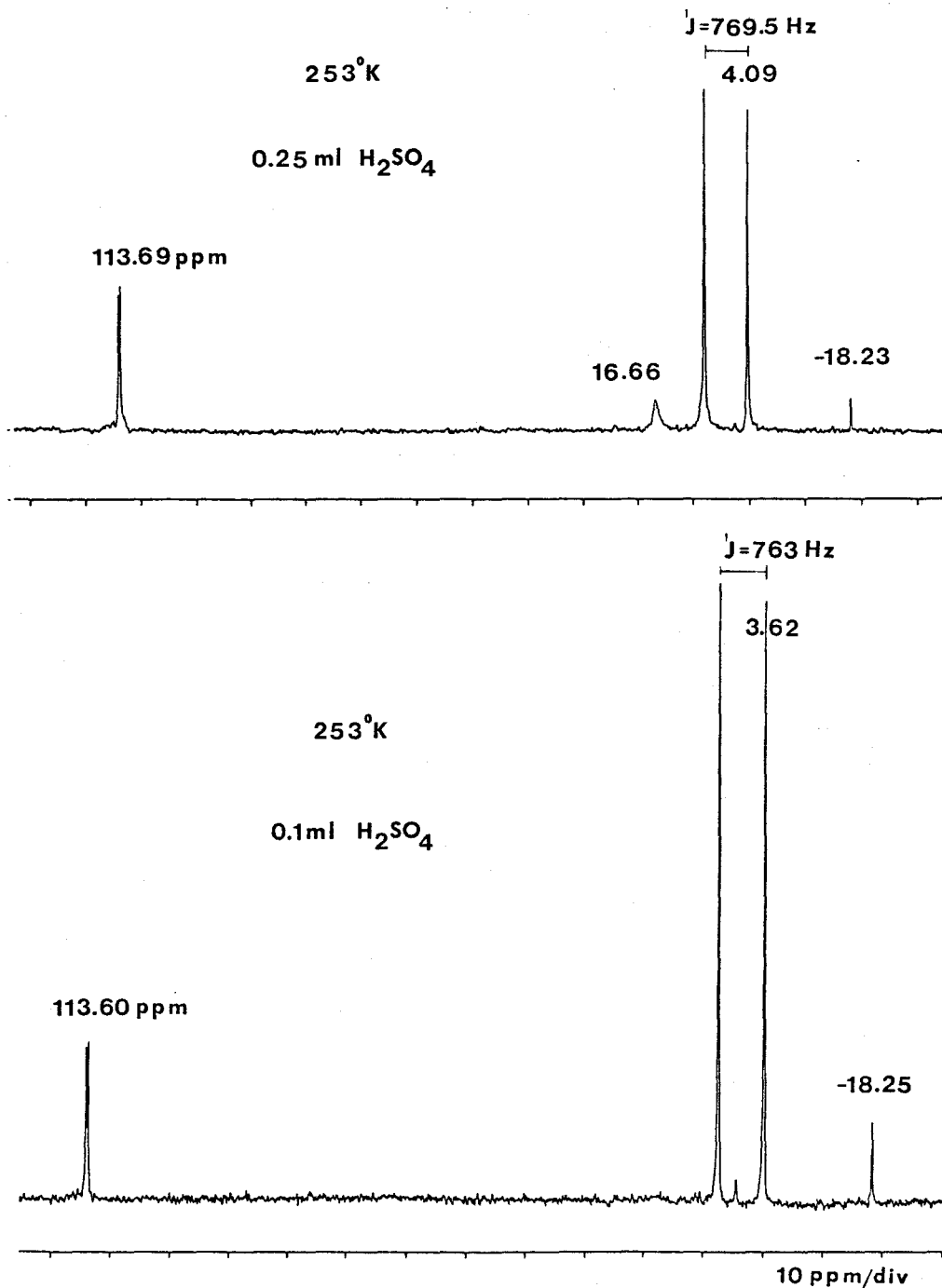


Figure 3.18:  $^{31}\text{P}$  NMR Spectra of  $\text{Ni}[\text{P}(\text{O-p-tolyl})_3]_4$ , Free Ligand and Various Concentrations of  $\text{H}_2\text{SO}_4$  Upfield from  $85\% \text{H}_3\text{PO}_4$  (161.98 MHz).

Cont...

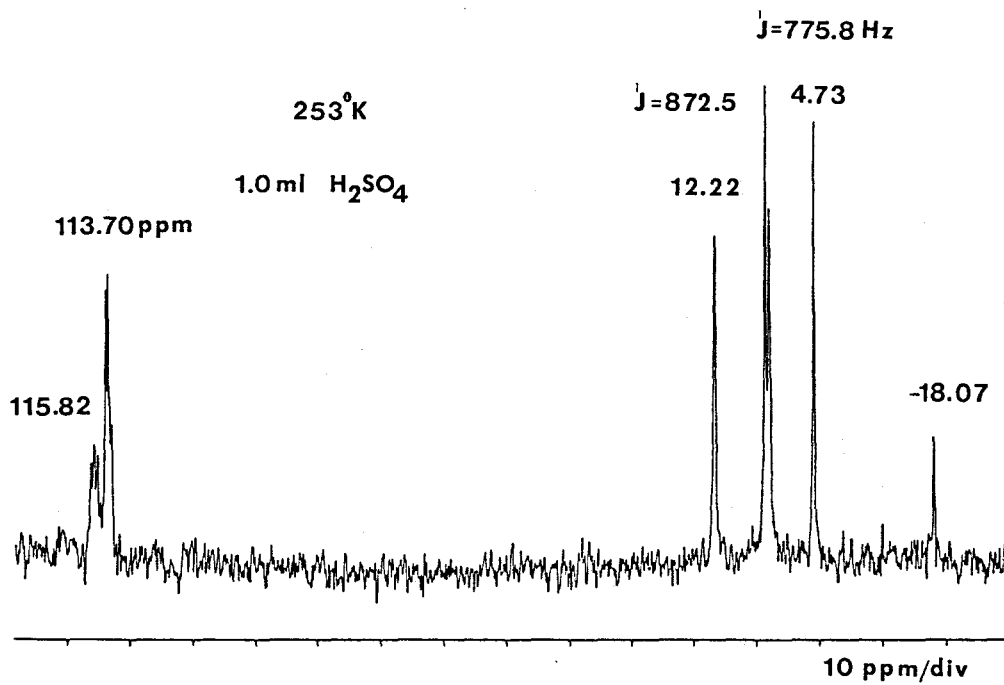
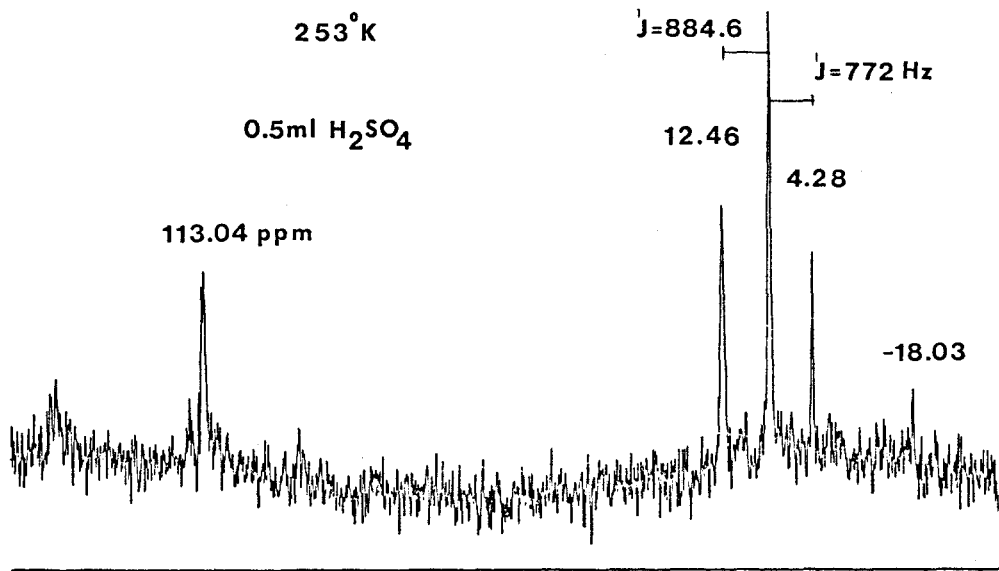


Figure 3.18: Cont.

substituted by deuterium. This shift is known as an isotope chemical shift. The  ${}^1J_{D-P}$  is approximately one-sixth of the  ${}^1J_{H-P}$ .

Deuterium ( $I=1$ ) NMR spectra were obtained on a system that contained  $Ni[P(O-p-C_6H_4CH_3)_3]_4$ ,  $D_2SO_4$ ,  $CH_2Cl_2$  and  $CD_2Cl_2$ . The deuterated sulphuric acid reacted directly with the nickel to give  $DNi[P(O-p-C_6H_4CH_3)_3]_4^{+}DSO_4^{-}$  and  $DNi[P(O-p-C_6H_4CH_3)_3]_3^{+}DSO_4^{-}$ . The low field region of the spectrum showed a  $CD_2Cl_2$  peak at 5.30 ppm and an acid peak at 9.54 ppm at 263°K. As the temperature was lowered and then raised again, these resonances increased in intensity and a deuterated aromatic resonance appeared at 6.60 ppm as shown in Figure 3.20.

In the high field region at -11.40 ppm and -13.50 ppm peaks appeared that belonged to the four and five-coordinated nickel deuterium compounds. The  $DNiL_3^{+}DSO_4^{-}$  species produced a high field resonance at -11.40 ppm which was similar to the hydride resonance shown in the  ${}^1H$  NMR spectrum. The multiplicities of these resonances are not very clear. As the temperature was increased to a point where the peaks began to be resolved, the system started to decompose and this prevented a well resolved multiplet from forming. The  $DNiL_3^{+}$  compound should ideally show a quartet with a  ${}^2J_{D-P} = [173-2(47)]/6 = 13$  Hz. At best, the resonance showed a doublet with a  ${}^2J_{D-P} = 12.8$  Hz. These two lines are the outer two peaks of the quartet. Since the  ${}^2J_{H-P_{trans}}$  and  ${}^2J_{H-P_{cis}}$  have opposite coupling constant signs, the last two peaks to form will appear in the middle of the multiplet (Figure 3.21).

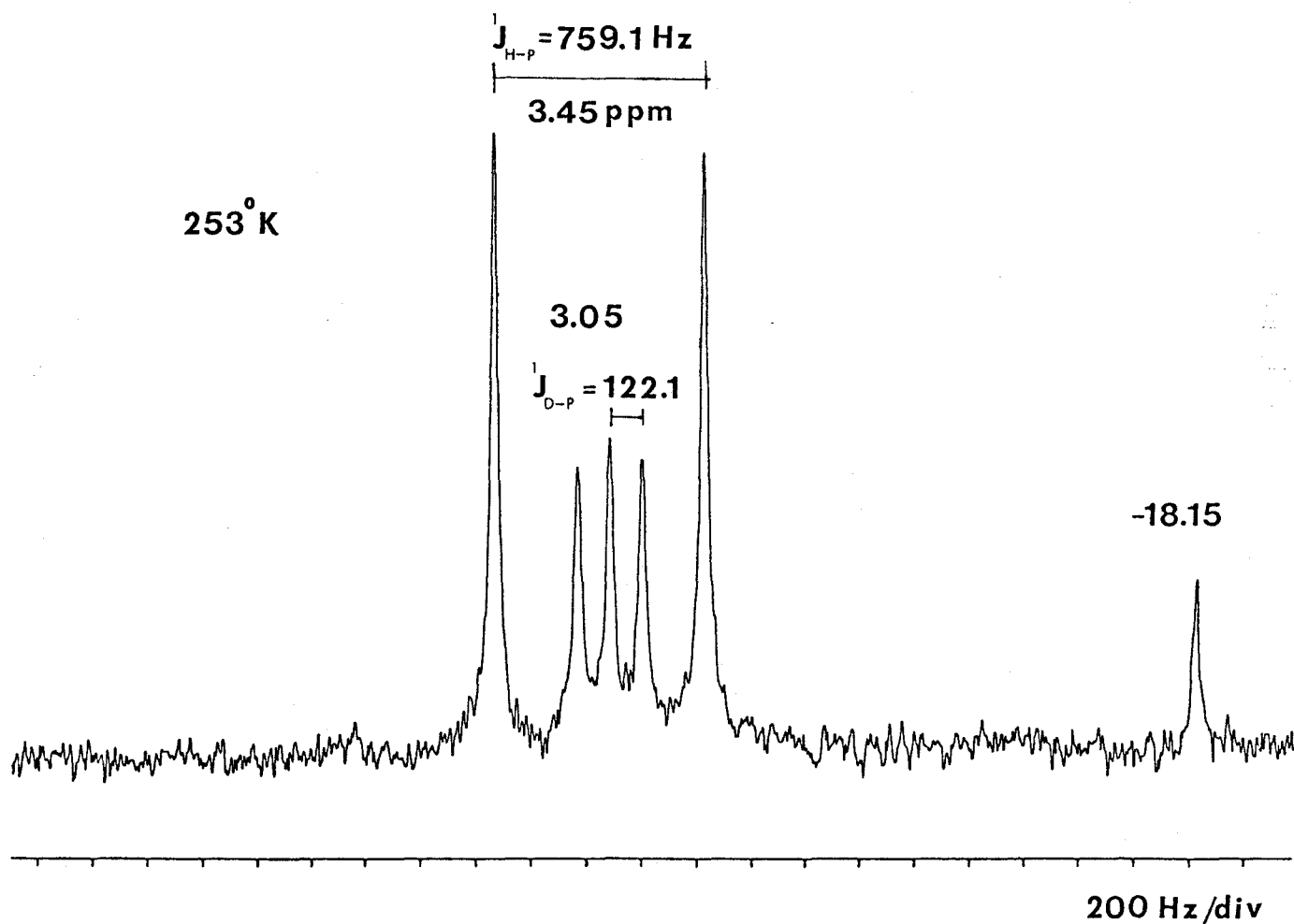


Figure 3.19:  $^{31}\text{P}$  NMR Spectrum of  $\text{HP}(\text{O})(\text{O-p-tolyl})_2$  and  $2\text{HP}(\text{O})(\text{O-p-tolyl})_2$  in  $\text{CH}_2\text{Cl}_2$  at  $253^\circ\text{K}$  Upfield from  $85\% \text{H}_3\text{PO}_4$  ( $101.26 \text{ MHz}$ ).

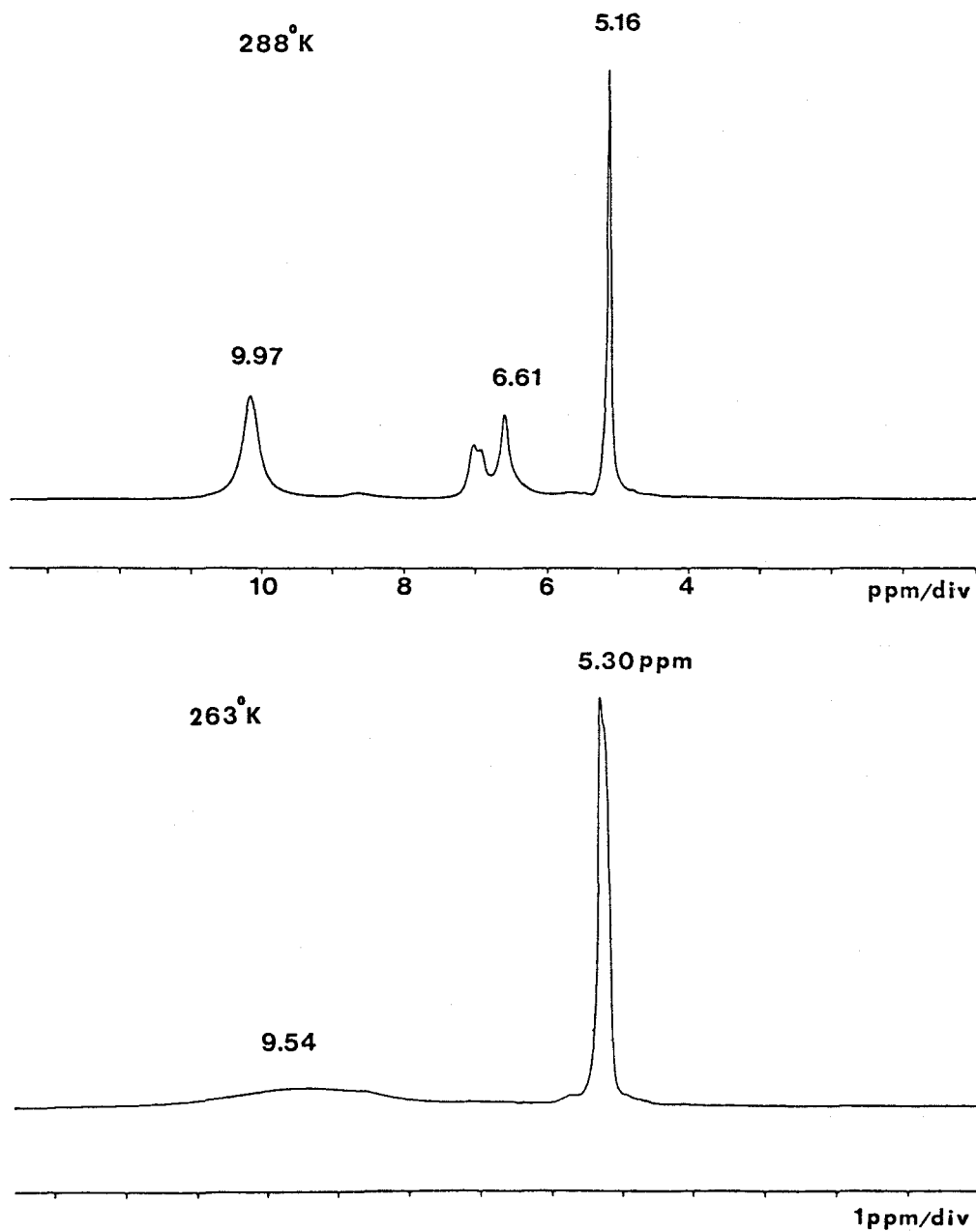


Figure 3.20: The  $^2\text{H}$  NMR Spectra Downfield from TMS of the  $\text{DNiL}_4^+$ ,  $\text{DNiL}_3^-$  System at  $263^\circ\text{K}$  and  $283^\circ\text{K}$  (38.39 MHz).

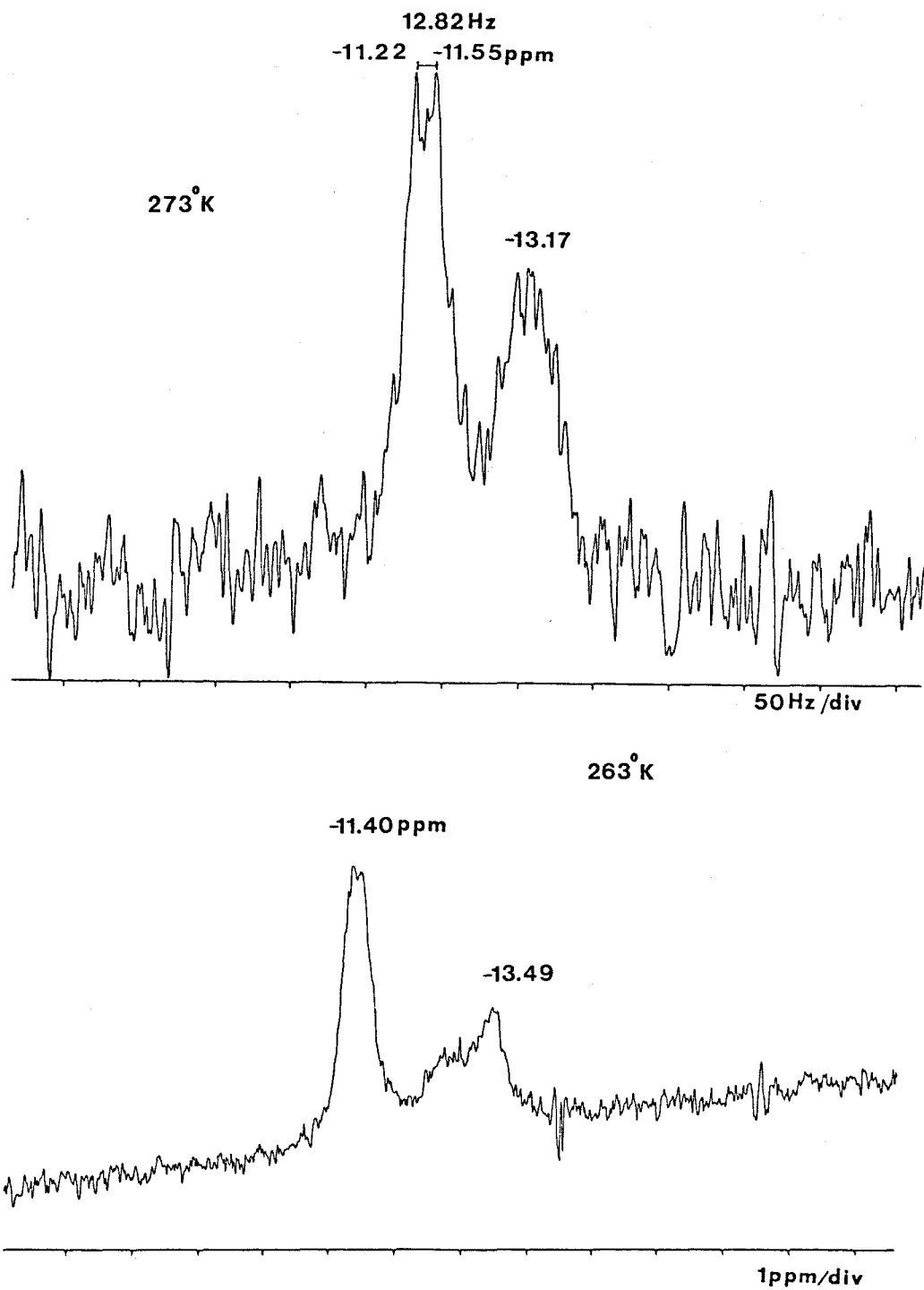


Figure 3.21: The  $^2\text{H}$  NMR Spectra of the Hydride Region of  $\text{DNiL}_4^+$  and  $\text{DNiL}_3^+$  at  $263^\circ\text{K}$  and  $273^\circ\text{K}$  (38.39 MHz).



The five-coordinate compound  $\text{DNiL}_4^+\text{DSO}_4^-$  was less resolved than the four-coordinate complex. This resonance should of appeared as a quintet but the best resolved spectrum only showed a doublet (Figure 3.22). Again, the temperature had a great effect on the lack of resolution.

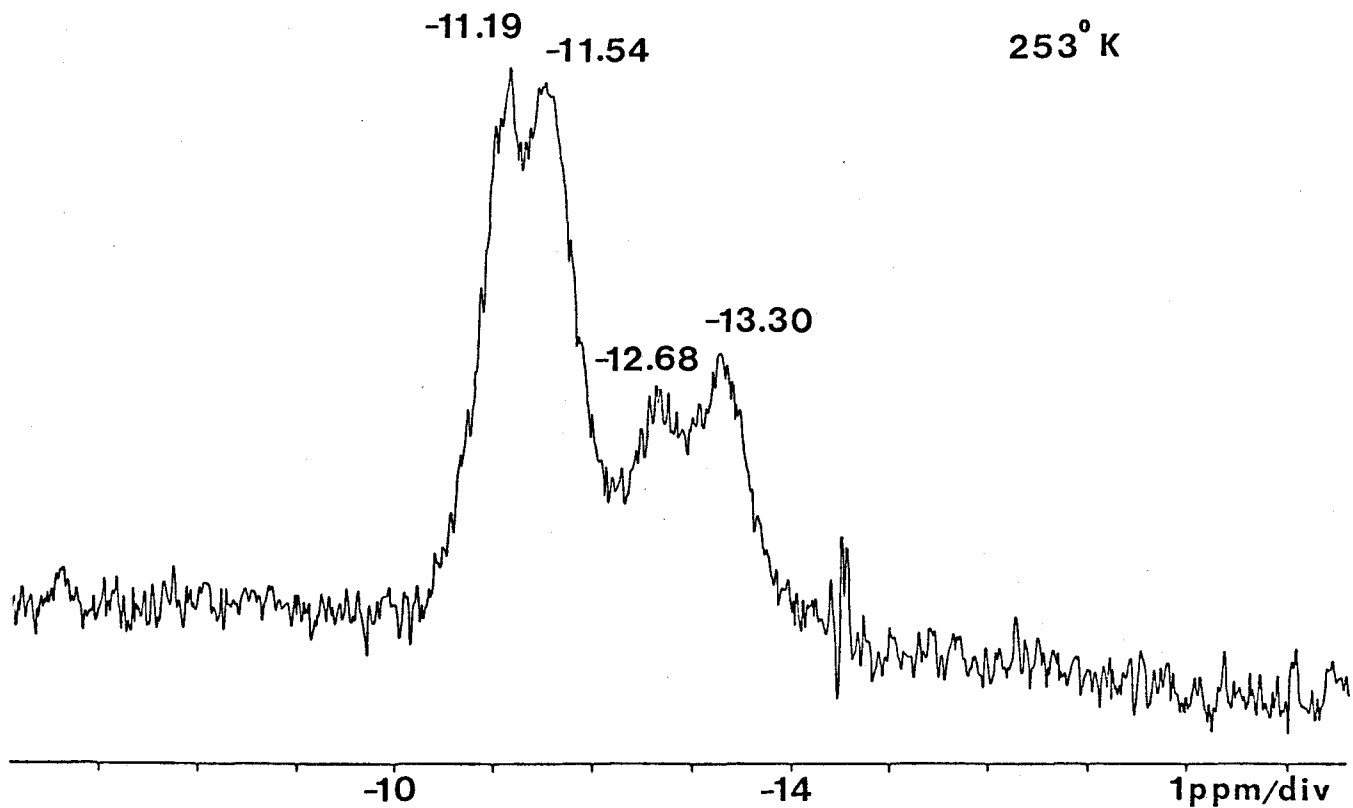


Figure 3.22: The  $^2\text{H}$  NMR Spectrum of the Hydride Complex  $\text{DNiL}_4^+$  at  $253^\circ\text{K}$  (38.39 MHz).

## CHAPTER FOUR

### Discussion of Variable-Temperature and Spin-Saturation Experiments

#### 4.1 Spin-Saturation Transfer

Spin-saturation transfer is one of the many double resonance NMR techniques available today.

In double resonance experiments, transitions between energy levels of a nuclear spin system in a polarizing static magnetic field  $H_0$  are measured in the presence of two oscillating magnetic fields,  $H_1$  and  $H_2$ .  $H_1$  is used to observe the resonance of one type of nucleus, and  $H_2$  is used to perturb a second nucleus. The method is based on a proposal made by Bloch in 1954.

The deduction of chemical lifetimes involved in a system by NMR is usually obtained from the line shapes. This method is suitable for very fast reactions (short lifetimes) with rate constants up to  $10^6 \text{sec}^{-1}$ , but small rate constants could not be studied.

In a series of papers Forsén and Hoffman (85,86,87) have described an alternative method using nuclear magnetic double resonance for the study of exchange rates in systems with longer lifetimes.

When a nuclear species X can move reversibly between two non-equivalent sites A and B, a disturbance of the magnetization of B (such

as a saturation with a large  $H_2$  field) can be detected at site A by a weak nonsaturating observing field  $H_1$ . The saturation of nuclei X at site B can move to site A by an exchange process, thereby decreasing the signal intensities observed for site A. The rate of decrease of the signal corresponding to site A and its new equilibrium intensity are governed by both the exchange lifetime ( $\tau$ ) and the spin-lattice relaxation time  $T_1$ . This is true provided that the spin-lattice relaxation time ( $T_{1A}$ ) in site A is not negligible compared with the lifetime ( $\tau_A$ ) of X in site A.

If the saturation of the resonance of X in B can be assumed to occur instantaneously at the time  $t=0$ , when the z magnetization  $M_z^A = M_0^A$ , then the decay of  $M_z^A$  is given by (86):

$$M_z^A = M_0^A \left[ \frac{\tau_{1A}}{\tau_A} \exp(-\tau/\tau_{1A}) + \frac{\tau_{1A}}{T_{1A}} \right] \quad [4.1]$$

The new equilibrium value of  $M_z^A$  is

$$M_z^A (t \rightarrow \infty) = M_0^A \left( \frac{\tau_{1A}}{T_{1A}} \right) \quad [4.2]$$

and  $M_z^A$  will attain its new equilibrium value through an exponential decay with the time constant  $\tau_{1A}$ .  $M_z^A$  is the instantaneous z magnetization of X at site A and  $M_0^A$  is the equilibrium z magnetization of X at site A. The ratio between the initial and final values of  $M_z^A$  gives the quotient  $T_{1A}/\tau_{1A}$ , and thus, by plotting the value of  $\log[M_z^A(t) - M_z^A(t \rightarrow \infty)]$  versus time, one obtains a straight line, the slope of which is  $-1/\tau_{1A}$ .  $\tau_{1A}$  is a time constant measuring the exponential decay of the resonance

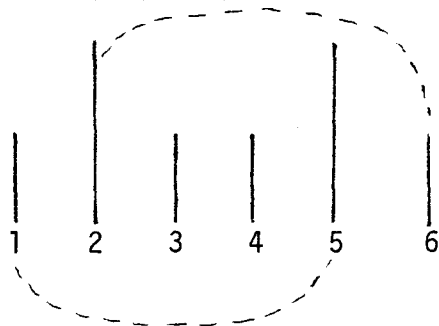
(site A).

From the known values of  $T_{1A}/\tau_{1A}$  and  $\tau_{1A}$ , the values of  $\tau_A$  and  $T_{1A}$  are obtained from the following equation:

$$\frac{1}{\tau_{1A}} = \frac{1}{\tau_A} + \frac{1}{T_{1A}} \quad [4.3]$$

where  $\tau_A$  is the lifetime of X at site A and  $T_{1A}$  is the spin-lattice relaxation time at site A.

The spin-saturation experiment was performed on the  $^1\text{H}$  NMR spectrum of the doublet of triplets characteristic of the four-coordinate nickel hydride cation,  $\text{HNi}[\text{P}(\text{O}-p\text{-C}_6\text{H}_4\text{CH}_3)_3]^+$  and are illustrated in Figure 4.1. If the lines in the low temperature limiting spectrum are labelled 1-6 as shown below, then the results of the double resonance experiments



are as follows. Upon irradiation of line 1 with a strong  $\text{H}_2$  field, line 5 decreases in intensity. Irradiation of peak 2 with a strong  $\text{H}_2$  field results in the disappearance of line 6. Also, irradiation of peak 3 does not cause a significant decrease in intensity of any of the other five lines. If a strong  $\text{H}_2$  field is applied at the center of lines 3 and 4, there is no visible decrease in intensity of any of the 6 lines.

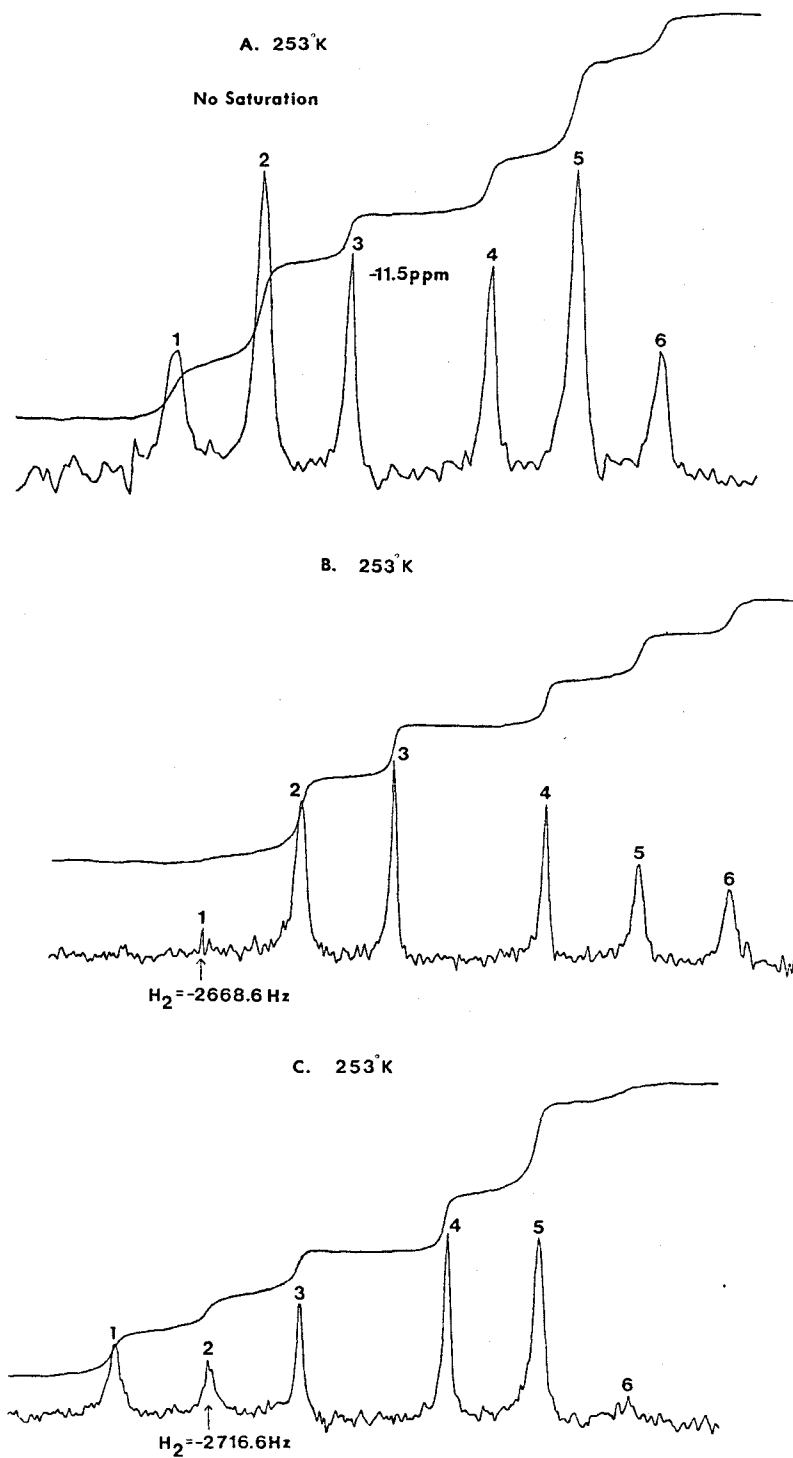


Figure 4.1: Spin-saturation Experiments of the Hydride Resonance of  $\text{HNi}[\text{P}(\text{O}-\text{C}_6\text{H}_4\text{CH}_3)_3]_3^+$  at 253°K in  $\text{CD}_2\text{Cl}_2$ . (250.13 MHz)

Cont...

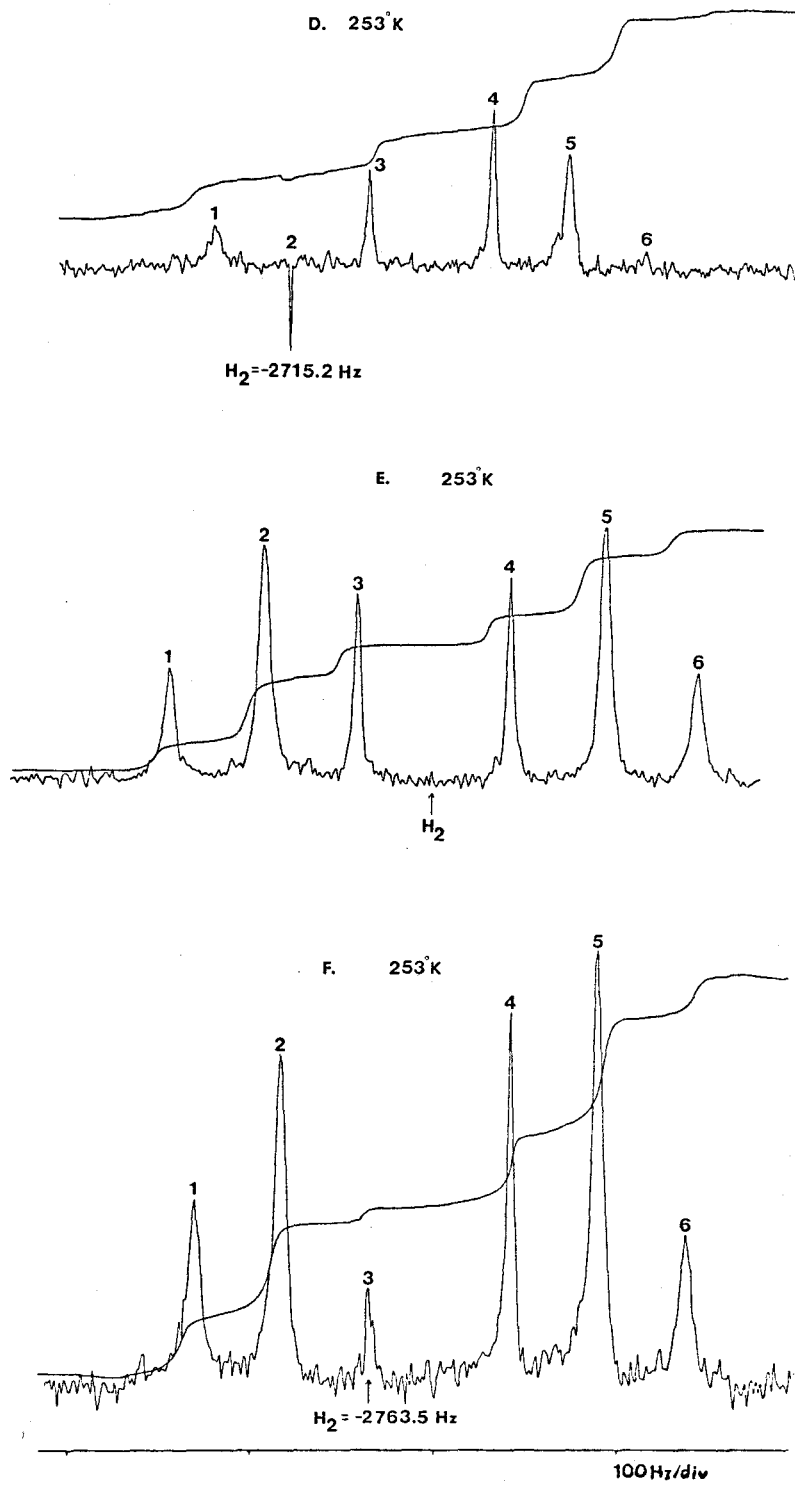


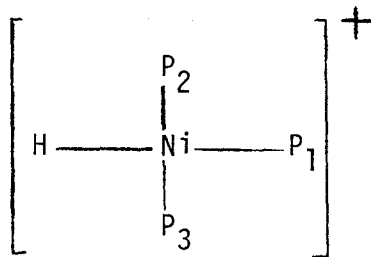
Figure 4.1: Cont..

The decrease in intensity of line 5 upon irradiation of line 1 shows that there is an exchange process occurring between these two sites. The saturation of site A (line 5) can transfer magnetization to site B (line 1) via the intramolecular exchange. Similarly, lines 2 and 6 are connected resulting in a decrease in intensity of line 2 when line 6 has been saturated with a strong  $H_2$  field.

A disturbance of the magnetization in line 3 by a saturating field does not affect any of the other lines present in the multiplet. Thus, line 3 is not involved in an exchange process with the other sites in the doublet of triplets. The same is true for line 4. These two lines remain sharp over the complete temperature range.

#### 4.2 The Intramolecular Exchange Process in $HNiL_3^+$

The hydride spectrum of the four-coordinate nickel hydride cation shows six lines in the form of a doublet of triplets. As explained previously this is characteristic of three phosphorus atoms in two different magnetic environments. One phosphorus atom  $P_1$  is trans to the proton and the other two phosphorus atoms  $P_2$  and  $P_3$  are cis to the hydride.



The rearrangement of  $P_1$  and  $P_2$  by  $90^\circ$  about an axis bisecting the  $P_3$ -hydride edge of the square plane gives a tetrahedral intermediate complex. A further rotation by  $90^\circ$  restores the square planar complex.



These three phosphorus atoms generate eight nuclear wavefunctions and the effect of a rearrangement on the spin wavefunctions is as follows:

flipping of two spins ( $P_1$  and  $P_2$ )

$\alpha_1 \alpha_2 \alpha_3$	→	$\alpha \alpha \alpha$	$\alpha \alpha \beta$	→	$\alpha \alpha \beta$
$\alpha \beta \alpha$	→	$\beta \alpha \alpha$	$\alpha \beta \beta$	→	$\beta \alpha \beta$
$\beta \alpha \beta$	→	$\alpha \beta \beta$	$\beta \alpha \alpha$	→	$\alpha \beta \alpha$
$\beta \beta \alpha$	→	$\beta \beta \alpha$	$\beta \beta \beta$	→	$\beta \beta \beta$

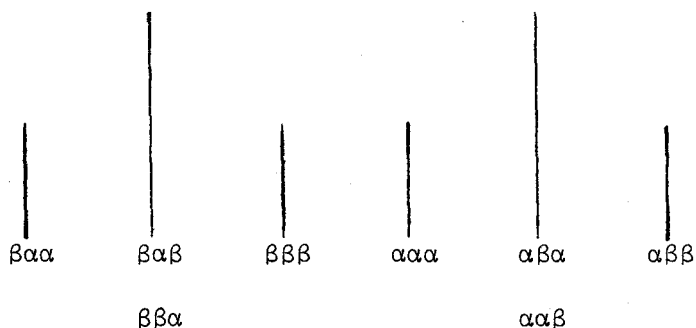
Since  $P_2$  and  $P_3$  are equivalent then  $\alpha \alpha \beta = \alpha \beta \alpha$  and  $\beta \alpha \beta = \beta \beta \alpha$ .

These pairs of wavefunctions are associated with the central lines of the triplets since two equivalent wavefunctions will produce an intensity of two.

The spin-spin coupling constants determine the exact assignments of the wavefunctions of the lines. If the two coupling constants  ${}^2J_{H-P_{trans}}$  and  ${}^2J_{H-P_{cis}}$  have the same sign, then  $\alpha \alpha \alpha$  and  $\beta \beta \beta$  will be assigned to the outer-most lines of the multiplet. But if the coupling constants are opposite in sign such as  ${}^2J_{H-P_{trans}} = \pm$  and  ${}^2J_{H-P_{cis}} = \mp$ , then the inner two lines will be assigned the nuclear spin wavefunctions  $\alpha \alpha \alpha$  and  $\beta \beta \beta$ .

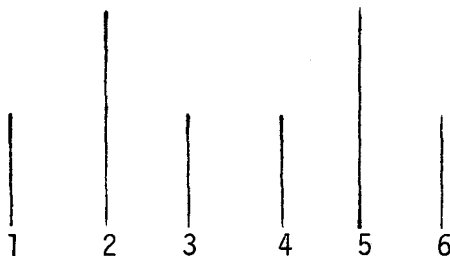
The two wavefunctions  $\alpha \alpha \alpha$  and  $\beta \beta \beta$  are unaffected by any permutation of the phosphorus spins and the spectral lines associated with these wavefunctions must therefore be unaffected by the exchange process. Inspection of the hydride temperature-dependent spectra shows that the inner lines of the triplets satisfy this condition. If it is assumed that

${}^2J_{\text{H-P trans}}$  is positive and  ${}^2J_{\text{H-P cis}}$  is negative then the labelling of the lines from low field to high field is as follows:



If  ${}^2J_{\text{H-P cis}}$  is positive and  ${}^2J_{\text{H-P trans}}$  is negative then the labelling of the lines in the multiplet is completely opposite but the conclusions drawn are unaffected.

If the lines in the low temperature spectrum are labelled 1-6,



then the results stated above for the effect of rearrangement on the nuclear spin wavefunctions produces the following deductions:

1) There is a 100% probability that line 1 will exchange with line 5 during a rearrangement and a 0% probability that it will exchange with any other line.

2) There is a 50% probability that line 2 will exchange with line 6 during rearrangement and a 0% probability that it will exchange with any other line.

3) There is a 0% probability that line 3 will exchange with any other line. Similarly line 4 of the other triplet will not exchange with any other line.

4) Similar results apply to line 5 exchanging with line 1 and line 6 exchanging with line 2.

The rearrangement process discussed above is only one possible exchange process. Any process that interchanges the trans ligand with a cis ligand leads to identical predictions with regard to NMR spectra. A tetrahedral intermediate is not necessary to obtain the above results. The only information that the NMR spectra give is that the rearrangement is by an intramolecular exchange process and not an intermolecular process.

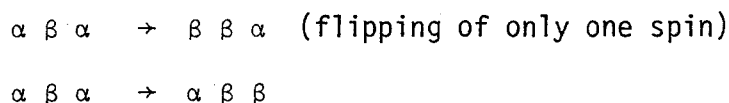
The above conclusions show that raising the temperature from the slow exchange limiting spectrum should not broaden the inside lines of the triplets and should broaden the outside lines twice as rapidly as the central lines of the triplets. This is shown in the temperature-dependent spectra in section 4.3, Figure 4.2.

Quantitative analysis of the spin-saturation spectra are straightforward. Since only the pairs of lines 1 and 5, and 2 and 6 are exchanging and the frequency separations and intensities of the two pairs are

identical, the exchange is only a simple two site exchange problem which can be treated using the standard formula obtained from Pople, Schneider and Bernstein (88). For a two site slow exchange process the spectrum will consist of two distinct signals in the vicinity of the frequencies  $\omega_A$  and  $\omega_B$ .  $G$  is the total complex moment given by  $G = G_A + G_B$ . If the radio frequency  $\omega$  is close to  $\omega_A$  and therefore, far away from  $\omega_B$ ,  $G_B$  is effectively zero and the solution of the complex moment becomes

$$G \approx G_A \approx -i\gamma H_1 M_0 \frac{P_A \tau_A}{1 + \alpha_A \tau_A} \quad [4.4]$$

There is also the possible relaxation of a phosphorus spin (a  $T_1$  process) that can occur along with the exchange of spins (88).



This is seen in the spin saturation experiment as a slight decrease in intensity of adjacent lines and other lines that usually are not affected by double resonance experiments. This spin flipping of only one spin state is also shown in the ratio of peak heights at the low temperature limiting spectrum for  $\text{HNiL}_3^+$ . The triplets should be in the ratio of 1:2:1 but the ratio is actually less (1:1.8:1).

A decrease in intensity of adjacent peaks can also be due to the fact that the coupling constants between adjacent lines are less than 50Hz (47 to be exact). If coupling constants are less than 100Hz, the spin saturation transfer will affect adjacent peaks along with the de-

sired site. This is more pronounced when  $J < 50\text{Hz}$ .

#### 4.3 The Temperature Dependence of $\text{HNiL}_3^+$

The formation of the four-coordinate nickel hydride complex  $\text{HNi}[\text{P}(\text{O-p-C}_6\text{H}_4\text{CH}_3)_3]_3^+$ , and the identification of this species by the hydride resonance at  $-11.0\text{ ppm}$  in the proton spectra has been discussed in the previous chapters. An intramolecular rearrangement mechanism of  $\text{HNiL}_3^+$  was illustrated by the use of variable-temperature experiments. The geometry of  $\text{HNiL}_3^+$  is characteristic of a square planar complex with two types of magnetically inequivalent phosphorus atoms observed at the low limiting temperature, one trans and two cis to the hydride. A fast rearrangement of these three phosphorus atoms on the NMR time scale will result in only one type of phosphorus and should show a quartet for the high field hydride resonance. This is not the situation observed at  $283\text{-}288^\circ\text{K}$ . The resonance appears as a doublet. Upon raising the temperature higher than  $288^\circ\text{K}$ , the doublet is expected to form a quartet with the two new lines appearing in between the present doublet. Unfortunately, raising the temperature results in rapid decomposition of  $\text{HNiL}_3^+$ . The high temperature enhances the fast intramolecular exchange. The two bond  $^1\text{H}\text{-}^{31}\text{P}$  coupling constant is  $78\text{Hz}$  which is an average of the cis and trans  $^1\text{H}\text{-}^{31}\text{P}$  couplings observed at low temperature (see Figure 4.2 at  $283^\circ\text{K}$ ).

As the temperature is lowered to  $273^\circ\text{K}$ , two broad peaks begin to appear, one on each side of the doublet already present. Lowering the

temperature has slowed down the intramolecular exchange process so that the three phosphite ligands are not magnetically equivalent (see Figure 4.2 at 273°K). Upon lowering the temperature further; at five degree intervals, these two broad peaks increase in intensity and sharpen. Simultaneously, two more lines are observed which go on to eventually form the doublet of triplets present at 203°K. With lowering the temperature the chemical shift of the multiplet moves downfield by a maximum of 0.3 ppm. This is characteristic of variable-temperature dependence. As the temperature is lowered to 183°K, the lines begin to broaden again due to increasing viscosity of the solution. Figure 4.2.

The decomposition of  $\text{HNiL}_3^+$  is evident by the liberation of  $\text{H}_2$  gas. If deuterated sulphuric acid is used to make  $^2\text{HNiL}_3^+$ ; the  $^2\text{H}$  NMR spectrum obtained at a high temperature, should show a quartet with reduced couplings. The  $^2\text{H}$ - $^{31}\text{P}$  coupling constants are approximately one-sixth ( $200/30.7=6.51$ ) the coupling constants of  $^1\text{H}$ - $^{31}\text{P}$  since the ratio of the magnetogyric ratios of  $^2\text{H}$ :  $^1\text{H}$  is 1:6.51. The estimated  $^2\text{H}$ - $^{31}\text{P}$  coupling constant is  $(174-2(48))/6.51=12\text{Hz}$ . This means that the temperature will not have to be as high in the  $^2\text{H}$  spectrum to obtain a well resolved quartet. The best resolution obtained for this resonance was a doublet centered at -11.38 ppm with  $^2J_{^2\text{H}-^{31}\text{P}} = 12.82\text{Hz}$  at 273°K as illustrated in Figure 3.21. At 288°K (Figure 4.3) a possible quartet was observed for the deuteride resonance but the signal to noise level was very poor and upon scanning for a longer period of time the complex totally decomposed.

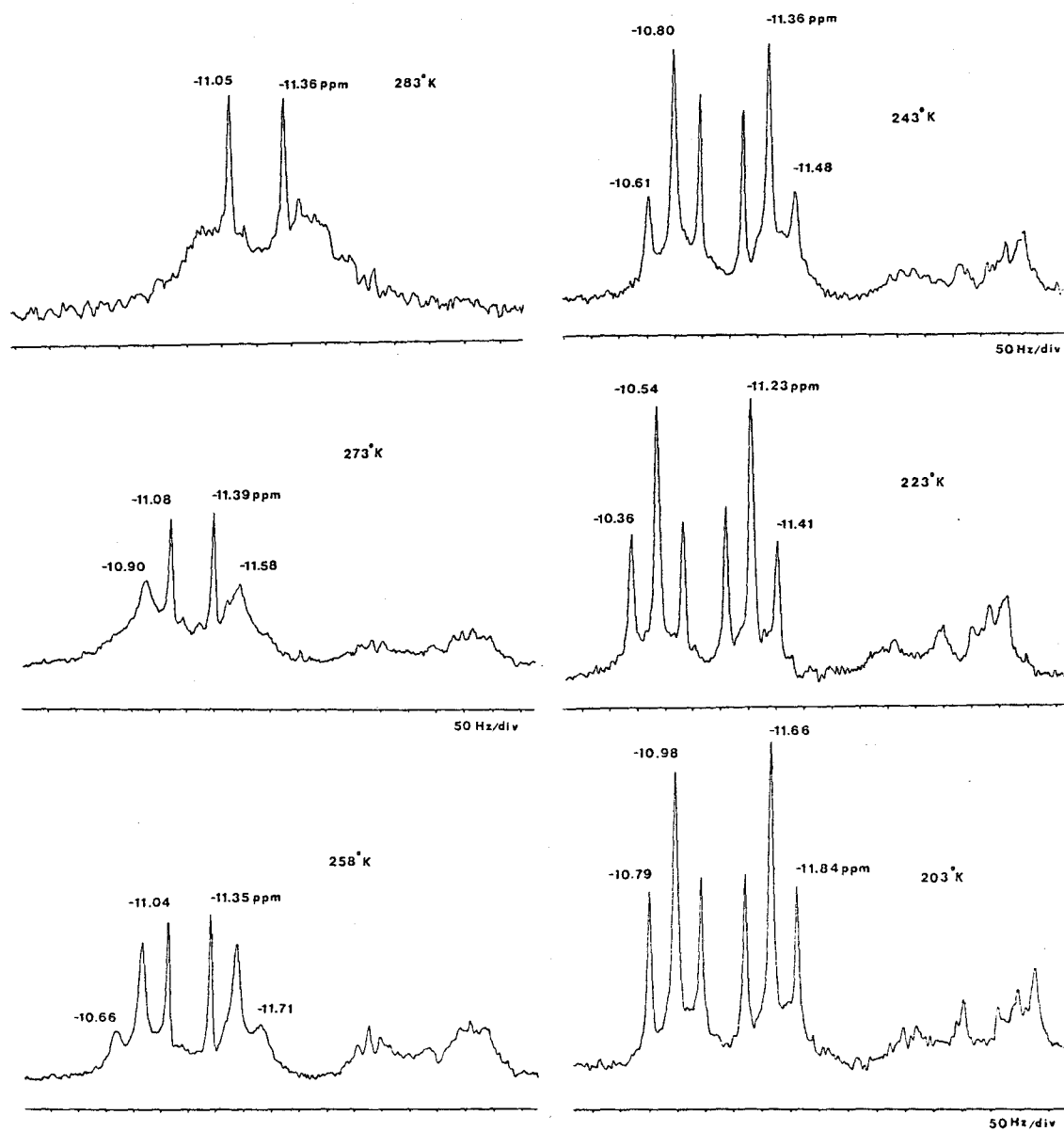


Figure 4.2: The  $^1\text{H}$  NMR Variable-Temperature Spectra of the Hydride Resonance of  $\text{HNi}[\text{P}(\text{O}-p\text{-C}_6\text{H}_4\text{CH}_3)_3]_3^+$  (250.13 MHz).

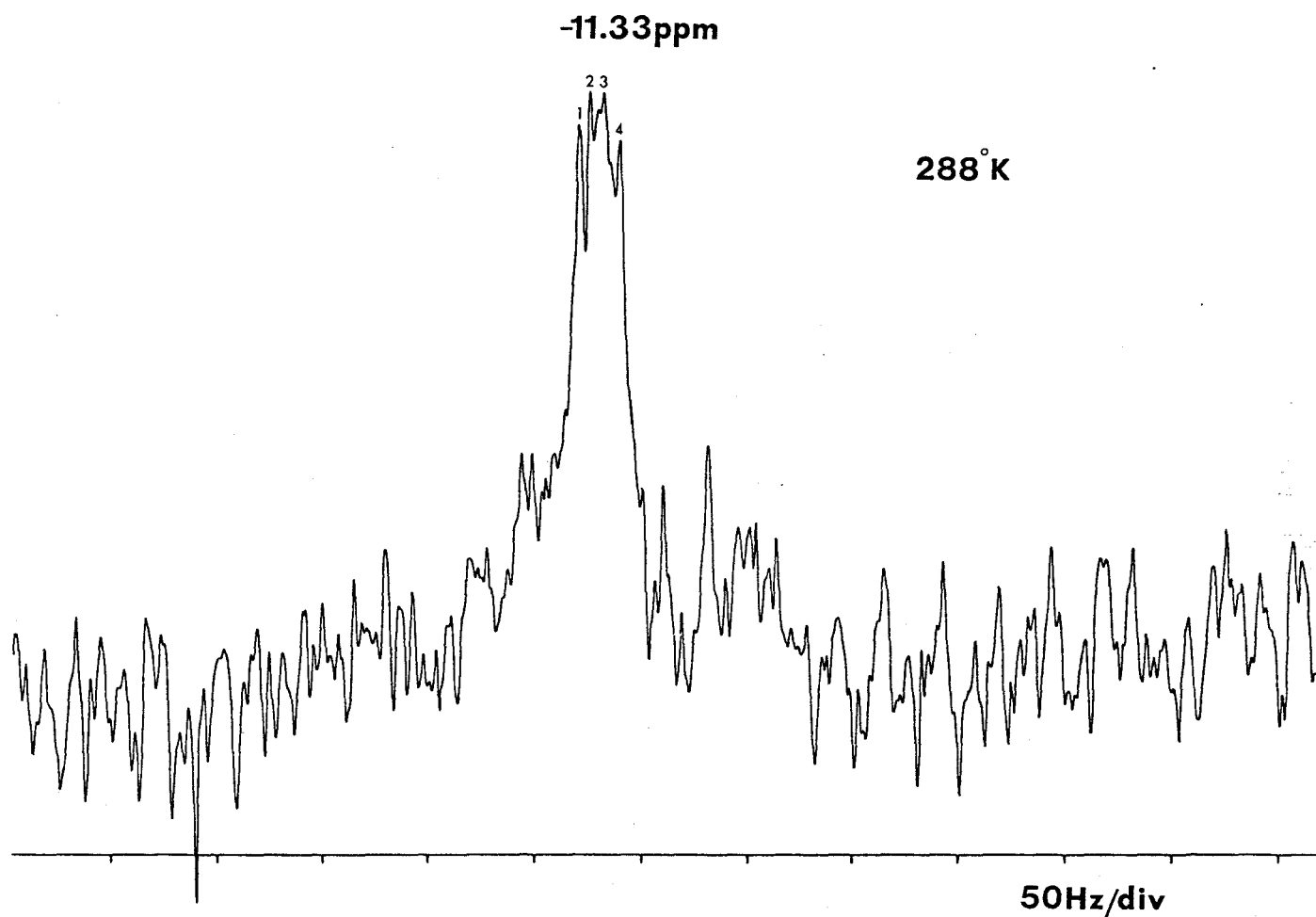


Figure 4.3:  $^2\text{H}$  NMR Spectrum of  $^2\text{H NiL}_3^+$  at  $288^\circ\text{K}$  (38.39 MHz)



Variable temperature work was also done on the phosphorus nucleus. The low temperature limiting spectrum has already been discussed in Chapter 3 and is illustrated in Figure 3.14 and 3.15. The high temperature limiting spectrum of  $\text{HNi}[\text{P}(\text{O}-p\text{-C}_6\text{H}_4\text{CH}_3)_3]_3^+$  is expected to show a doublet. The three equivalent phosphorus atoms are coupled to one proton. This doublet was expected to appear somewhere between the doublet of triplets and the triplet which were due to the trans  $^{31}\text{P}$  and cis  $^{31}\text{P}$  atoms respectively. Again, the higher temperature limiting spectrum was not well resolved showing a broad resonance at 114.4 ppm.

Variable-temperature NMR experiments were not performed on the five-coordinate complex  $\text{HNi}[\text{P}(\text{O}-p\text{-C}_6\text{H}_4\text{CH}_3)_3]_4^+$ . From previous variable-temperature studies using triethyl phosphite the system showed a more rapid intramolecular exchange which prevented the observation of the low temperature limiting spectrum. The theoretical low limiting spectrum is a triplet of triplets assuming the complex is in a trigonal bipyramidal geometry. The hydride is coupled to two equatorial phosphorus atoms forming a triplet which is further split into a triplet of triplets by two axial phosphorus atoms. The spectrum observed at 253°K is the high temperature limiting spectrum where all phosphorus atoms are magnetically equivalent via the intramolecular exchange. Since the slow exchange limit was not obtained for the  $\text{HNi}[\text{P}(\text{O}-p\text{-C}_6\text{H}_4\text{CH}_3)_3]_4^+$  complex or any other five-coordinated hydride, the activation parameters are approximate. The calculation of the activation energy is only a limit of <5Kcal/mole for the intramolecular rearrangement.

#### 4.4 Enthalpy and Entropy of Activation for the $\text{HNiL}_3^+$ System

Since the central lines in the  $^1\text{H}$  spectra of the doublet of triplets are unaffected by the exchange, they provide a calibration to allow for variation of the non-exchange broadened line width with temperature. Figure 4.4 shows a set of calculated spectra which are compared with the experimental results. The calculated spectra were obtained using the computer program DNMR 3 (89a).

The variable temperature  $^{31}\text{P}$  spectra of the four-coordinated hydride is shown in Figure 4.5 along with the simulated  $^{31}\text{P}$  spectra. The temperature dependence in the phosphorus spectra show that all the lines in the spectrum are affected by the exchange process. At 273°K the resonances of the four and five-coordinated nickel hydrides have started to overlap, which broadens the peak at 115.18 ppm. This is not reproduced in the simulated spectrum since the five-coordinate hydride is not involved in the simulation. The activation parameters obtained from the proton spectra, together with the chemical shift difference and  $J(\text{PP})$  obtained from the low temperature  $^{31}\text{P}$  spectrum were used to calculate the simulated spectra shown in Figure 4.5.

The agreement between observed and calculated spectra is reasonably good. There is a small doublet slightly upfield from the triplet at 233°K and 253°K which was not simulated by the DNMR 3 program. This weak resonance has not been assigned, but it may be related to the five-coordinated species.

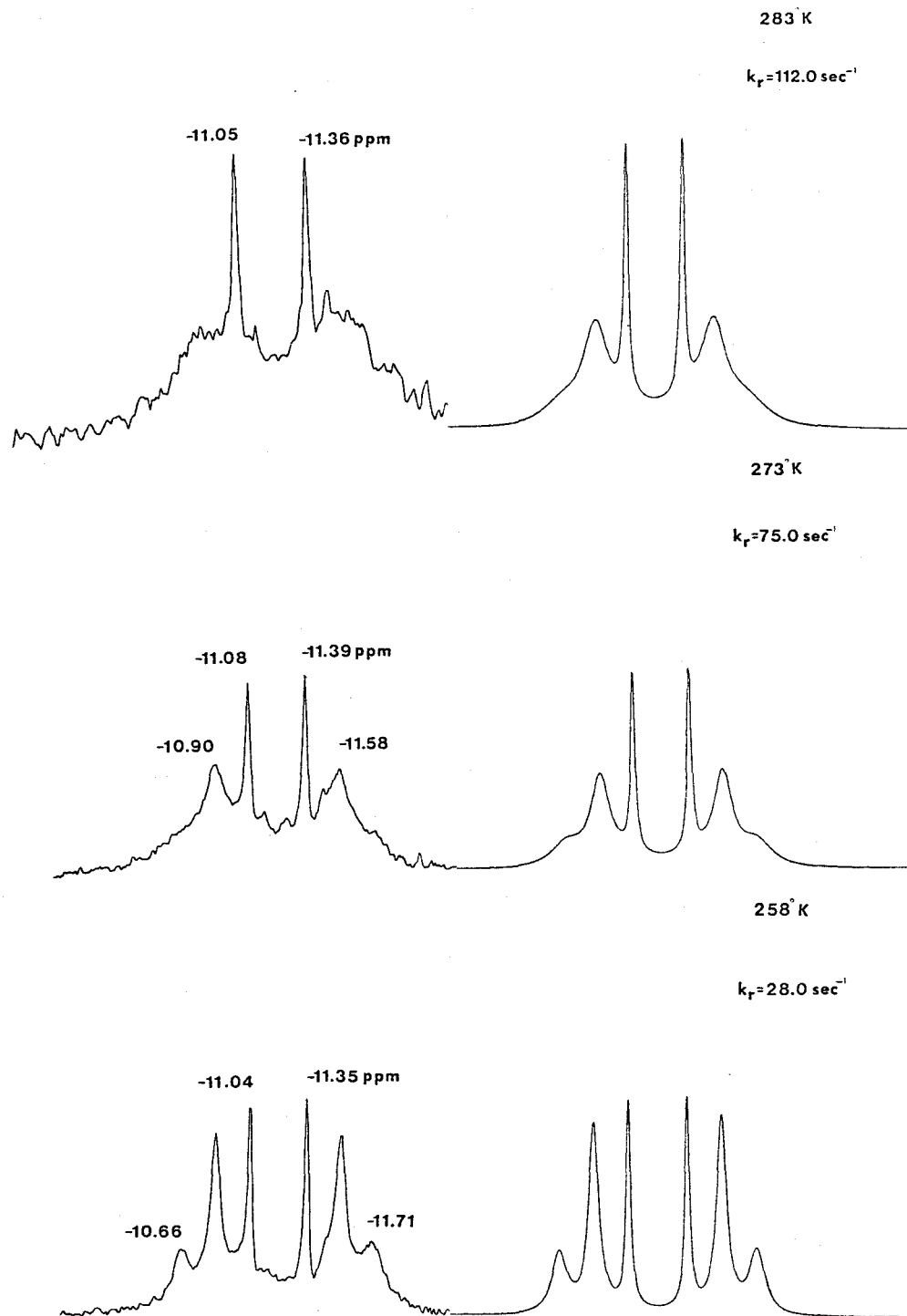


Figure 4.4: The  $^1\text{H}$  Simulated and Experimental Spectra of the Hydride Resonance of  $\text{HNi}[\text{P}(\text{O}-p\text{-C}_6\text{H}_4\text{CH}_3)_3]_3^+$  (250 MHz)

Cont..

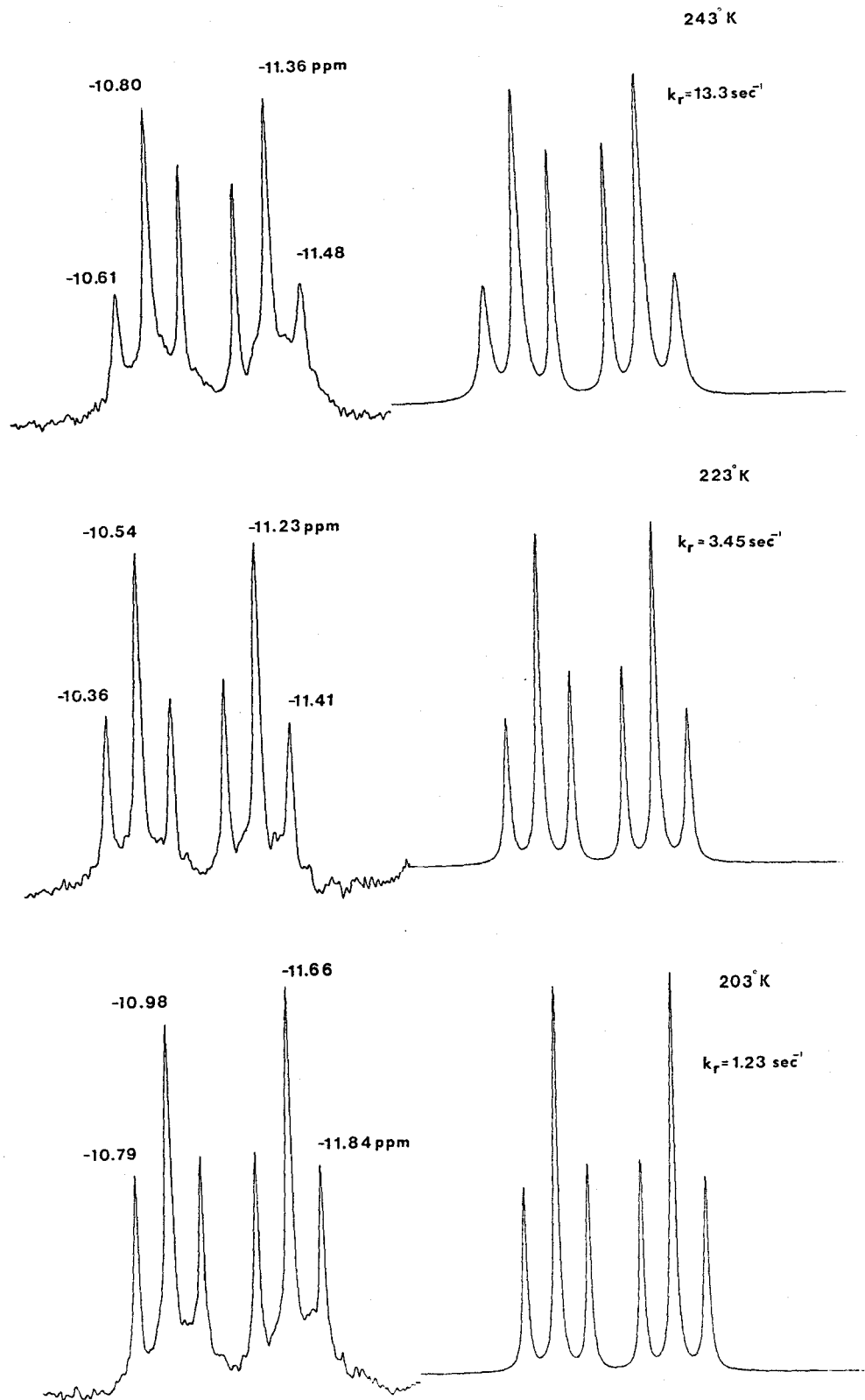


Figure 4.4: Cont..

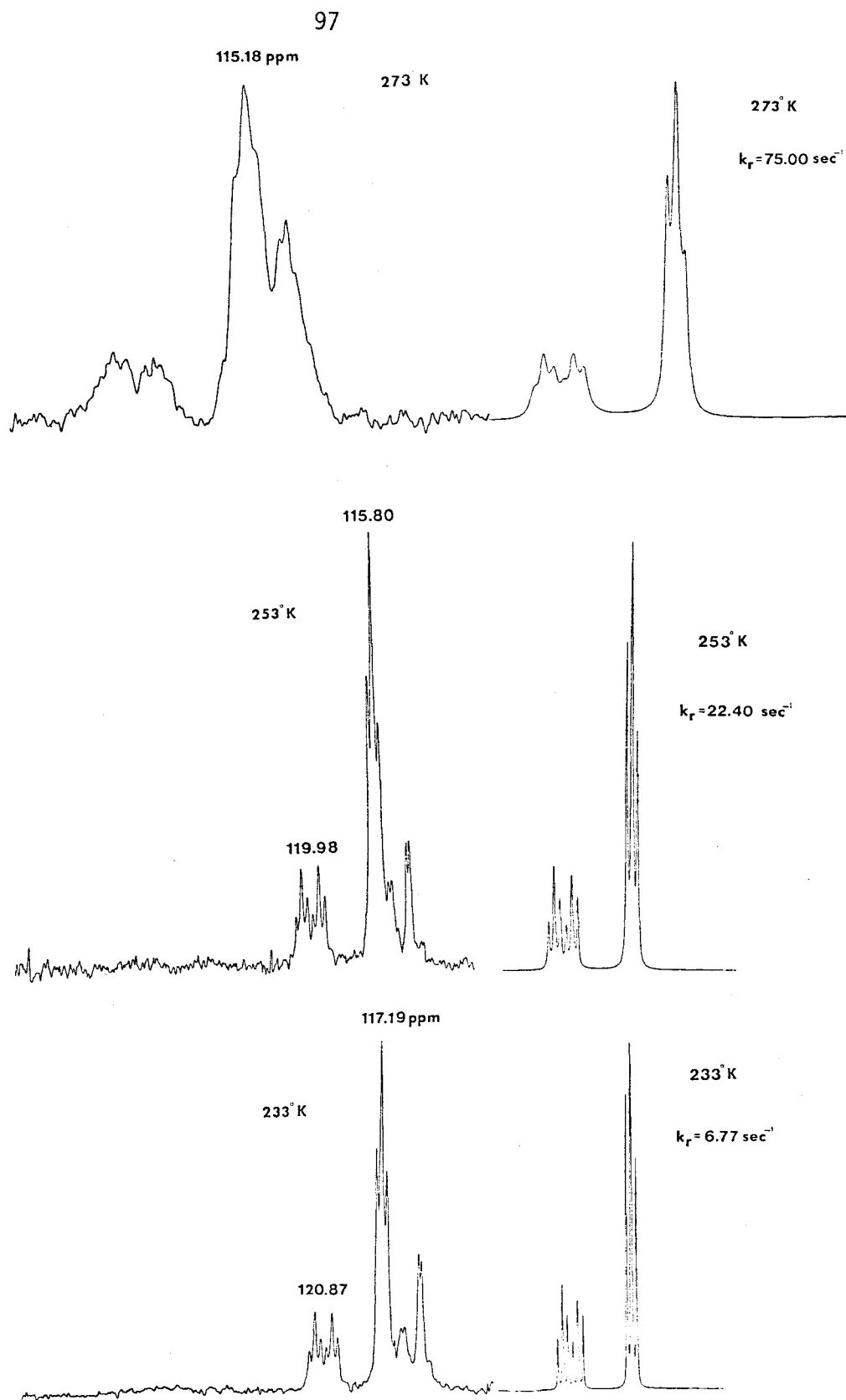


Figure 4.5: The  $^{31}\text{P}$  Simulated and Observed Spectra of  $\text{HNi}[\text{P}(\text{O}-p\text{-C}_6\text{H}_4\text{CH}_3)_3]_3^+$  at 161.92 MHz.

The activation energy of a reaction can be calculated using two different methods. The simplest approach involves solving the Arrhenius Activation Energy Equation which is stated as follows:

$$k_r = Ae^{-E_a/RT} \quad [4.5]$$

where  $k_r$  is the first order rate constant, A is the pre-exponential or frequency factor (a constant),  $E_a$  is the activation energy, R is the gas constant and T is the temperature in °K. Taking the natural logarithm gives

$$\log k_r = \log A - \frac{E_a}{2.303RT} \quad [4.6]$$

A plot of  $\log k_r$  versus  $1/T$  should produce a straight line of slope  $-E_a/2.303R$  ( $R=1.98717 \text{ cal K}^{-1} \text{ mole}^{-1}$ ) which is shown in Figure 4.6.

The first order rate constants corresponding to the different temperatures are listed in Table 4.1. The rate constants for the four lowest temperatures are not included in the calculations since they were very difficult to fit. Also calculated rate constants were obtained from the best fit line using linear regression.

The other method involves the Eyring equation [4.14] which is derived from the activated complex theory. The Eyring equation may be used to calculate the enthalpy and entropy of activation from the first order rate constants obtained at different temperatures. An elementary first order reaction is

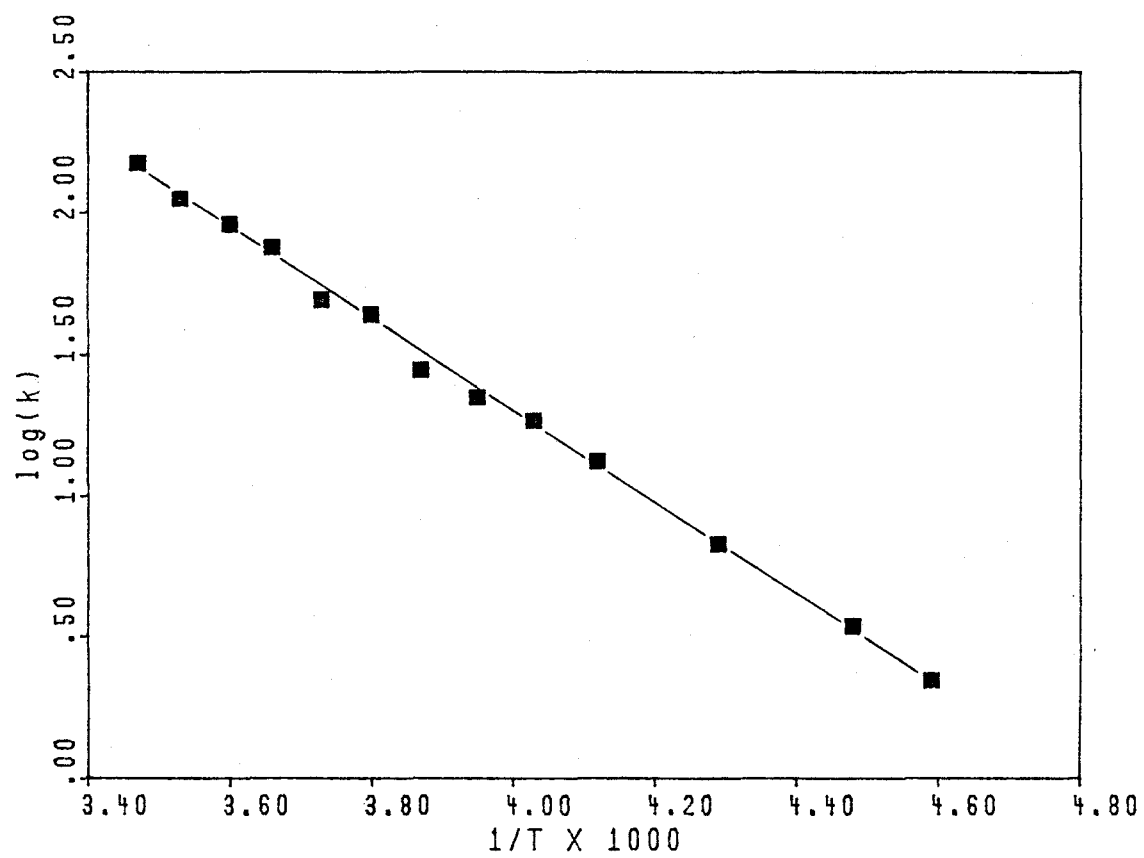


Figure 4.6: The Plot of  $\log k_r$  versus  $1/T$

Table 4.1: Temperature and Rate Data for Activation Energy Parameters

Temp. (°K)	$1/T \times 10^3$	$k_r(\text{sec}^{-1})$	Calc'd $k_r(\text{sec}^{-1})$	$\log(k_r/T)$
188	5.32	0.80	0.15	-2.371
198	5.05	0.96	0.41	-2.314
203	4.93	1.23	0.64	-2.218
208	4.81	1.29	0.99	-2.207
218	4.59	2.23	2.23	-1.990
223	4.48	3.45	3.34	-1.811
233	4.29	6.77	6.77	-1.537
243	4.12	13.30	12.75	-1.262
248	4.03	18.50	17.80	-1.127
253	3.95	22.40	23.94	-1.053
258	3.87	28.00	32.30	-0.965
263	3.80	43.65	41.97	-0.780
268	3.73	49.00	54.55	-0.738
273	3.66	75.00	70.89	-0.561
278	3.60	91.00	88.93	-0.485
283	3.53	112.00	115.47	-0.403
288	3.47	150.00	144.77	-0.283



$$k_r = \frac{k_B T}{h} K_{eq} \quad [4.7]$$

$$K_{eq} = \frac{k_r h}{k_B T} \quad [4.8]$$

If  $K_{eq}$  is regarded as an equilibrium constant then;

$$-RT \ln K_{eq} = \Delta G^{0\ddagger} \quad [4.9]$$

$$-RT \ln K_{eq} = \Delta H^{0\ddagger} - T \Delta S^{0\ddagger} \quad [4.10]$$

$$\ln K_{eq} = \frac{-\Delta H^{0\ddagger}}{RT} + \frac{\Delta S^{0\ddagger}}{R} \quad [4.11]$$

$$\ln \frac{k_r h}{k_B T} = \frac{-\Delta H^{0\ddagger}}{RT} + \frac{\Delta S^{0\ddagger}}{R} \quad [4.12]$$

$$\ln k_r = \frac{-\Delta H^{0\ddagger}}{RT} + \frac{\Delta S^{0\ddagger}}{R} + \ln \frac{k_B T}{h} \quad [4.13]$$

$$k_r = \frac{k_B T}{h} \exp \left( \frac{-\Delta H^{0\ddagger}}{RT} + \frac{\Delta S^{0\ddagger}}{R} \right) \quad [4.14]$$

$$\ln \frac{k_r}{T} = \frac{-\Delta H^{0\ddagger}}{RT} + \frac{\Delta S^{0\ddagger}}{R} + \ln \frac{k_B}{h} \quad [4.15]$$

$$\log \frac{k_r}{T} = \frac{-\Delta H^{0\ddagger}}{2.303RT} + \frac{\Delta S^{0\ddagger}}{2.303R} + \log \frac{k_B}{h} \quad [4.16]$$

Thus, a plot of  $\log(k_r/T)$  versus  $1/T$  will produce a straight line with the slope equal to  $-(\Delta H^{0\ddagger}/2.303R)$  as shown in Figure 4.7. The rate constant is  $k_r$ ,  $k_B$  is the Boltzmann constant,  $h$  is Planck's constant and  $R$  is

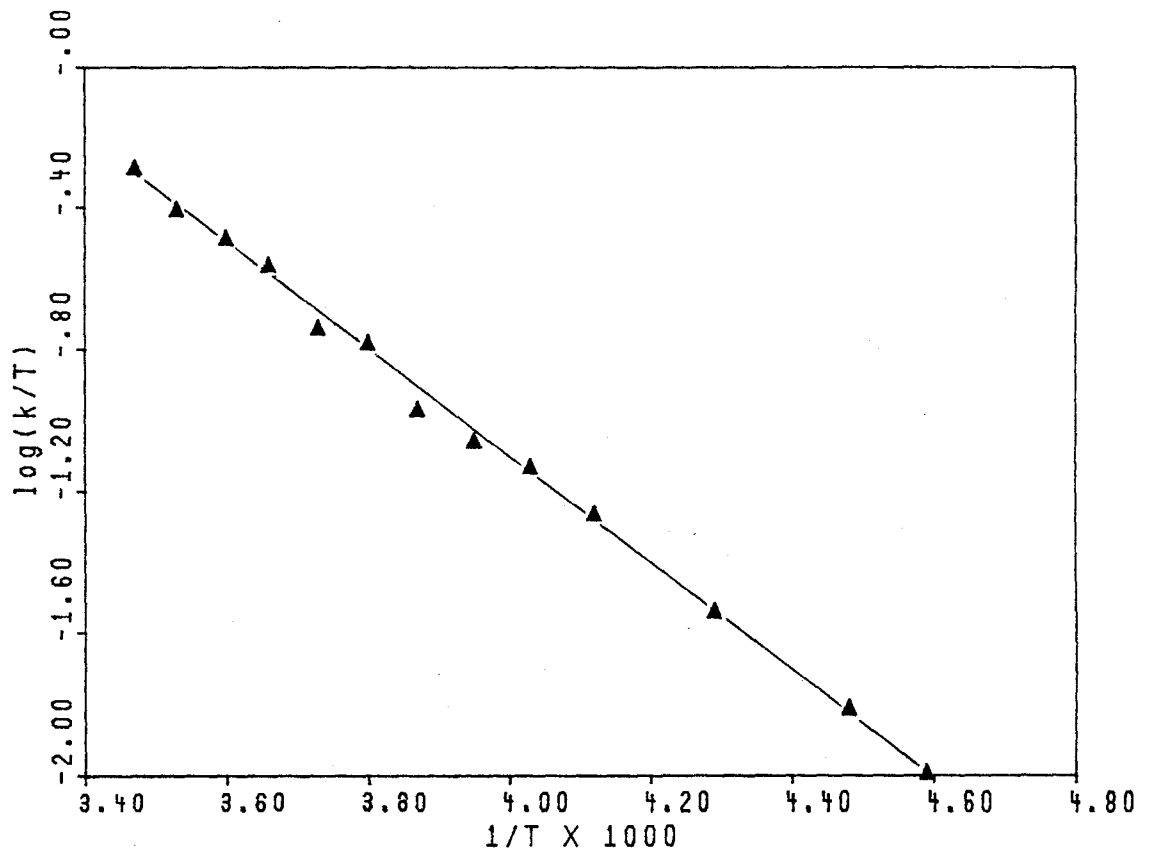


Figure 4.7: The Plot of  $\log(k_p/T)$  versus  $1/T$

the gas constant. When  $1/T$  equals zero then the y-intercept is equal to

$$b = \frac{\Delta S^{0\ddagger}}{2.303R} + \log \frac{k_B}{h} \quad [4.17]$$

which enables the calculation of the entropy of activation.

The plot of  $\log k_r$  versus  $1/T$  is linear and yields an activation energy of  $-7.51\text{Kcal/mole}$  with a correlation coefficient of 0.9979. Also, the plot of  $\log(k_r/T)$  versus  $1/T$  is linear with a correlation coefficient of 0.9959 and yields the activation parameters  $\Delta H^{0\ddagger} = 7.28\text{Kcal/mole}$  and  $\Delta S^{0\ddagger} = -24.6\text{cal/mol}\cdot\text{K}$ .

A relatively wide temperature range was covered with the present data and with the simple nature of the spectra, a rather precise fit of the first order rate constants was obtained. Binsch (89b) has discussed problems that arise in obtaining accurate activation parameters from NMR data. The probable errors associated with these parameters have been estimated by examining the fit of other straight lines to the data with different values of  $\Delta H^{0\ddagger}$  and  $\Delta S^{0\ddagger}$ . Based on these considerations the error is estimated in  $\Delta H^{0\ddagger}$  to be  $\pm 2.0\text{Kcal/mole}$  and in  $\Delta S^{0\ddagger}$  to be  $\pm 3.0\text{cal/mol}\cdot\text{K}$ .

In Table 4.2 are some literature data on the activation parameters of rearrangement reactions of four, five and six-coordinated hydride complexes and on the rates of square planar/tetrahedral isomerization of nickel complexes (33,34,79,90-96). Five, seven and higher coordinated complexes are usually considered stereochemically labile and octahedral

Table 4.2: Activation Parameters for Metal Complex Reactions

Reaction	$\Delta H^\ddagger$ (kcal/mol)	$\Delta S^\ddagger$ (cal/mol.K)	Ref.
Isomerization $H_2Fe[P(OCH_2H_5)_3]_4$	13.7	-8.8	34
Isomerization $HRh[P(OC_2H_5)_3]_4$	5.2	-11.9	33
Isomerization $HNi[P(O-p-C_6H_4CH_3)_3]_3^+$	7.3	-24.6	This work
Isomerization $HNi[P(C_2H_5)_3]_3^+$	9.6	-7.9	68
Isomerization $(PPh_3)_2Pt(HgGePh_3)GePh_3$	14.2	6.3	96
Isomerization $Ni[P(OCH_2)_3CC_2H_5]_5^+$	8.2	-0.5	91
Isomerization $Fe[P(OC_2H_5)_3]_5^{2+}$	9.9	-7.1	92
Ligand Exch. $HPd[P(C_2H_5)_3]_3^+$	1.9	-27.8	68
Ligand Exch. $HPt[P(C_2H_5)_3]_3^+$	2.4	-28.5	68
Tet/Planar $Ni[C_2H_5P(C_6H_5)_2]_2Br_2$	9.0	-4.7	94
Tet/Planar $Ni[(C_6H_5)_2PCH_3]_2Br_2$	11.0	-6.0	95

and four coordinated square planar complexes stereochemically inert. This is based on the smaller ligand field stabilization energies of the trigonal prismatic and tetrahedral geometries which are the likely intermediates in the isomerization processes. The present value of 7.3Kcal/mol for the enthalpy of activation for a square planar isomerization is not in line with these expectations. Neither is the large negative value for the entropy of activation. It is interesting to note that the only known examples of stereochemically labile octahedral or square planar complexes contain hydride ligands. The enthalpy of activation is not dissimilar to the values found for six and five-coordinated hydrides.

Thus, a six-coordinated Fe(II) phosphite hydride has an enthalpy of activation for rearrangement of 13.7 and an entropy of -8.8. The corresponding values for a five-coordinated Rh(I) compound are 5.18 and -11.9. English et al. (68) reported the only values available for a four-coordinated complex  $\text{HNi}[\text{P}(\text{C}_2\text{H}_5)_3]_3^+$  which are  $\Delta H^\ddagger = 9.6\text{Kcal/mol}$  and  $\Delta S^\ddagger = -7.9\text{cal/mol}\cdot^\circ\text{K}$ . Also, note the complications encountered in the fitting of the NMR spectra. For rearrangements of five-coordinated phosphites the  $\Delta H^\ddagger$ 's values are in the range 8-10Kcal/mol and the  $\Delta S^\ddagger$ 's are from -7.1 to 6.5cal/mol·K. The single example (96) of stereochemical nonrigidity in a non-hydride square complex gives a relatively high  $\Delta H^\ddagger = 14.2\text{Kcal/mole}$  and a positive  $\Delta S^\ddagger$ . The rates of isomerization of the tetrahedral to square planar of Ni(II) phosphine halides yield  $\Delta H^\ddagger$  around 7-13 and  $\Delta S^\ddagger$  of -1 to -6. Simple considerations would suggest that the  $\Delta S^\ddagger$  value for an intramolecular rearrangement should be close

to zero and values from +7 to -7 are usually considered consistent with a unimolecular rearrangement mechanism. The large negative value (-24.6) found in the present instance is much more suggestive of a bimolecular substitution mechanism as is illustrated by the values of -28.5 and -27.8 quoted in Table 4.2 for square planar Pd and Pt hydride substitutions. It is noted that there is a tendency for hydride rearrangements to show negative  $\Delta S^\ddagger$ 's and Meakin et al. (33) did remark that the value of -11.9 quoted above for the Rh complex "is larger than might be expected for a simple intramolecular rearrangement". From the NMR spectra it is clear that the process is indeed an intramolecular exchange since the phosphorus-hydrogen coupling constant is not lost as would be the case for intermolecular exchange.

The direct implication of the large negative entropy of activation is that the transition state for the process, presumably a ligand arrangement close to tetrahedral, is more highly ordered than the square planar ground state. In cases where both the square planar and the tetrahedral state are accessible to study there is usually a positive difference in entropy between the two states (95,96). This has been attributed to interactions of donor solvent molecules at axial positions of the square planar molecule. Methylene chloride is a poor donor and the large bulk of the phosphite ligands prevents axial coordination in the present case. A probable reason for the negative entropy difference is the existence of a more tightly bound ion pair in the tetrahedral configuration. In a non-polar solvent such as methylene chloride, ion pairing would certainly be anticipated. The involvement of hydrogen bonding to the hydride ligand

is a probable structure for such an ion pair. A model indicates that steric crowding in the square planar complex would prevent direct interaction of the bisulphate counter ion and the hydride. The result would probably be a loose, solvent-separated ion pair. The fact that the hydride chemical shifts are invariant with the anion is consistent with a solvent-separated ion pair. In the tetrahedral geometry, the steric crowding is much less, therefore, direct hydrogen bonding to the anion could occur. Hydrogen bonding interactions between metal complexes and second sphere ligands are well documented (97). In terms of the entropy change, complexing of the anion by hydrogen bonding is equivalent to the addition of another ligand. The low enthalpy of activation of the rearrangement can also be accounted for by the formation of a strong hydrogen bond in the transition state. Only hydrides can form ion pairs of this type and such a mechanism, therefore, accounts for the unique stereochemical lability of square planar and octahedral complexes containing this ligand. It has been argued (98) that the intramolecular isomerization of a square planar complex is a thermally "forbidden" but photochemically "allowed" reaction and requires the participation of a fifth ligand or, in the present case, a counter ion if it is to be a rapid reaction. There is no requirement of this nature for tetrahedral to square planar transitions and all the reported  $\Delta S^\ddagger$ 's are in the range for unimolecular rearrangements (94,95). The only other reported non-rigid square planar complex(96) shows a small positive entropy of activation for the rearrangement process. This complex has very bulky ligands probably leading to distortion from square planar geometry in the ground state and to rearrangement through a digonal twist.

#### 4.5 Proposals for Future Research

There are many areas of future research that could be developed from the results presented in this thesis. One such project is an investigation of the possible loose, solvent-separated ion pair involving hydrogen bonding between the hydride and the counter bisulphate ion. This is the explanation we have advanced for the large negative entropy, but more work is necessary to verify this. The use of the four-coordinate hydride  $\text{HNi}[\text{P}(\text{O}-\text{p}-\text{C}_6\text{H}_4\text{CH}_3)_3]_3^+$  as an active catalyst in the coupling of dienes with olefins and also its possible use in polymerizations or hydrogenations should be undertaken and compared with previous work reported in the literature. Furthermore, the formation of a four-coordinated nickel hydride involving a bidentate ligand may form a reasonably stable hydride similar to the para-tolyl phosphite system investigated in this thesis.



## REFERENCES

1. E.L. Muetterties, "Transition Metal Hydrides", Marcel Dekker, Inc., New York, (1971).
2. M.L.H. Green, D.J. Jones, Advan. Inorg. Chem. Radiochem. 7, 115 (1965).
3. R.V.G. Ewens, M.W. Lister, Trans Faraday Soc., 35, 681 (1939).
4. a) W. Hieber, Die Chemie 55, 24 (1942)  
b) M.L.H. Green, D.J. Jones, Advan. Inorg. and Radiochem., 7, 129 (1965).  
c) A.P. Ginsberg, Transition Metal Chem., 1, 111 (1965).  
d) G. Wilkinson, J.M. Birmingham, J. Amer. Chem. Soc., 77, 3421 (1955).
5. F.A. Cotton, G. Wilkinson, Chem. Ind. (London), 1305 (1956).
6. P.G. Ouston, J.M. Partridge, J.M. Rowe, Acta Crystallogr. 13, 246 (1960).
7. P.L. Orioli, L. Vaska, Proc. Chem. Soc., 333 (1962).
8. S.J. LaPlaca, J.A. Ibers, J. Am. Chem. Soc. 85, 3501 (1963).
9. S.C. Abrahams, A.P. Ginsberg, K. Knox, Inorg. Chem. 3, 558 (1964).
10. S.J. LaPlaca, W.C. Hamilton, J.A. Ibers, A. Davison, Inorg. Chem. 8, 1928 (1969).
11. A. Pidcock, R.E. Richards, L.M. Venanzi, J. Chem. Soc. A., 1707 (1966).
12. C. Masters, B.L. Shaw, R.F. Stainbank, Chem. Commun. 209 (1971).
13. J.A. Pople, D.P. Santry, Mol. Phys. 8, 1 (1964).
14. R.M. Stevens, C.W. Kern, W.N. Lipscomb, J. Chem. Phys. 37, 279 (1962).

15. A.D. Buckingham, P.J. Stephens, *J. Chem. Soc.*, 2747 (1964).
16. G.W. Parshall, "Homogeneous Catalysis, The Applications and Chemistry of Catalysis by Soluble Transition Metal Complexes", John Wiley and Sons, Toronto, (1980).
17. J.C. Kotz, D.G. Pedrotty; *J. Organometal. Chem.*, 22, 425 (1970).
18. W.C. Drinkard, D.R. Eaton, J.P. Jesson, R.V. Lindsay Jr., *Inorg. Chem.* 9, 392 (1970).
19. R.A. Schunn, *Inorg. Chem.* 9, 394 (1970).
20. L. Vaska, *Chem. Commun.*, 614 (1966).
21. J. Knight, M.J. Mays, *J. Chem. Soc. A.* 711 (1970).
22. M. Meier, F. Basolo, R.G. Pearson, *Inorg. Chem.* 8, 795 (1969).
23. C.A. Tolman, *J. Am. Chem. Soc.*, 92, 6777 (1970).
24. C.A. Tolman, *J. Am. Chem. Soc.*, 92, 4217 (1970).
25. J.P. Durand, F. Dawans, Ph. Teyssie, *J. Polym. Sci. Part A-1*, 8, 979 (1970).
26. R.W. Barker, P. Pauling, *Chem. Commun.* 1495 (1969).
27. E.L. Muetterties, *Inorg. Chem.* 4, 769 (1965).
28. P. Meakin, J.P. Jesson, E.N. Tebbe, E.L. Muetterties, *J. Am. Chem. Soc.*, 93, 1797 (1971).
29. E.L. Muetterties. *J. Am. Chem. Soc.*, 91, 1636 (1969).
30. E.L. Muetterties, *Accounts. Chem. Res.* 3, 266 (1970).
31. E.L. Muetterties, *Rec. Chem. Progr.* 31, 51 (1970).
32. R.S. Berry, *J. Chem. Phys.* 32, 933 (1960).
33. P. Meakin, E.L. Muetterties, J.P. Jesson. *J. Am. Chem. Soc.* 94, 5271 (1972).

34. P. Meakin, E.L. Muetterties, F.N. Tebbe, J.P. Jesson, J. Am. Chem. Soc., 93, 4701 (1971).
35. F.N. Tebbe, P. Meakin, J.P. Jesson, E.L. Muetterties, J. Am. Chem. Soc. 92, 1068 (1970).
36. S.A.R. Knox, H.D. Kaesz, J. Am. Chem. Soc. 93, 4594 (1971).
37. D.D. Titus, A.A. Orio, R.E. Marsh, H.B. Gray, Chem. Commun. 322 (1971).
38. K.C. Dewhirst, W. Keim, C.A. Reilly, Inorg. Chem. 7, 546 (1968).
39. G.C. Bond, Surface Sci. 18, 11 (1969).
40. R.P.H. Gasser, K. Roberts, A.J. Stevens, Trans. Faraday Soc. 65, 3105 (1969).
41. M.L.H. Green, T. Saito, P.J. Tanfield, J. Chem. Soc. A. 152 (1971).
42. M.L.H. Green, H. Munakata, T. Saito, J. Chem. Soc. A. 469 (1971).
43. F. Cariati, R. Ugo, F. Bonati, Inorg. Chem. 5, 1128 (1966).
44. M.J. Church, M.J. Mays, J. Chem. Soc. A. 3074 (1968).
45. L. Toniolo, M. Giustiniani, U. Belluco, J. Chem. Soc. A., 2666 (1969).
46. M. Giustiniani, G. Dolcetti, U. Belluco, J. Chem. Soc. A. 2047 (1969).
47. H.C. Clark, K.R. Dixon. J. Am. Chem. Soc., 91, 596 (1969).
48. M.J. Church, M.J. Mays, J. Chem. Soc. A., 1938 (1970).
49. A.J. Deeming, B.F.G. Johnson, J. Lewis, Chem. Commun., 598 (1970).
50. J.D. Druliner, A.D. English, J.P. Jesson, P. Meakin, C.A. Tolman, J. Am. Chem. Soc., 98, 2156 (1976).

51. M.L.H. Green, T. Saito, Chem. Commun. 208 (1969).
52. K. Jonas, G. Wilke, Angew. Chem. Int. Ed. Engl. 8, 519 (1969).
53. U.A. Gregory, B.T. Kilbourn, private communication.
54. H. Bönemann, Angew. Chem. Int. Ed. Engl. 9, 736 (1970).
55. H. Munakata, M.L.H. Green, Chem. Commun. 881 (1970).
56. T. Saito, Chem. Lett. 1545 (1974).
57. G.K. McEwen, C.J. Rix, M.F. Traynor, J.G. Verkade, Inorg. Chem. 13, 2800 (1974).
58. P. Meakin, R.A. Schunn, J.P. Jesson, J. Am. Chem. Soc. 96, 277 (1974).
59. R.A. Schunn, Inorg. Chem. 15, 208 (1976).
60. C.A. Tolman, J. Am. Chem. Soc. 92, 6785 (1970).
61. C.A. Tolman, J. Am. Chem. Soc. 94, 2994 (1972).
62. C.A. Tolman, Inorg. Chem. 11, 3128 (1972).
63. J.A. Chopoorian, J. Lewis, R.S. Nyholm, Nature 190, 528 (1961).
64. K. Jonas, G. Wilke, Angew. Chem. Int. Ed. Engl. 9, 312 (1970).
65. W. Hieber, J. Ellermann, Z. Naturforsch B18, 595 (1963).
66. W. Hieber, W. Kroder, E. Zahn, Z. Naturforsch B15, 325 (1960).
67. P. Meakin, A.D. English, J.P. Jesson, J. Am. Chem. Soc. 98, 414 (1976).
68. A.D. English, P. Meakin, J.P. Jesson, J. Am. Chem. Soc. 98 422 (1976).
69. J.J. Levison, S.D. Robinson, J. Chem. Soc. A. 96 (1970).
70. J.J. Levison, S.D. Robinson, Inorg. Syn. 13, 105 (1972).
71. H.J. Lucas, F.W. Mitchell, C.N. Scully, J. Am. Chem. Soc., 72, 5491 (1950).

72. P. Haake, J.P. McNeal, E.J. Goldsmith. *J. Am. Chem. Soc.* 90, 715 (1968).
73. R. Burgada, H. Germa, M. Wilson, F. Mathis, *Tetrahedron*, 27, 5833 (1971).
74. D.H. Gerlach, W.G. Peet, E.L. Muetterties, *J. Am. Chem. Soc.*, 94, 4545 (1972).
75. E.L. Muetterties, F.J. Hirsekorn, *J. Am. Chem. Soc.*, 96, 7920 (1974).
76. W. Kruse, R.H. Atalla, *Chem. Commun.* 921 (1968).
77. C.A. Tolman, *J. Am. Chem. Soc.* 92, 2956 (1970).
78. E.L. Muetterties, F.J. Hirsekorn, *J. Am. Chem. Soc.*, 96, 7920 (1974).
79. P. Meakin, L.J. Guggenberger, J.P. Jesson, D.H. Gerlach, F.N. Tebbe, W.G. Peet, E.L. Muetterties, *J. Am. Chem. Soc.* 92, 3482 (1970).
80. K.B. Dillon, T.C. Waddington, D. Younger, *J. Inorg. Nucl. Chem.*, 43, 2665 (1981).
81. H.R. Hudson, J.C. Roberts, *J. Chem. Soc. Perkin (II)* 1575 (1974).
82. E.J. Griffith, M. Grayson, ed. by "Topics in Phosphorus Chemistry Volume 8", J. Wiley and Sons, New York, 1976, pp.99-192.
83. C.F. Callis, J.R. VanWazer, J.N. Schoolery, W.A. Anderson, *J. Am. Chem. Soc.*, 79, 2719 (1957).
84. W.G. Schneider, A.D. Buckingham, *Disc. Faraday, Soc.*, 34, 147 (1962).
85. S. Forsen, R.A. Hoffman, *Acta, Chem. Scand.*, 17, 1787 (1963).
86. S. Forsen, R.A. Hoffman, *J. Chem. Phys.*, 39, 2892 (1963).

87. S. Forsen, R.A. Hoffman, J. Chem. Phys., 40, 1189 (1964).
88. J.A. Pople, W.G. Schneider, H.J. Bernstein, "High-Resolution Nuclear Magnetic Resonance", McGraw-Hill Book Company Inc., New York, (1959).
- 89.a) D.A. Kleier, G. Binsch, Q.C.P.E. No165 Indiana University (1969).  
b) G. Binsch, "Band-Shape Analysis" in "Dynamic Nuclear Magnetic Resonance Spectroscopy" ed. by L.M. Jackman, F.A. Cotton, Academic Press, New York 1975 pg. 45.
90. P. Meakin, J.P. Jesson, J. Am. Chem. Soc., 96, 5751 (1974).
91. J.P. Jesson, P. Meakin, J. Am. Chem. Soc., 96, 5760 (1974).
92. A.D. English, S.D. Ittel, C.A. Tolman, P. Meakin, J.P. Jesson, J. Am. Chem. Soc., 99, 117 (1977).
93. P. Meakin, E.L. Muetterties, J.P. Jesson, J. Am. Chem. Soc., 95, 75 (1973).
94. G.N. LaMar, E.O. Sherman, J. Am. Chem. Soc., 92, 2691 (1970).
95. L.H. Pignolet, W. DeW. Horrocks, R.H. Holm, J. Am. Chem. Soc., 92, 1855 (1970).
96. Yu. K. Grishin, V.A. Domrachev, Yu.A. Ustynyuk, S.N. Titova, G.A. Domrachev, G.A. Razuvaev, Polyhedron 2, 895 (1983).
97. D.R. Eaton, W.D. Phillips, D.J. Caldwell, J. Am. Chem. Soc., 85, 397 (1963).
98. P. Beck, Coord, Chem. Rev. 3, 91 (1968).